SEMMELWEIS EGYETEM DOKTORI ISKOLA

Ph.D. értekezések

3232.

KEMECSEI RÓBERT GERGELY

Neuromorfológia és sejtbiológia

című program

Programvezető: Dr. Alpár Alán, egyetemi tanár

Témavezető: Dr. Zachar Gergely, tudományos főmunkatárs

Network-Level Analysis of Social Brain Activation in Mice with Autistic Phenotypes

PhD thesis

Róbert Gergely Kemecsei

János Szentágothai Neurosciences Doctoral School Semmelweis University



Supervisor: Gergely Zachar, Ph.D

Official reviewers: László Négyessy, D.Sc

András Horváth, Ph.D

Head of the Complex Examination Committee:

Alán Alpár, MD, D.Sc

Members of the Complex Examination Committee:

Zsuzsanna Várnainé Tóth, Ph.D Krisztina Kovács, D.Sc

Budapest 2025

Table of contents

Li	st of abbi	reviations	5
1	Introdu	ıction	9
	1.1 Au	tism Spectrum Disorder	9
	1.1.1	Historical overview	9
	1.1.2	VPA Syndrome	. 11
	1.2 AS	ED CNS pathology	. 12
	1.2.1	Explored differences in CNS	. 12
	1.2.2	Gray-matter differences	. 12
	1.2.3	Microstructure	. 15
	1.2.4	White matter	. 15
	1.2.5	Sex differences	. 17
	1.3 Ro	dent VPA model	. 18
	1.3.1	Face validity of model	. 18
	1.3.2	Rodent social behavior	. 19
2	Objecti	ives	. 23
3	Materia	als and methods	. 24
	3.1 An	imals and housing conditions	. 24
		perimental design	
	3.2.1	Dopamine assay	
		.1 Sample preparation	
		.2 DA ELISA assay	
	3.2.2	Three-chamber sociability test	
	3.2.3	Immunhistochemistry	
	3.2.3	·	
	3.2.3	* * *	
	3.2.3.		
	3.2.3		
	3.2.4	Behavioral analysis	. 31

3.3	Statystical analysis	31
3.3	3.1 Comparisons	31
3.3	Network analysis	33
3.3	Network construction	34
3	3.3.3.1 Centrality measures	34
3	3.3.3.2 Cluster analysis	35
3	3.3.3.3 Validation of network analyses	35
3.3	Behavioral correlations	37
3.4	Identifying of potentially affected neurodevelopmental genes	(gene library
analy	ysis)	
4 Re	esults	30
4.1	DA ELISA	39
4.2	Three-chamber sociability test	39
4.2	2.1 Habituation	39
4.2	2.2 Social Preference	41
4.2	2.3 Social Memory	41
4.3	C-Fos Activity	41
4.3	3.1 Laterality	41
4.3	3.2 Activation pattern	41
4	4.3.2.1 Decision-Making Network	42
4	4.3.2.2 Lateral Septum and Bed Nucleus of the Stria Terminalis	47
4	4.3.2.3 Social Network	47
4	4.3.2.4 Stress Network	
4	4.3.2.5 Putative non-social regions	49
4.4	Network Analysis	50
4.4	Visual Inspection of Network Structure	50
4.4	1.2 Validation of Connectome Threshold	53
4	4.4.2.1 Statistical Analysis	53
4.4	Functional Connectivity after social stimulation	53
4	4.4.3.1 Connectome filtered and Random Matrix Analysis	53
44	1.4 Functional Sub-networks	57

	4.4.4.1	Analysis of Sub-networks	57
	4.4.4.2	Identification of Functional Core Networks- Social reinstatement	59
	4.4.4.3	Identification of Functional Core Networks- Social isolation	62
	4.4.5	Behavioral analysis	64
	4.4.6	Gene library analysis	67
5	Discussio	on	68
	5.1 Socia	ability deficits	68
	5.2 Activational pattern of ROI		69
	5.3 Fund	ctional Connectivity and Network Changes	72
6	Conclusion	on	85
7	Summary		
8	References		
9	List of Own Publications		
10	Ackno	wledgement	124

List of abbreviations

5-HT 5-Hydroxytryptamine

ACC Anterior Cingulate Cortex

ADHD Attention Deficit Hyperactivity Disorder

AH Anterior Hypothalamus

ANOVA Analysis of Variance

ASD Autism Spectrum Disorder

blAMY Basolateral Amygdala

bmAMY Basomedial Amygdala

BNST Bed Nucleus of the Stria Terminalis

CA Cornu Ammonis

ceAMY Central Amygdala

CPU Caudate Putamen

CTR Control

D1/2/3 Dopamine type 1/2/3 (receptor)

DA ELISA Dopamine Enzyme-Linked Immunosorbent Assay

DA Dopamine

dCA 1/2/3 Dorsal Cornu Ammonis

dGD Dorsal Dentate Gyrus

DMH Dorsomedial Hypothalamus

dmPAG Dorsomedial Periaqueductal Gray

dlPAG Dorsolateral Periaqueductal Gray

DMN Default Mode Network

DSM Diagnostic and Statistical Manual of Mental Disorders

DTI Diffuse Tensor Imaging

E13.5 13.5th day of gestation/ embryonic day

ELISA Enzyme-Linked Immunosorbent Assay

FDR False Discovery Rate

fMRI Functional Magnetic Resonance Imaging

FVS Fetal Valproate Syndrome

GABA Gamma Amino Butyrate

GD Dentate Gyrus

GM Gray Matter

HIP Hippocampus

IF Interfascicular Nucleus

IPN Interpeduncular Nucleus

LHA Lateral Hypothalamic Area

IHb Lateral Habenula

IPAG Lateral Periaqueductal Gray

IPOA Lateral Preoptic Area

LS Lateral Septum

MCL Markov Cluster Algorithm

meAMY Medial Amygdala

mHb Medial Habenula

mHb-IPN Habenulo-Interpeduncular Axis

mPOA Medial Preoptic Area

MRS Mesolimbic Reward System

NAcc Nucleus Accumbens

NiDAB 3,3'-Diaminobenzidine + Nickel chloride

P Postnatal day

PAG Periaqueductal Gray

PBS Phosphate Buffered Saline

PDD Pervasive Developmental Disorders

PDD-NOS Pervasive Developmental Disorder Not Otherwise Specified

PFA Paraformaldehyde

POA Preoptic Area

PVT Paraventricular Thalamus

ROI Regions of Interest

RSC Retrosplenial Cortex

SBN Social Behavior Network

SDMN Social Decision Making Network

TD Typically Developing

TH Tyrosine Hydroxylase

TO Olfactory Tubercle

vCA1/3 Ventral Cornu Ammonis

vGD Ventral Dentate Gyrus

VMH Ventromedial Hypothalamus

VP Ventral Pallidum

VPA Valproic Acid

vPAG Ventral Periaqueductal Gray

VTA Ventral Tegmental Area

WM White Matter

ZI Zona Incerta

1 Introduction

1.1 Autism Spectrum Disorder

1.1.1 Historical overview

Autism spectrum disorder (ASD) is a neurodevelopmental condition characterized by deficits in social communication and the presence of restricted interests and repetitive behaviors (1,2). The term "autism" was first used by Bleuler to describe severely withdrawn schizophrenic patients (3,4). Kanner later described ASD as "autistic disorder," "childhood autism," or "infantile autism." He distinguished it from schizophrenia by noting that children with ASD exhibited consistent behaviors from birth, such as a preference for solitary activities and a heightened interest in non-living objects (5). Kanner outlined key criteria for ASD, including a lack of interest in social interactions and behaviors such as 'resistance to change' or 'insistence on sameness.' Around the same time, Asperger identified similar traits in boys with normal intelligence and language skills, coining the term "autistic psychopathy." These boys demonstrated difficulties in social interactions, specific interests, and deficits in communication skills (6,7).

In the early editions (I-II) of the Diagnostic and Statistical Manual of Mental Disorders (DSM), autism was initially classified as a subtype of schizophrenia, reflecting the limited understanding of neurodevelopmental conditions at the time. However, as research progressed and awareness of autism increased, it became evident that autism represented a distinct disorder with unique characteristics (8).

With the publication of DSM-III, a significant shift occurred in the classification of autism. It was no longer considered a subtype of schizophrenia but was instead recognized as a separate entity within a new category known as Pervasive Developmental Disorders (PDD). This marked a crucial step in acknowledging the distinct nature of autism and paved the way for further research and understanding of the condition (9).

DSM-III primarily focused on infantile autism but also addressed other forms of autism, including late-onset autism. The diagnostic criteria for autism outlined in DSM-III included various behavioral and developmental characteristics, such as onset before 30 months of age, deficits in language development, and peculiar speech patterns like

echolalia and metaphorical language. Importantly, these criteria aimed to distinguish autism from other psychiatric disorders like schizophrenia by emphasizing specific behavioral patterns unique to autism (10).

In DSM-III-R, a comprehensive set of 16 criteria was introduced, categorized into three primary domains:

- Qualitative impairments in reciprocal social interaction
- Impairments in communication
- Restricted interests/resistance to change and repetitive movements

To receive a diagnosis of autistic disorder, individuals needed to meet a minimum of eight positive criteria, with at least two from the social domain and at least one from each of the other two categories (10,11).

DSM-IV aimed to streamline the classification of disorders associated with autistic features, encompassing newly identified conditions like Rett syndrome (12). Diagnostic subcategories, including autistic disorder, Asperger's disorder, PDD-NOS (Pervasive Developmental Disorder Not Otherwise Specified), Rett's disorder, and childhood disintegrative disorder, were grouped under the umbrella term "Pervasive Developmental Disorders". However, studies highlighted significant variability in symptom severity both within and between these subcategories (13–15). These discrepancies, coupled with limited predictive capacity for later outcomes and diagnostic ambiguity, led to reliability concerns. Additionally, treatment eligibility and coverage often hinged on these subtypes.

DSM-5 marks a significant shift from the previous multi-categorical diagnostic approach to a single diagnosis based on multiple dimensions. This change addresses the challenges in categorizing the diverse manifestations of autism into distinct subcategories, as highlighted by past unsuccessful attempts (11,16).

In DSM-5, the term "spectrum" is used to describe the disorder, recognizing the wide range of presentations within ASD. This includes variations in social communication difficulties. To receive an ASD diagnosis, individuals must meet criteria for specific fixated interests and repetitive behaviors. Symptoms must appear in early development and cause significant impairments in social, occupational, or other important areas of

functioning. Additionally, the diagnosis should not be better explained by intellectual disability (17,18).

1.1.2 VPA Syndrome

Twin studies and extensive genetic investigations have not provided conclusive results but emphasize the importance of environmental risk factors in the development of autism (19,20). Consequently, researchers propose that the development of autism primarily involves the interaction between susceptible genes and environmental factors (21,22). Among these environmental factors, gestational exposure to Valproic acid (VPA) is particularly noteworthy (23).

VPA, originally synthesized in 1882 by Burton as a derivative of valeric acid—a naturally occurring fatty acid found in both plants and animals— remained pharmacologically inactive until 1962, when Eymard serendipitously discovered its anticonvulsant properties (24). Since then, VPA, a branched short-chain fatty acid, has been widely used to treat epilepsy, bipolar disorder, migraine, and other neuropsychiatric conditions. Its antiepileptic efficacy is primarily attributed to the modulation of ion channels and the enhancement of gamma-aminobutyric acid (GABA) signaling. Furthermore, VPA functions as a histone deacetylase inhibitor, promoting gene transcription by inhibiting histone deacetylation and thereby increasing chromatin accessibility (25,26).

Reports since the early 1980s have indicated that exposure to VPA during pregnancy is associated with an increased risk of congenital malformations and compromised developmental outcomes (27–29). These adverse effects include impaired cognition and neurodevelopment, as well as an elevated susceptibility to attention deficit hyperactivity disorder (ADHD) and ASD. Initially overlooked, these associations are now recognized as part of the Fetal Valproate Syndrome (FVS) phenotype (30–32).

Classical autism has been identified as one of the behavioral outcomes associated with VPA exposure during pregnancy. In several reported cases, children born to mothers who received VPA treatment during pregnancy exhibited various symptoms: 53% showed poor social interaction, 49% demonstrated deficits in communication skills, and 46% displayed insistence on routines (29,33,34).

1.2 ASD CNS pathology

1.2.1 Explored differences in CNS

The physiological changes underlying the behavioral manifestations of autism are not yet fully understood. However, numerous structural alterations have been identified through advancements in neuroimaging technologies. Differences have been observed in the size of various cortical and subcortical structures, alongside alterations in the microscopic structure, connectivity, and developmental synchronization of these brain areas in individuals with ASD. Subsequent functional Magnetic Resonance Imaging (fMRI) studies have demonstrated that these structural changes are related to the behavioral characteristics of autism.

1.2.2 Gray-matter differences

The first indication of structural changes in brain architecture in individuals with autism was highlighted by Kanner, who observed that 5 out of 11 autistic children examined had relatively large heads (5). Subsequent imaging studies revealed that individuals with ASD exhibit a whole-brain volume enlargement of 5-10% (35–37). This enlargement affects both gray matter (GM) and white matter (WM), particularly in toddlers and children, but not in later developmental stages. This phenomenon suggests an early overgrowth followed by a decelerated developmental trajectory (38–40). Moreover, research has demonstrated that GM volume enlargement persists into adulthood (21-34 years), and structural abnormalities correlate with autistic symptoms (41,42).

Further investigation into the theory of whole-brain enlargement was conducted through a meta-analysis spanning from 2002 to 2010, which found no significant difference in whole-brain GM volume in ASD patients (43). Later studies revealed age-dependent disparities between autistic and typically developing (TD) brains, particularly in regions including the parietal lobe, occipital lobe, temporal lobe, and cingulate gyrus (44). During early childhood in ASD, enlargement primarily affects the frontal and temporal lobes and the amygdala (45,37), followed by decelerated development in later years (10-15 years of age) (46).

Publications have documented asymmetric decreases in various brain regions in ASD children. For instance, the right superior temporal gyrus, associated with language (47)

and social cognition (48), and the right inferior parietal lobule, implicated in image thinking, imitative action (49), and eye contact (50), show significant reductions (44).

Additionally, structural changes include reduced regional GM volume in the right orbitofrontal cortex and increased cortical thickness in the right pars triangularis (51), along with decreased cortical thickness in the left orbitofrontal cortex and pars triangularis (52). The pars triangularis may be related to expressive language deficits in some individuals with ASD (53) and facilitates cross-talk with other social brain regions, such as the pars orbitalis of the frontal lobe, potentially contributing to social communication difficulties linked to higher autistic traits (54).

Furthermore, decreased GM volume has been observed in the post- and paracentral gyrus and parahippocampal gyrus, while increases have been noted in the right-sided precentral gyrus, fusiform gyri, left precuneus, and anterior cingulate cortex (52,55,51). The left lingual gyrus also exhibits higher GM thickness (51). The lingual gyrus, along with the lateral occipital cortex, fusiform gyrus, and posterior superior temporal sulcus, is crucial for object/face recognition and following biological motion cues (56).

While a smaller right inferior parietal lobule is noted in children with autism, an enlargement of the left inferior parietal lobule is observed in older ASD cohorts (44). Additionally, the right middle occipital gyrus, responsible for processing body language and emotional regulation (57), is enlarged (44). The left posterior cingulate gyrus, which plays roles in cognitive control (58), conflict monitoring (59), and social cognition (60), shows a decrease in volume in individuals with ASD (44).

fMRI studies have revealed significant differences in brain activity during tasks involving the recognition of emotional states in others. In children with ASD, exposure to fearful faces results in lower activation in key brain regions, such as the right amygdala, right superior temporal sulcus, and right inferior frontal gyrus, compared to TD children. Conversely, when presented with happy faces, children with ASD exhibit lower activity in the left insular cortex (61,62).

Research has also identified distinct activation patterns in brain areas crucial for communication, such as the left superior temporal gyrus (Wernicke's area) and left inferior frontal gyrus (Broca's area), which play pivotal roles in language processing and

higher-order communication skills. These differences in activation patterns may contribute to the pragmatic language deficits often observed in individuals with ASD (63).

These findings provide valuable insights into the neural mechanisms underlying emotional processing and communication difficulties in ASD, illuminating the complex interplay between brain function and behavior in individuals with neurodevelopmental disorders. Studies have shown hypo-activation in the bilateral fusiform face area and occipital face area during emotion processing (64–66). The anterior cingulate cortex (ACC) is also crucial in regulating cognitive and emotional processing. Hypo-activity of the ACC is strongly correlated with decreased function (67) and may contribute to restricted and repetitive behaviors. During correct and error response tasks, the rostral ACC shows higher activity in individuals with ASD (68).

Analysis of deeper brain structures, such as the basal ganglia and thalamus, reveals increased GM volume in the bilateral putamen in individuals with ASD (51). This increase is associated with restricted and repetitive behavior (69,70). The putamen and the right globus pallidus exhibit age-related shape changes in ASD, characterized by a reduction in tissue volume, leading to a more inwardly curved (concave) surface facing the ventricular system. These maturational alterations may reflect underlying changes in neuronal pruning, connectivity, or gray matter integrity. Additionally, an enlargement of the surface area has been observed in the bilateral thalamus, with the right thalamus showing similar localized inward curvature. The surface area of the left medial thalamus has been found to positively correlate with ASD symptom severity. Among thalamic subdivisions, the mediodorsal nucleus — a key hub for prefrontal-thalamic communication — appears particularly affected and may contribute to executive function deficits, while the pulvinar nucleus, involved in sensory integration and social attention, also exhibits ASD-related alterations (71).

ASD children also show higher structural covariance between the putamen and the right globus pallidus, potentially due to hyper-synchronous developmental coordination and maturation (72). Conversely, decreased structural covariation is observed between the right globus pallidus and the left nucleus accumbens, as well as between the left globus pallidus and the right nucleus accumbens. Similar structural tendencies are noted in the

thalamus, with decreased structural covariation between the left and right thalami. Overall, covariance analysis reveals decreased inter-hemispheric structural covariation and enhanced intra-hemispheric structural covariation. These subcortical structural abnormalities collectively predict social communication difficulties and repetitive, stereotypic behavior in ASD (73).

1.2.3 Microstructure

The differences in GM volume in individuals with ASD may be attributed to microstructural alterations within cortical columns. Post-mortem studies have revealed fewer minicolumns in the orbitofrontal cortex, which may explain the reduced regional GM volume (74,75). This abnormal cytoarchitecture could result from differences in neuronal migration within radial minicolumns (76), leading to reduced alignment and increased density of pyramidal cells (51). Mislocated neurons may lose proper innervation by fibers that normally travel to and target specific cortical lamina, resulting in improper firing (77,78).

Misplaced neurons in individuals with ASD exhibit delayed maturation, immature dendritic arborization and spine formation, insufficient dendritic spine pruning, and a delayed switch from excitatory to inhibitory GABAergic synaptic transmission (79,80). These individuals also show smaller cell size and increased cell density in regions such as the hippocampus, limbic system, entorhinal cortex, and amygdala (81). Irregularly distributed neurons and disruptions in the boundary between cortical layers IV and V, particularly in the posterior cingulate gyrus, have also been observed (82). Additionally, a decrease in 5-hydroxytryptamine (5-HT) receptors in the left posterior cingulate cortex has been noted in individuals with ASD. 5-HT plays an important role in neuronal migration, synaptogenesis, and nerve growth (83).

Microstructural changes can also result from atypical myelination development. Without synchronized myelination, axons can be misrouted to incorrect areas of the brain, may never reach their targets, or may arrive late, which can have devastating effects (84).

1.2.4 White matter

Another explanation for the expanded cortical surface in individuals with ASD involves differences in WM structure. Research suggests that the enlarged gyrification and sulcal

patterns might be caused by mechanical tension from axon fibers of white matter pulling on the neocortex (85,86). Atypical cortical folding and accelerated cortical surface expansion have been observed in the frontal lobe of children and adolescents with ASD in several studies (87,88). However, differences in cortical thickness have not been found in children with ASD before the age of two years (89).

Studies on connectivity in ASD have produced mixed results. Some researchers have found long-range hyper-connectivity (90,91), while others have reported long-range hypo-connectivity (92,93). These variations may reflect age-related patterns in WM differences. Research on the default mode network (DMN), which includes the posterior cingulate gyrus, retrosplenial cortex, lateral parietal cortex, medial prefrontal cortex, superior frontal gyrus, and temporal lobe, shows that it is hypo-connected in adults with ASD but hyper-connected in ASD children (94). These early developmental patterns and age-related changes in frontal fiber tracts may underlie impaired social and communication behaviors in ASD (95).

Additionally, studies have found local-range hyper-connectivity within the frontal lobe and hypo-connectivity between the frontal cortex and other brain systems (96,97). This hypo-connectivity predominates in cortico-cortical and interhemispheric functional connectivity (98). Diffusion tensor imaging (DTI) studies also highlight these differences in functional connections. Abnormalities in the WM structure of the corpus callosum, frontal tract pathways, inferior longitudinal fasciculus, fronto-occipital fasciculus, and superior longitudinal fasciculus have been reported (99,94,84,100).

Studies on thalamic connectivity have identified widespread hyper-connectivity between the thalamus (including prefrontal, motor, temporal, and posterior parietal regions) and the cerebral cortex (101–103). Functional connectivity analyses indicate that this hyper-connectivity leads to decreased variance (flexibility) in these connections, correlating with deficits in social motivation and social interaction in individuals with ASD (104,105). Additionally, impairments in social cognitive tasks, such as face-name associations, are linked to these connectivity patterns (106).

Similarly, hyper-connectivity has been observed in the striatal networks of individuals with ASD (107,108). This connectivity pattern reflects an initial phase of overgrowth

followed by a subsequent decline in volume, mirroring trajectories seen in gray matter development in ASD (109).

1.2.5 Sex differences

Most of the knowledge about autism comes from observations of males, as ASD is more prevalent in males. The male-to-female ASD ratio is estimated to range between 8:1 and 2:1 (110,111). Even after accounting for under- and misdiagnosis, as well as camouflaging in females, the ratio remains at approximately 3:1 (112). This difference may be explained by the hyper-masculinized brain theory.

Autistic individuals exhibit a masculinized shift in scores on two key sexually dimorphic psychological traits: empathy and systemizing (113). There are regions in the brain where size and function depend on exposure to sex steroids. Prenatal estrogens can dysregulate many aspects of brain development in areas that are not restricted to sexual differentiation (114). Excessive exposure to prenatal androgens results in the "masculinization" of biological females, while an absence of androgens results in the "feminization" of biological males (115,116).

Fetal testosterone levels predict GM volumes in a pattern reflecting more extreme "masculinization," including positive associations in regions linked to mental state inference and negative associations in regions linked to language and emotional processing (117). Moreover, the brain in different sexes presents age-dependent sensitivity to sexual hormones. Age-related patterns of regional GM volumes are generally more linear in males and curvilinear in females (118). Females show U-shaped age patterns in GM development into puberty (119).

In contrast to GM, the development and myelination of WM in females persist into their late 30s (120). Studies generally show that WM integrity is greater in male youth compared to female youth (121). However, evidence suggests that androgens play a significant role in brain development across sexes. These hormones have been linked to pubertal changes in various brain structures, including those associated with the frontoparietal, limbic, ventral attention, default mode, and visual networks. Additionally, androgens influence WM integrity in regions such as the thalamus, precentral gyrus, genu

of the corpus callosum, superior and anterior corona radiata, and superior frontal WM tracts (122).

1.3 Rodent VPA model

1.3.1 Face validity of model

The VPA syndrome and the VPA animal model can only mimic certain aspects of the etiology of autism (123). While not all cases of ASD can be traced to VPA exposure, this exposure may share pathways with other etiological factors leading to the development of the disorder (124). Regarding face validity, human diagnosis of autism is based on three core criteria: (1) qualitatively abnormal social interactions, (2) impairments in communication, and (3) stereotyped and repetitive behavior with restricted interests and resistance to change (125–128).

Animal models have demonstrated that these categories are altered in VPA-treated animals. Social preference decreases in these animals, as evidenced by their reduced inclination to spend time with a conspecific over an object in the three-chamber test (129,13). Additionally, VPA-treated pups exhibit reduced ultrasonic vocalization, indicating impaired communication skills (129,130). Several repetitive behavioral aspects are also observed in the VPA rodent model, including increased repetitive/stereotypic-like movements, elevated self-grooming, digging, jumping, and headshaking (131–133,129). VPA-treated animals also show increased re-entry into previously explored arms in a Y-maze and increased marble-burying, both of which indicate repetitive tendencies (134,135,133).

Rigidity is another observed trait in these animals, as VPA-exposed rodents demonstrate reduced preference for unfamiliar conspecifics in Social Novelty Preference Tests (136). This tendency is also evident in Novel Object Recognition Tests, where VPA-treated animals spend more time exploring familiar objects than novel ones (137,124).

In rodents, the VPA-induced behavioral deficits are consistent with the unbalanced sex ratio observed in human autism, where males are more often affected than females (138,139). VPA-exposed males show more robust social impairments than VPA-exposed females, while females are more likely to exhibit stereotypies and elicit shorter distress-call durations (140,138,141,136,142).

1.3.2 Rodent social behavior

Similar to humans, rodents exhibit significant changes in social interactions during adolescence. Adolescent male rats show a greater preference for social stimuli in conditioned place preference tests compared to adults (143,144). They also place a higher value on peer-directed activities, including play behaviors, which is particularly evident in males deprived of social interactions (145). This underscores the critical role of social interactions during this developmental stage.

All mammals exhibit some degree of social behavior, but the extent of sociality varies widely across species. While social behavior involves costs such as increased disease transmission and competition for resources, it also offers significant benefits, including enhanced predator detection, defense, and, in some species, cooperative breeding (146). These benefits can drive the evolution of sociality, emphasizing its adaptive value.

For rodents, social interactions during adolescence are particularly important for their social development. Disruptions in these interactions can lead to adverse social and emotional outcomes in adulthood. Therefore, forming social connections during early development is crucial for their proper growth, highlighting the similarities between rodents and humans in the importance of adolescent social experiences(147).

Several studies have established that the so-called "social behavior network" (SBN) functions as an integrated circuit in regulating aggressive behavior (148). As shown in Figure 1, the core nodes of the SBN are involved in regulating multiple forms of social behavior, are reciprocally connected, and contain sex steroid hormone receptors. The nodes that make up this network include the lateral septum (LS), preoptic area (POA), ventromedial hypothalamus (VMH), anterior hypothalamus (AH), periaqueductal gray/central gray (PAG), medial amygdala (meAMY), and bed nucleus of the stria terminalis (BNST). Each of these brain regions has been shown to be important in regulating both reproductive and aggressive behavior in mammals(149).

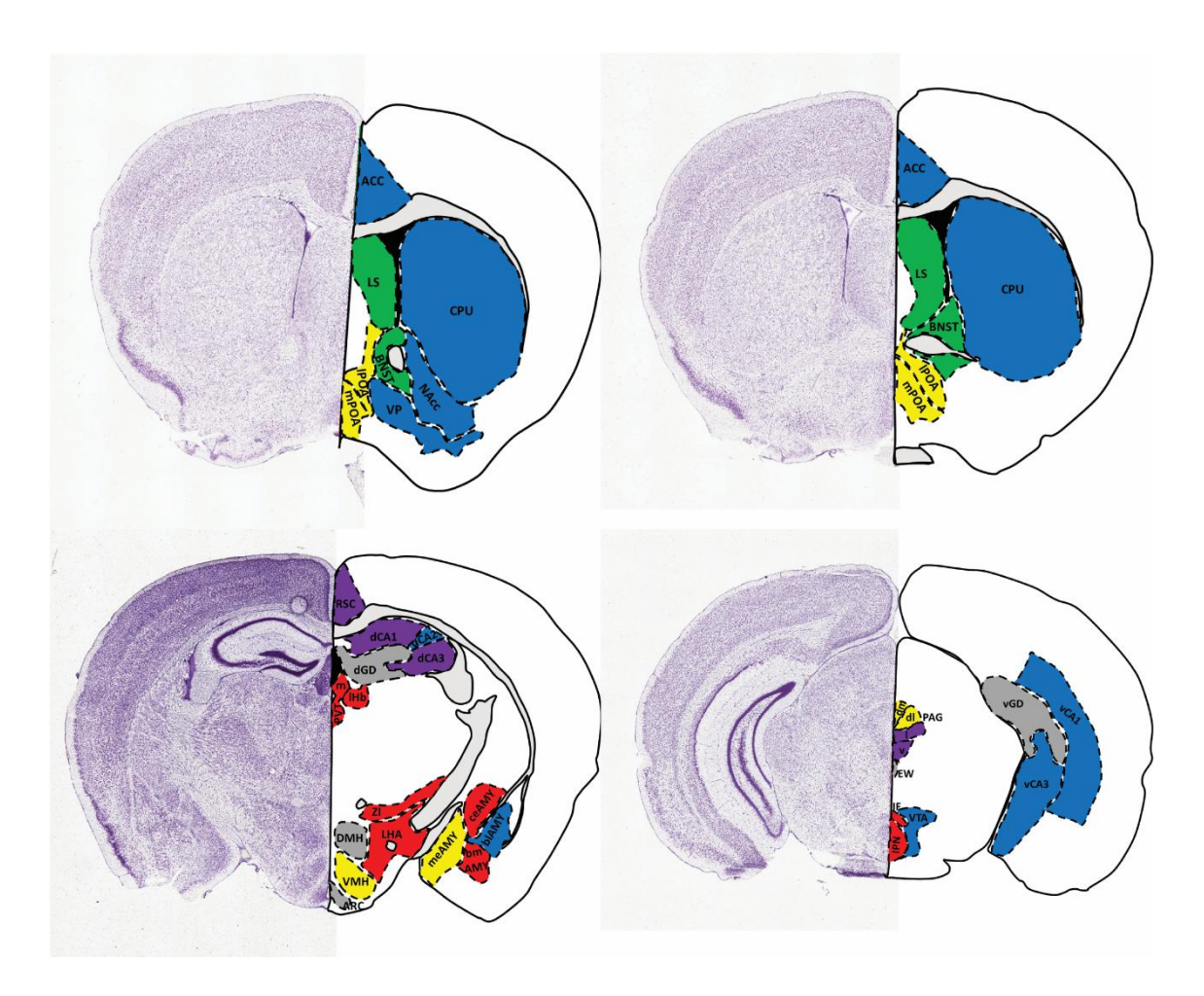


Figure 1: The examined nuclei following the concept of the Social Decision-Making Network created by O'Connell and Hoffman (149). The blue color represents the nuclei of the Mesolimbic Reward System (MRS), the yellow nuclei represent the Social Behavioral Network (SBN), and the green nuclei belong to both the MRS and the SBN. The red-labeled nuclei are those involved in stress regulation in social contexts associated with the habenulopeduncular axis. The purple areas are those found to show differences in the autistic brain but cannot be attached to the previously mentioned systems. Grey color represents the nuclei that served as control regions, as they do not play a role in the regulation of behavior nor were differences found in them in autism (150).

For example, hypothalamic stimulation elicits a stronger aggressive response when SBN nodes located in the forebrain (e.g., the BNST, LS, and meAMY) are activated simultaneously (151). Similarly, the PAG is another node of the SBN that regulates aggressive behavior in concert with the remainder of the circuit (152,153). In general, regions of the SBN form an interactive network, and a single node can mediate many behaviors, such as various forms of aggression (154–157). For instance, the POA mediates male—male aggression (158), male sexual behavior (159,160), and maternal care (161,162).

Besides sex-derived behaviors, animals must evaluate the relative importance and implications of environmental stimuli to generate the appropriate behavioral response. Many studies indicate that the "mesolimbic reward system" (MRS) is the neural network where the salience of such stimuli is evaluated (163,164). The dopaminergic pathway most involved in reward is the mesolimbic system, formed by projections of midbrain dopamine neurons from the ventral tegmental area (VTA) to the nucleus accumbens (NAcc). The conventional reward system also includes the basolateral amygdala (blAMY), LS, ventral pallidum (VP), caudate putamen (CPU), hippocampus (HIP), and BNST (165). Given the ancient nature of the functional contexts in which animals behave (i.e., mate choice, male-male aggression, foraging, etc.), it is reasonable to hypothesize that the mesolimbic dopamine system plays a conserved role in reinforcing these behaviors in vertebrates (149).

The LS and BNST form the junction between the two networks. Both regions play a role in social behavior and reward processing, making them well-positioned to serve as relay stations that mediate information about the salience of social stimuli into adaptive behavioral outputs, such as aggression toward an intruder or sexual behavior toward a potential mate. These regions form the so-called social decision-making network (SDMN), which appears to be involved in regulating many social and, more broadly, reward-related behaviors (149).

The SDMN model primarily describes the regulation of reciprocal social behavior, with notable modulation by an animal's stress levels, which significantly influence behavioral outcomes (166). The habenulo-interpeduncular (mHb-IPN) pathway is particularly involved in both addiction to multiple drugs of abuse and mood-associated conditions,

serving as a junction for signaling underlying both sets of conditions (167). Specifically, the mHb-IPN circuit has been implicated in mood-related conditions (168).

Lesions in projections from the bed nucleus of the anterior commissure, which terminate in the dorsal subnucleus of the medial habenula (mHb), disrupt fear-associated behavior. Conversely, lesions in projections from the triangular septum, which terminate in the ventral subnucleus of the mHb, disrupt anxiety-associated behavior (169). Additionally, studies have implicated the interpeduncular nucleus (IPN) in regulating anxiety and fear, with early research identifying a role for the IPN in the retention of avoidance conditioning (167,170).

The mHb receives projections from several nodes of the SDMN, including the POA, LS, and NAcc. Similarly, the lateral habenula (lHb) receives inputs from the SDMN, including the meAMY, VP, and BNST (171). The lHb also acts on SDMN nodes, including the VTA and PAG, via the rostromedial tegmental nucleus (172,173). The mHb sends its densest efferent projections to the mesencephalic IPN through the core of the fasciculus retroflexus (174), which, in turn, sends efferents to a variety of mid- and hindbrain structures implicated in regulating affective states. These structures include the hippocampus, lateral hypothalamus, VTA, septum, and POA (167,175–177).

Different habenular subnuclei selectively regulate various states of social behaviors. The mHb-IPN pathway modulates experience-dependent behavioral responses, such as anxiety, toward social threats (178).

2 Objectives

This study investigates behavioral differences between normally developing CTR and VPA-treated mice during social reinstatement with familiar animals following one day of social separation. The goal is to identify nuclei that activate in parallel with these behavioral changes, providing insight into the neural basis of altered social behavior.

Differences in nuclear activation across various social environments (social separation, social reinstatement, and normal social conditions) are examined to determine how VPA treatment modulates these patterns. The study explores whether social behavior can be interpreted through the activity of nuclei within the Social Decision-Making Network (SDMN).

Network-level analyses focus on identifying differences in the organization of activated regions between VPA-treated and normally developing CTR mice, with attention to potential shifts in functional connectivity and changes in regulatory hubs.

Functional connectivity alterations resulting from embryonic VPA treatment are assessed, with emphasis on a priori identified networks and pathways. Core networks and hub regions are identified a posteriori through data-driven analysis.

The study also aims to identify genes expressed during VPA treatment that influence tract morphology development, comparing them to genes expressed at other developmental stages.

3 Materials and methods

3.1 Animals and housing conditions

Young adolescent C57BL/6 mice were used for this study. The animals were maintained on a 12:12 light cycle, and food was provided ad libitum. For breeding, two female mice were housed together in a single cage, and a male mouse was introduced to the cage for 24 hours for timed mating. The weights of the dams were monitored throughout the experiment.

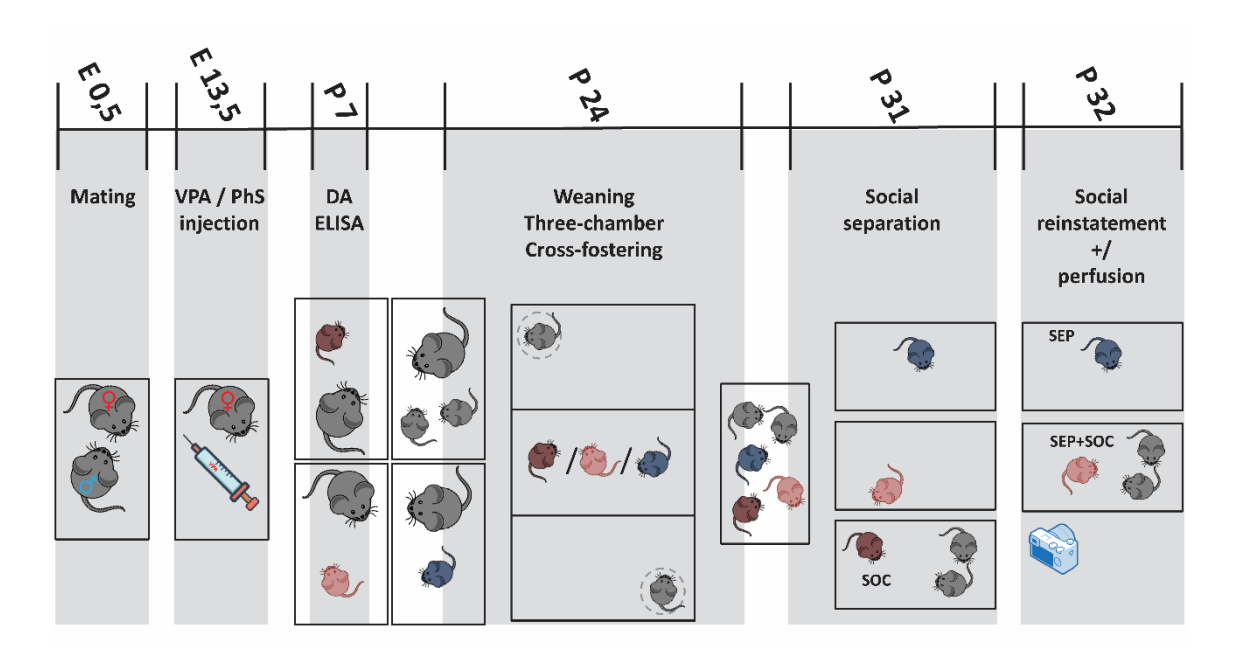


Figure 2: Experimental design. The grey boxes represent the events of one day. The mating of the parent animals was considered embryonic day 0.5 (E0.5). 500 mg/bwkg VPA or physiological saline (PhS) injection was administered to the dam on E13.5. The pups were kept with their dam until postnatal day 24 (P24). On P7, the sex of the pups was validated, and some animals from the litters were taken for the Dopamine Enzyme-Linked Immunosorbent Assay (DA ELISA). On P24, directly after weaning, the animals were tested for sociability using the three-chamber. After the testing groups of five were formed, ensuring that group members were not from the same litter. On P31, two animals were separated from the group (Sep, Sep+Soc) while one stayed with the groupmates (Soc). On P32, one of the separated animals was reintroduced to the cagemates (Sep+Soc), while the other remained alone (Sep).

Animals that had gained more than 2 grams by the 13.5th gestational day were injected subcutaneously with either VPA (Depakine® (400 mg/4 mL injection) at 500 mg/bwkg, 100 mg/mL) or with a volume-matching physiological saline injection.

The first cohort, which was used for DA ELISA, was separated from the dam and sacrificed at P7. The sex of the pups was identified immediately before dissection. A total of 23 pups were used in this experiment ($n_{CTR-female} = 5$, $n_{CTR-male} = 5$, $n_{VPA-female} = 6$, $n_{VPA-male} = 7$) (Figure 2).

The pups in the second cohort were kept with their dam until the 24th postnatal day. For this experiment, only male pups were used (n total = 41, $n_{CTR-Soc} = 7$, $n_{VPA-Soc} = 5$, $n_{CTR-Sep+Soc} = 8$, $n_{VPA-Sep+Soc} = 9$, $n_{CTR-Sep} = 7$, $n_{VPA-Sep} = 5$).

The animal study was approved by the Food Chain Safety and Animal Health Directorate of the Government Office for Pest County, Hungary (XIV-I-001-2269-4/2012; PE/EA/926-7/2020).

3.2 Experimental design

3.2.1 Dopamine assay

3.2.1.1 Sample preparation

The P7 mice of the first cohort were decapitated, and their brains were removed, placed in ice-cold saline, and then cut into coronal slabs using a brain matrix (Stoelting Co., USA). Two slabs, each 2 mm thick, were obtained from the appropriate coordinates. These slabs were placed on a black aluminum box containing ice, and the regions of interest were dissected from both sides under a stereomicroscope (Figure 3). The first, more rostral slab was centered on the NAcc, also including parts of the olfactory tubercle (TO), substantia innominata, LS, the nucleus of the diagonal band, and the bed nucleus of stria terminalis. The second, more caudal slab was centered on the dorsal CPU, also including a part of the globus pallidus. The dissected brain specimens (with the combined bilateral samples counted as one) were immediately placed into pre-weighed plastic vials, weighed, sealed, and stored at -80° C until further processing.

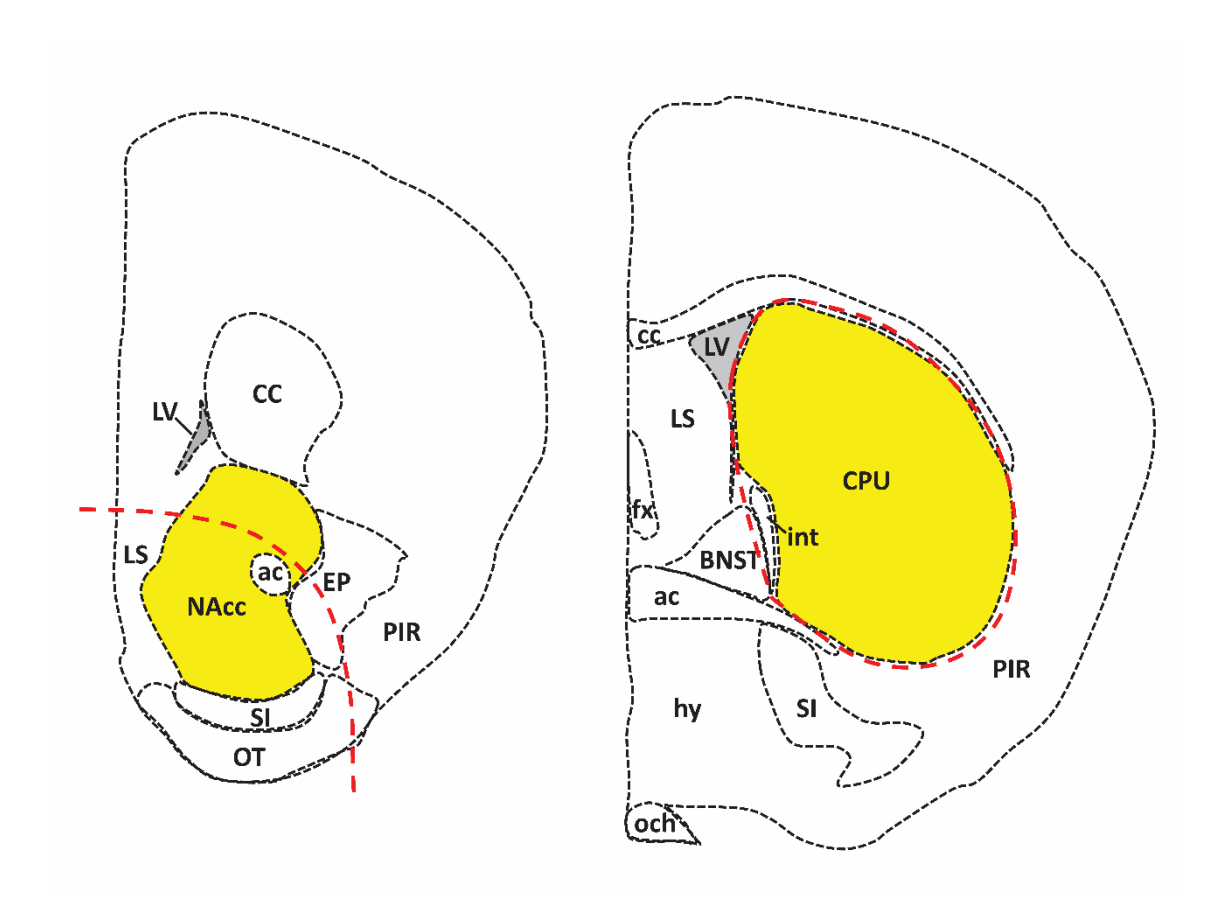


Figure 3: Slices used for the sample preparation for the DA ELISA assay. The red line represents the cutting line, while the yellow-filled areas are the regions of interest (ROI). A indicates the dissected area for NAcc DA content measurement, which also includes the substantia innominata (SI), the olfactory tubercule (OT), and part of the LS. B represents the slice from which the CPU sample was taken (179).

3.2.1.2 DA ELISA assay

For the quantitative measurement of tissue DA levels, the universal DA ELISA Kit by BioVision (#K4219-100) was used. The protocol recommended by the manufacturer was followed with minor modifications. The primary dilution of the tissue samples was set to 18 ml/g wet weight (instead of 9 ml/g) to obtain sufficient homogenate for duplicate measurements. This dilution was accounted for in the final calculation of results. The brain samples were homogenized in ice-cold PBS (0.01 M, pH = 7.4) by rapid sonication. Halt (protease inhibitor, Thermo Fisher, 1:100) and EDTA (Thermo Fisher, 1:100) were added to the PBS. The homogenates were then centrifuged at $5000 \times g$ for 5 minutes at 4° C, and the supernatants were recovered. From these, duplicate samples (2 × 50 μ l) were

transferred onto the ELISA plate. Based on preliminary experiments, the standard calibration curve was adjusted by preparing and measuring two additional intermediate dilutions (5 μ g/ml and 2 μ g/ml) compared to the recommended protocol, and the highest standard concentration was reduced from 100 ng/ml to 25 ng/ml, in order to better match the expected lower concentration range of the samples. Optical density was read using a Bio-Rad iMark Microplate reader at 450 nm. The protein concentration of the supernatant fraction of the brain homogenates was determined using the BCA method (180). Since the protein concentration values proved to be highly uniform (owing to the adjustment of the primary dilutions to the wet weight of the tissue), giving a mean \pm SEM value of 6992.261 \pm 70.809 μ g/ml, the measured DA data were not standardized with the protein values.

3.2.2 Three-chamber sociability test

On the day of weaning (Figure 2) for the second cohort, the "three-chamber" social preference and social memory tests were conducted on the pups. The experimental setup consisted of three Plexiglass boxes (19×45 cm) connected by doors measuring 10×7.5 cm (Figure 2). In the initial session of the test, the animals were placed alone in the device for 5 minutes to habituate to their surroundings. Each of the two side chambers were equipped with an empty 7.5×7.5 cm metal cage, which later housed the unfamiliar mice (181).

In the second session (Social Preference), a non-VPA-treated, age-matched mouse was placed in the cage in one of the terminal boxes (randomly chosen), while the other chamber remained empty. During this session, the test mice spent a total of 10 minutes in the device. However, analysis revealed that the mice only spent an average of 5 minutes actively exploring. Therefore, only the data from the first 5 minutes were analyzed for statistical purposes.

In the third session (Social Memory), another unfamiliar, age-matched, non-VPA-treated mouse was introduced, and the test mouse spent an additional 10 minutes in the device (with 5 minutes used for statistical analysis) to assess social memory.

Video recordings were made for all three sessions, which were subsequently analyzed.

After the three-chamber test, the animals were placed in new home cages into groups of five. Care was taken to ensure that the animals in each group were not closely related and that each group consisted of a mix of VPA-treated (2 or 3) and CTR individuals. This approach was intended to provide similar social conditions for animals originating from different cages and treatment groups. The animals remained undisturbed under these conditions for the next week.

On the 31st postnatal day, the groups were disbanded. One mouse from each group was randomly selected and separated individually for 24 hours from the group (Sep group). Another 3 mice were placed into a new home cage together for the next 24 hours (Soc group).

Another animal was kept alone in its home cage to avoid the effects of a new environment. After 24 hours two of the familiar groupmates were reintroduced to the cage for social stimulation (Sep+Soc group). The first 10 minutes of the reinstatement were video recorded and analyzed for behavioral data. The Sep+Soc animals spent 1.5 hours under these conditions before being anesthetized and perfused. All of the animals spent 2 hours deprived from food and water before they were anesthetized using isoflurane (Forane®) and perfused with 20 ml of physiological saline followed by 20 ml of 4% paraformaldehyde (PFA).

3.2.3 Immunhistochemistry

3.2.3.1 *Sample preparation*

The brains were stored in 4% PFA for one week at 4°C. One day before sectioning, the samples were transferred to 25% sucrose diluted in 0.01M phosphate-buffered saline (PBS). Fifty-micrometer slices were collected using a freezing microtome (Leica). The appropriate sectional planes for immunohistochemistry were selected based on the Allen Brain Atlas(182).

The slides were rinsed in PBS, and endogenous peroxidase activity was blocked using PBS with 2% H₂O₂. The slices were then blocked for 1 hour in a solution of PBS with 1% normal goat serum and 0.2% Tween-20. Following this, the slices were incubated with an anti-c-Fos antibody (1:5000, Abcam, ab190289) in a solution containing 1%

normal goat serum and 0.02% Tween-20 for 1 hour at room temperature, and then overnight at 4°C.

The following day, the slices were incubated for two hours at room temperature in a secondary solution (1:200, Biotinylated IgG, Vector Laboratories). They were subsequently incubated overnight at 4°C in an avidin-biotin solution (1:500, ELITE ABC kit, Vector Laboratories) containing 0.01% Tween-20. The next day, the samples were rinsed in PBS and then in Tris buffer (pH = 8.0). The samples were then incubated in a 3,3'-Diaminobenzidine + nickel chloride (NiDAB) solution (0.15 mg/ml DAB + 4.25 mg/ml Ammonium nickel sulfate Hexahydrate).

3.2.3.2 *Image acquisition*

Images of the entire brain areas were captured using a Nikon Eclipse E800 microscope with 4X magnification.

3.2.3.3 *ROI*

We focused on socially relevant brain regions based on the Social Decision-Making Network (SDMN) framework proposed by O'Connell and Hofmann (149). The network was modified in several aspects, with each alteration supported by recent literature. For instance, the Decision-Making Network was expanded to include the ACC, given its wellestablished role in social cognition, emotional regulation, and decision-making (183). Additionally, certain regions were divided into subregions to reflect functional specialization: the POA was separated into lateral and medial subdivisions, with the lateral POA associated with reward-driven motivation (184) and the medial POA implicated in parental and aggression-related behaviors (185,186). Within the PAG, we selectively included the dorsomedial (dmPAG) and dorsolateral (dlPAG) columns known to mediate social defensive behaviors (187,188) — while excluding lateral and ventral columns primarily involved in non-social defensive responses (189,190). Moreover, a third subnetwork, focusing on social stress processing, was integrated, incorporating nuclei such as the IF, LHA, and meAMY, based on their established roles in stress-reactivity and social challenge processing (191–193). Finally, regions implicated in ASD but not traditionally categorized within the SDMN, such as the RSC, were

included due to emerging evidence linking them to social salience and cognitive dysfunctions in ASD (194–196) (Figure 4).

3.2.3.4 *Cell counting*

For every brain region one representative coronal section from the same rostrocaudal coordinate was carefully selected based on anatomical landmarks to count the number of c-Fos nuclei. To quantify the positive signals, a semi-automatic method in ImageJ was utilized. The procedure included using the "Find Edges" plugin for background subtraction, applying a "Gaussian Blur" filter, and then separating overlapping signals using the "Watershed" function. The "Triangle" method was employed for thresholding, and the counting of thresholded signals was conducted using the "Analyze Particles" function. The areas of ROI-s were also measured.

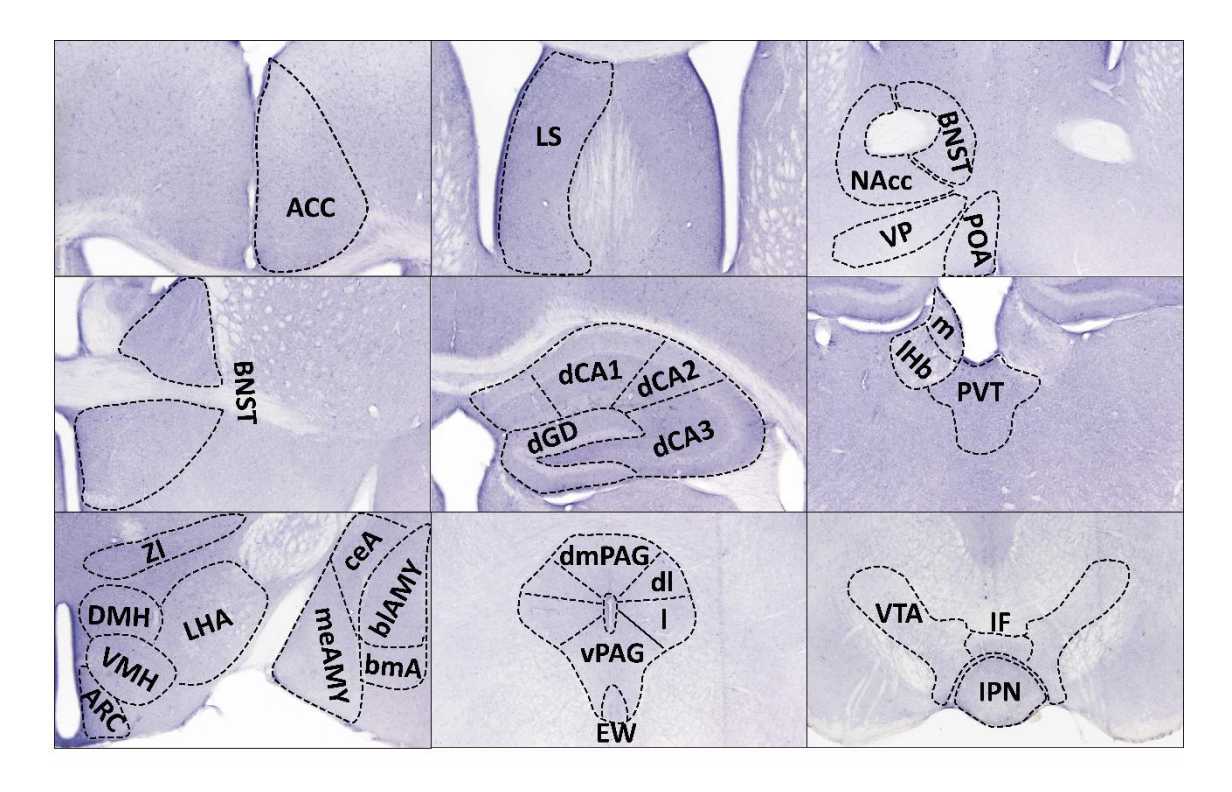


Figure 4: Regions analysed for the immediate early gene activation. Dashed lines indicate the outline of the ROI where c-Fos values were measured. To compare c-Fos activity, the raw number of positive nuclei was used, with the dashed area values (mm²) used for correction as an offset variable.

3.2.4 Behavioral analysis

The videos captured during the Three-chamber test and the social reinstatement phase were analyzed using Solomon Coder (197). For the Three-chamber test, the parameters measured included the time spent in the peripheral two chambers and the middle chamber over a five-minute period.

During the social reinstatement phase, various behaviors were measured, including:

- Anogenital sniffing: The animal's nose is brought close to the other animal's anal area.
- Following: The test subject follows another moving animal at a distance of a few centimeters.
- Allogrooming: The animal engages in grooming behaviors with its familiar companions.
- Self-grooming: The animal cleans itself.
- Fighting: Aggressive, fast rolling-over behaviors are exhibited by two animals.
- Running away: The mouse rapidly flees from another approaching animal.
- Exploration: The animal actively examines the cage, separate from other animals.

3.3 Statystical analysis

3.3.1 Comparisons

The statistical analysis was performed using R.

For the analysis of the ELISA results, none of the data transformations met the preconditions of the linear model. To address this issue, a non-parametric repeated sampling test (198) was applied to the untransformed data.

To assess the time spent in different chambers during the three-chamber test, a linear mixed model was employed using the formula: "Time spent in chamber ~ Embryonic treatment * Chamber + random effect (Dam ID)". This model was applied to analyze the time each subject spent in different chambers during the sociability test. The fixed effects included Embryonic treatment (VPA-exposed vs. control) and Chamber (empty/unfamiliar animal/familiar animal), with their interaction (Embryonic treatment * Chamber) testing whether the preference for a chamber depended on the prenatal

treatment. Additionally, we included a random effect for Litter/test subject's ID to account for potential similarities among pups from the same litter due to shared genetics or prenatal environment. The time values for the middle chamber were excluded from this test. To evaluate potential differences in locomotion, the number of entries into the peripheral chambers was also compared. Pairwise comparisons were conducted using the Tukey method from the lmerTest library.

To compare the laterality of brain areas, the density values of the left and right sides were compared using a generalized linear model. The ID of the animal and the ID of the dam were included as random factors in the model.

To identify nuclei activated either by social isolation or by social stimulation within the treatment groups their cell density was compared to the average values of the saline treated group kept in standard social environment (Soc group). Subsequently, a one-sample t-test was employed to compare the density of each nucleus. To compare the number of c-Fos positive cells between VPA-treated and control groups under different social conditions, a negative binomial regression model with a log link function was applied using the following formula:

c-Fos positive cell number ~ Embryonic treatment * Social state + random effect (Dam ID/test subject) + offset(log(Area of nucleus)).

This model was specifically designed to examine whether c-Fos expression varied depending on both prenatal VPA exposure and the social state experienced by the test subjects. In this framework, embryonic treatment (VPA-treated vs. control) and social state (Soc/Sep/Sep+Soc) were treated as fixed effects, and their interaction term allowed us to assess whether the effect of social state on c-Fos expression differed between treatment groups. To account for dependencies within the data, random effects were incorporated. The Dam ID was used to control for shared genetic and prenatal environmental factors among littermates, while the subject ID accounted for repeated measurements within individuals (specifically, bilateral sampling from the left and right hemispheres). An offset term was added by including the logarithm of the area of the nucleus analyzed. This normalization ensured that the number of c-Fos positive cells was adjusted for the size of the brain region, preventing potential biases arising from

differences in region size across samples. This modeling approach enabled a robust evaluation of how prenatal VPA exposure and social conditions influenced neuronal activation, while appropriately addressing biological clustering and technical variation. For model diagnosis, Wald tests were used, and when the p-value was less than 0.1, pairwise comparisons were performed. Contrasts were calculated separately for individual brain nuclei. In cases where the p-value ranged between 0.05 and 0.1, Cohen's D values were calculated using the effsize library, and comparisons with an effect size value greater than 0.8 were separately visualized (199). Due to the large number of measured areas, p-values from the regressions underwent false discovery rate (FDR) analysis using the Holm-Bonferroni method, with the threshold value set to 0.05.

For the comparison of behavioral data between VPA-treated and control animals within each behavior type, two-sample t-tests were employed.

3.3.2 Network analysis

Our approach, combining c-Fos-based functional connectivity mapping with anatomical constraints, is consistent with methodologies previously applied in network-level analyses of immediate early gene expression (200,201).

The density of c-Fos-positive cells for each brain region was calculated by first summing the total c-Fos-positive signals detected across both hemispheres, and across multiple slides when applicable. The total cell count was then divided by the corresponding summed area, yielding the c-Fos density value for each nucleus.

To account for potential lateralization effects, c-Fos densities were initially quantified separately for the left and right hemispheres. Subsequently, hemisphere-specific values were compared using within-subject statistical analyses. Since no significant interhemispheric differences were detected in the CTR group, left and right hemisphere values were averaged for each nucleus prior to subsequent analyses.

To characterize functional relationships between brain regions, all possible pairwise Pearson correlation coefficients were computed within each experimental group, based on the regional c-Fos density values. The resulting matrices contained both the p-values and the coefficient of determination (R²) for each regional pair. R²-values, ranging between -1 and 1, quantify the proportion of variance shared between two regions, thereby

serving as a proxy for functional co-activation. These R² matrices were visualized as heatmaps using the heatmaply R package (202).

3.3.3 Network construction

To enhance biological relevance and reduce the probability of spurious functional connections, only correlations corresponding to known anatomical connections — as identified in the Allen Mouse Brain Connectivity Atlas (203) (Figure 5) — were retained for subsequent network analysis. This anatomical filtering ensured that observed correlations likely reflected direct or monosynaptic communication rather than co-activation due to shared upstream inputs.

Subsequently, further thresholding was applied according to two criteria: Only correlations with p-values lower than 0.05 were considered significant, and correlations with absolute R²-values greater than 0.7 were considered strong enough to infer functional connectivity.

The remaining connections were visualized as undirected graphs using the igraph R package (204). In these visualizations, edges between nodes (brain regions) represented significant, strong functional links. The width of each edge was proportional to the R²-value, and edge colors reflected the directionality (black: positive correlation; red: negative correlation (Figure 12)).

3.3.3.1 *Centrality measures*

To quantify the functional importance of individual brain regions within the network, two complementary centrality metrics were computed using the same package (204,205). Degree centrality reflects the number of direct connections a node maintains. High degree centrality suggests that a region is functionally well-integrated and interacts extensively with other nodes in the network. In contrast, betweenness centrality measures how often a node lies on the shortest path between other nodes(206,207). A high betweenness assesses the extent to which a node lies on the shortest paths between pairs of other nodes. It is defined as:

$$B(v) = \sum_{u \neq v \neq w} \frac{\sigma_{uw}(v)}{\sigma_{uw}}$$

where:

 σ_{uw} : number of shortest paths between nodes u and w

 $\sigma_{uw}(v)$: number of those paths that go through node v

A high betweenness score indicates that a node plays a key relay role, serving as a functional bridge between otherwise disconnected parts of the network.

Both centrality metrics were computed for each region in both experimental groups, and visualized to facilitate comparison. To identify functionally important "hubs", a stringent dual-threshold criterion was applied: regions exceeding the 80th percentile in both degree and betweenness centrality were classified as network hubs. This conservative approach ensured that selected hub regions were not only highly connected, but also strategically positioned to coordinate information flow between modules within the network. (201).

3.3.3.2 Cluster analysis

In addition to topology assessments based on centrality measures, a clustering analysis was performed to identify tightly interconnected groups of brain regions (modules) within the functional networks. Clustering was conducted using the Markov Cluster Algorithm (MCL), an unsupervised method designed to detect highly connected communities within complex networks (201,208). The MCL algorithm simulates random walks on the network graph, leveraging the intuition that more random walks will occur within densely connected subgraphs (clusters) than between them(208). For the statistical evaluation of variations in connectivity strength within specific subnetworks, an analysis of variance (ANOVA) model was employed, complemented by pairwise Tukey comparisons. The investigation encompassed the examination of R² values, comparing the overall networks with those specific to subnetworks.

3.3.3.3 *Validation of network analyses*

To validate whether the observed modular structures and network properties were significantly different from random expectations, a control analysis was conducted using randomly generated networks. A total of 1000 random networks were created, each consisting of 10 brain regions randomly sampled from the complete set of 36 regions. For each random network, functional connectivity matrices were constructed and analyzed

identically to the experimental data, generating distributions of network metrics such as mean degree, mean betweenness, and modularity. The properties of the experimental subnetworks were then statistically compared against these random distributions.

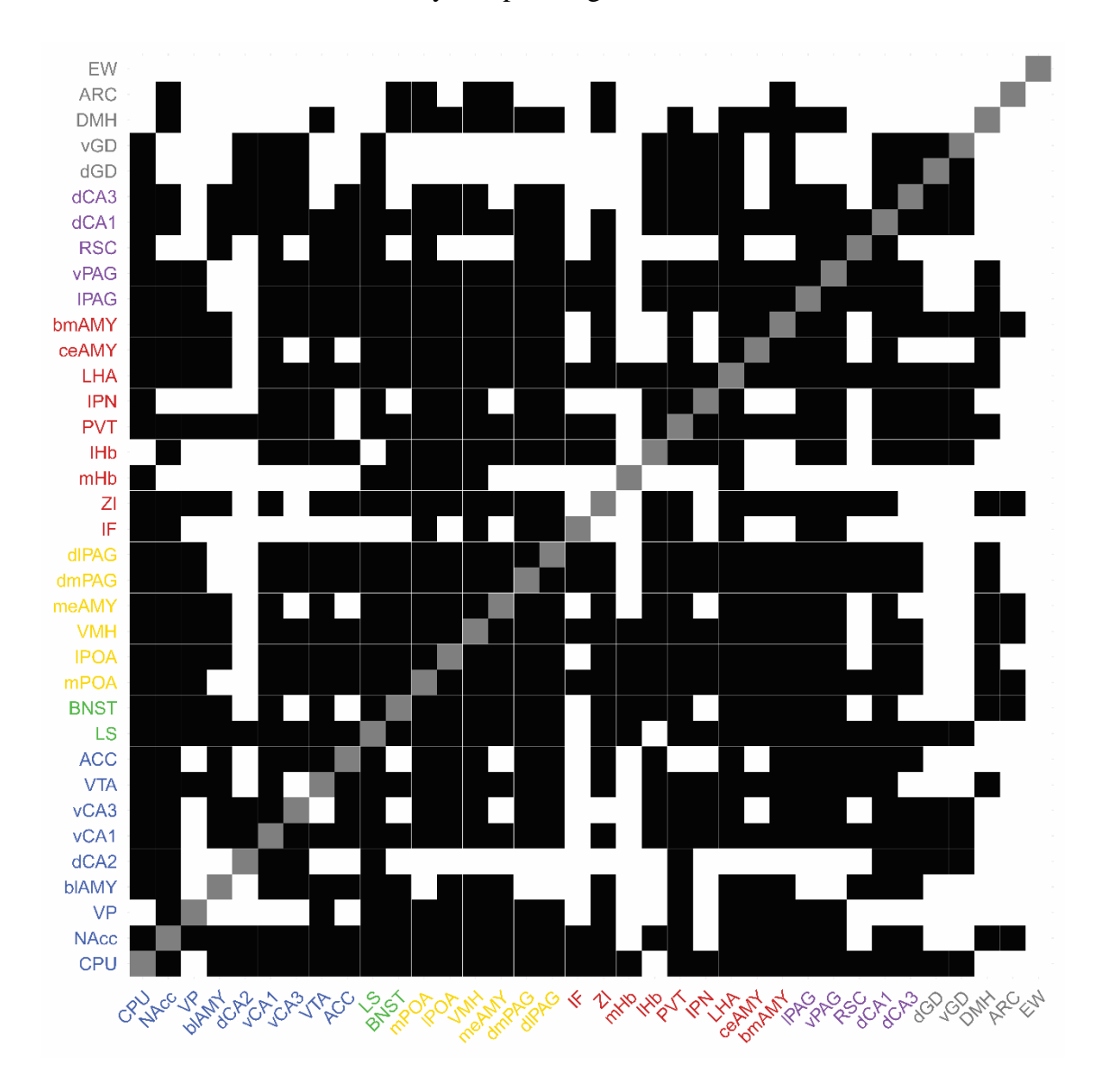


Figure 5: Matrix of the anatomical connectome used to threshold the correlational matrices. The matrix was constructed using projectional data from the Allen Mouse Brain Connectivity Atlas (209). Black squares represent the projectional connections between areas, while white squares indicate the absence of direct connections. Blue indicates the MRS, green represents the intersection between MRS and SBN, yellow stands for the SBN, red labels the nuclei involved in stress modulation, purple indicates areas where changes were found in autism(195,210–212), and grey represents the control regions.

3.3.4 Behavioral correlations

The previously utilized c-Fos density data were subjected to correlation analysis using Pearson's correlation to examine their relationship with the duration of various behaviors observed during social reinstatement. Only correlations with p-values below 0.05 were considered statistically significant. The correlations were color-coded: black for positive correlations and red for negative correlations. The GGally package was employed for visualizing these correlations (213).

3.4 Identifying of potentially affected neurodevelopmental genes (gene library analysis)

To investigate the genes active during the critical window of VPA administration, the Allen Developing Mouse Brain Atlas (214) was utilized. Genes overexpressed in the midbrain, diencephalon, and telencephalic vesicle at E13.5 were identified using the Temporal Search feature. Since VPA administration is ineffective after E15 (215), genes overexpressed at E15.5 were also collected for comparison. Genes uniquely overexpressed at E13.5 but not at E15.5 were selected for further analysis to elucidate the biological processes in which they are predominantly involved.

The enrichment analysis was performed using MouseMine to identify biological functions significantly overrepresented in the list of differentially expressed genes. Statistical significance was determined using the hypergeometric test, which calculates the probability of observing at least k genes associated with a given category by chance, based on the reference population. This method ensures that identified functional enrichments are unlikely to occur randomly, providing insight into the biological relevance of the observed gene expression patterns. (216).

$$p = \frac{\binom{M}{k} \binom{N-M}{n-k}}{\binom{N}{n}}$$

where N is the total number of objects (e.g., all genes in the reference population), n is the number of genes in the analyzed subset, M is the number of genes in the reference population associated with the category of interest, and k is the number of genes in the subset also associated with that category. Functional enrichment analysis of these genes was performed using the Holm-Bonferroni correction for FDR and ensure statistical significance (217). Additionally, genes exclusively expressed at E15.5 were analyzed to determine their functional roles.

This approach allowed the identification of specific genes and biological pathways responsive to VPA during early embryonic development, offering insights into the molecular mechanisms potentially underlying VPA-induced neurodevelopmental alterations.

4 Results

4.1 DA ELISA

The non-parametric ANOVA model revealed that, for the CPU, there was no significant difference in DA concentration between the CTR and VPA groups, regardless of treatment or the sex of the animals ($F_{(1, 13.343)} = 0.01$, p = 0.923). However, in the NAcc, the DA level was significantly lower in the VPA-treated animals ($F_{(1, 15.543)} = 7.423$, p = 0.015). No interaction between treatment and the sex of the animals was observed (Figure 6). A significant difference in DA levels was found between CTR and VPA males ($F_{(1, 8)} = 7.807$, p = 0.023), while no significant difference was observed in females ($F_{(1, 7.866)} = 1.382$, p = 0.274).

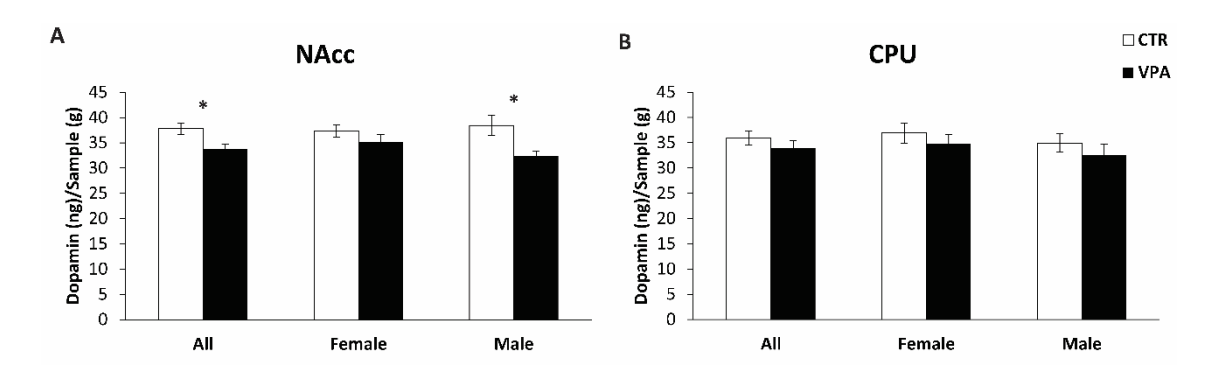


Figure 6: Results of the DA ELISA measurements. Block A represents the DA (ng/g) measured from samples taken from the NAcc. * indicates significant differences in dopamine levels between CTR and VPA-treated animals. Block **B** shows the measured DA values from the samples containing the CPU (179).

4.2 Three-chamber sociability test

4.2.1 Habituation

During the habituation phase of the three-chamber test, no significant differences were observed between VPA-treated and CTR groups in terms of the time spent in any of the chambers (Figure 7/B) ($F_{(1,52)} = 0.879$, p = 0.353). However, paired comparisons of the time spent in different chambers revealed a weak significant difference in the VPA-treated animals ($t_{(26)} = 2.081$, p = 0.047), whereas no such difference was observed in the CTR group ($t_{(26)} = 0.471$, p = 0.642). There was no difference in the number of chamber

entries between the CTR animals and the VPA-treated ones ($F_{(1,7.713)} = 1.2611$, p = 0.2952), indicating no difference in the locomotion of the animals.

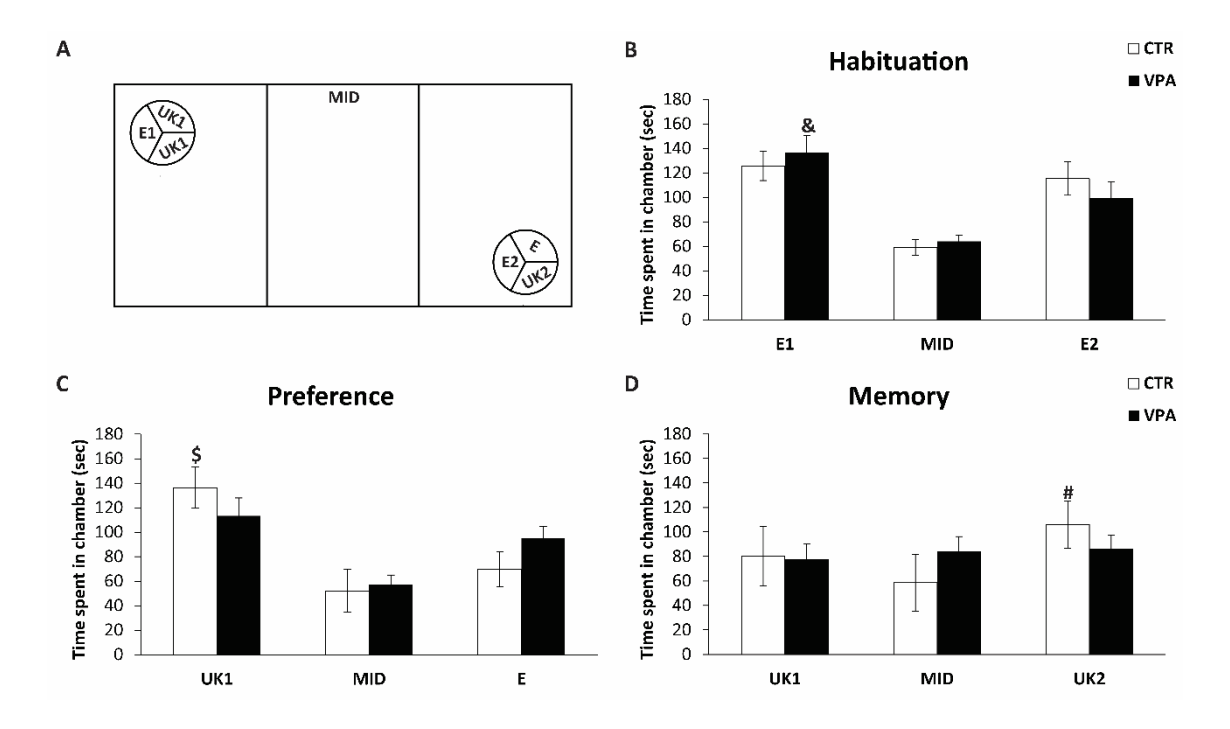


Figure 7: Results of the three-chamber sociability test. Block A shows the experimental design and setup of the test device. Circles indicate the positions of cages containing age-and sex-matched mice unfamililiar to the test subject. The text within the circles represents the content of each cage during different test sessions. "E" stands for empty cage, and "UK" stands for unknown individual. Block B depicts the habituation phase where both cages were empty. In this phase, VPA-treated animals showed a slight side preference (labeled by &). In the social preference phase (Block C), the cage previously labeled E2 remained empty, while an unknown individual (UK1) was placed in E1. During this phase, CTR animals spent more time in the chamber containing the UK animal than in the empty chamber (labeled by \$). Block D represents the social memory phase. The UK1 animal stayed in the same cage as the previous phase, while another unknown animal (UK2) was placed in the previously empty chamber (E). In this phase, CTR animals showed a preference shift, spending more time in the chamber with the UK2 animal compared to the previously empty chamber (E). This preference shift was not observed in VPA-treated animals (difference labeled by #).

4.2.2 Social Preference

In the social preference phase, a significant effect was found in the time spent in different chambers (Figure 7/C) ($F_{(1,52)} = 9.108$, p = 0.004). However, there was no significant interaction between treatment and time spent in the chambers ($F_{(1,52)} = 2.959$, p = 0.091). Pairwise comparison revealed that CTR animals spent more time in the chamber containing unfamiliar mice than in the empty chamber ($t_{(26)} = 3.040$, p = 0.005), while the VPA-treated mice did not show a significant difference in time spent between the chambers ($t_{(26)} = 1.035$, p = 0.310).

4.2.3 Social Memory

In the social memory phase, no significant differences (Figure 7/D) were observed in the time that animals spent in different chambers ($F_{(1,52)} = 1.128$, p = 0.293). However, compared to the social preference phase, the time spent by CTR animals in the chamber ($F_{(1,52)} = 9.078$, p = 0.004), which in this phase contained the novel animal, significantly increased ($t_{(26)} = -3.000$, p = 0.006). In contrast, the VPA-treated animals showed no such preference change; their choice remained random ($t_{(26)} = -1.078$, p = 0.291).

4.3 C-Fos Activity

4.3.1 Laterality

Comparisons of the density values revealed differences in the interaction between VPA treatment and laterality in three areas (central amygdala, cornu ammonis 3 of hipocampus, dorsomedial hypothalamus (DMH)), specifically in the central amygdala (ceAMY) ($\chi^2_{(1,659.113)} = 4.554$, p = 0.033). In VPA-treated animals, the right-sided ceAMY exhibited a higher density ($t_{(38)} = -2.029$, p = 0.050), whereas CTR animals did not show lateralization ($t_{(38.6)} = 0.960$, p = 0.343). No significant differences were observed in the density of other brain areas, therefore we combined the data of the two hemispheres for any further analysis.

4.3.2 Activation pattern

Differences in the activation patterns of the observed 36 nuclei were assessed by comparing the number of c-Fos positive cells, normalized to the region of interest (ROI) area. Among the absolute control animals (saline treated and kept under a standard social

environment), the interfascicular (IF) nucleus was the only one showing significantly higher activation ($t_{(6)} = 2.374$, p = 0.028) compared to the average activation density (14.197 c-Fos positive cells/mm²) (Figure 8).

Significant differences in activation, influenced by embryonic treatment and/or changes in social environment, were observed in several other nuclei during the analysis (Figure 9).

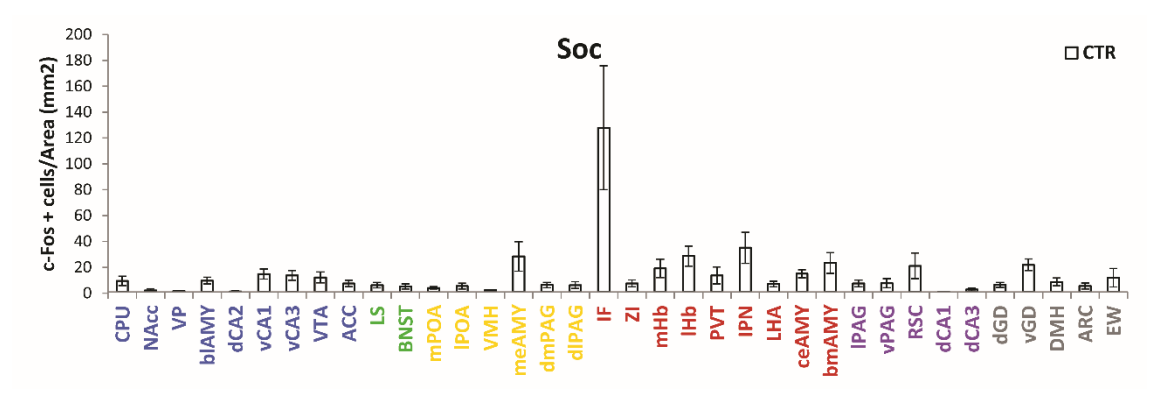


Figure 8: The measured c-Fos positive cell density in 1 mm² in CTR animals kept in an undisturbed social environment. These values were used as baseline values for the subsequent fold change diagrams. The different colors of the area names represent the subnetworks to which the nuclei are assigned. Blue indicates the MRS, green represents the overlap between MRS and SBN, yellow stands for the SBN, red labels the nuclei involved in stress modulation, purple indicates areas where changes were found in autism, and grey represents the control regions.

4.3.2.1 *Decision-Making Network*

The CPU showed no significant difference in activation in the socially consistent environment between the CTR and VPA groups. However, in the socially separated environment (Figure 10), CTR animals exhibited higher c-Fos activity than VPA-treated animals ($\chi^2_{(1,41)} = 6.376$, p = 0.012; $z_{(41)} = 2.525$, p = 0.056, Cohen's d = 1.222).

Following separation, higher activity was observed in the NAcc among VPA-treated animals compared to the consistent social environment ($\chi^2_{(1, 49)} = 3.9523$, p = 0.047; $z_{(49)} = -3.141$, p = 0.009, FDR = 0.043). The NAcc of the separated animals showed higher activation than those kept in a consistent social environment ($\chi^2_{(1, 41)} = 4.948$, p = 0.026).

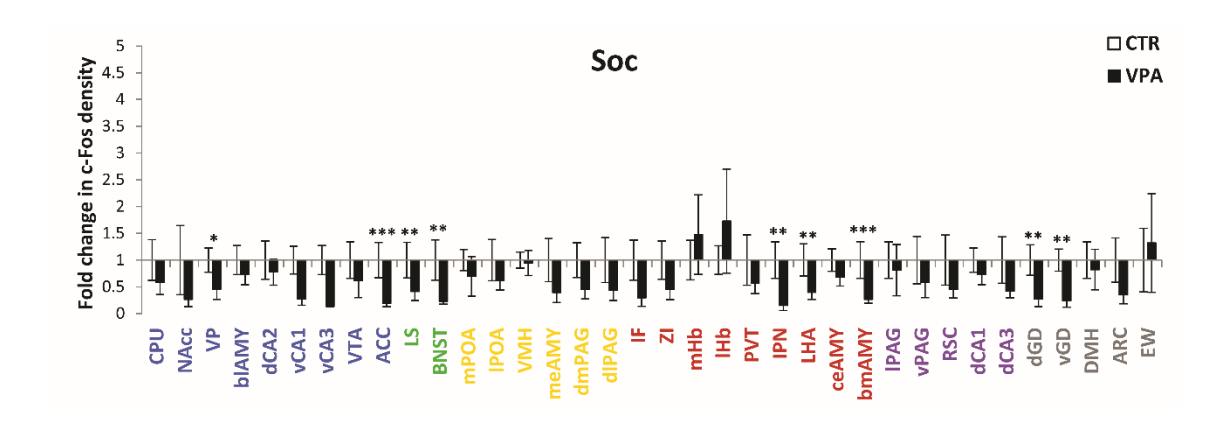


Figure 9: Fold change in the density of c-Fos⁺ cells across brain regions in a constant social environment (Soc group). Bar plots display the relative change compared to the mean c-Fos density of CTR animals maintained in a consistent social environment, as shown in Figure 8. Different colors indicate distinct functional groupings of nuclei: blue marks regions of the MRS, yellow denotes areas of the SBN, and green highlights nuclei involved in both (SDMN). Red indicates stress-responsive regions influencing social behavior, while purple represents autism-related areas not part of either main network. Gray indicates control regions with no known social relevance.

Asterisks denote statistically significant differences between the CTR and VPA-treated groups: a single asterisk (*) indicates a trend-level difference (0.05 accompanied by a Cohen's d greater than 0.8, double asterisks (**) indicate <math>p < 0.05, and triple asterisks (**) represent significance after FDR.

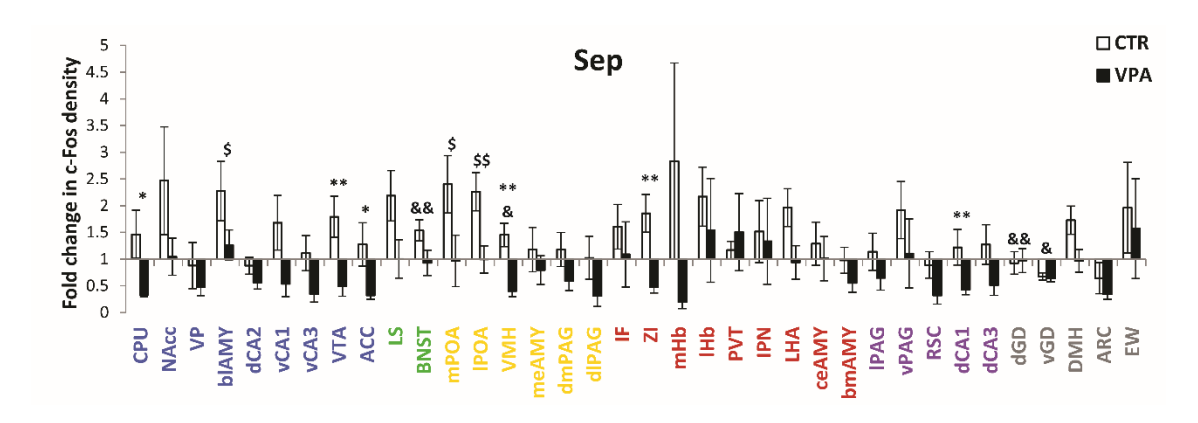


Figure 10:. Fold change in the density of c-Fos⁺ cells across brain regions in animals subjected to social separation (Sep group). All values are expressed relative to the mean c-Fos density of CTR animals maintained in a consistent social environment (Soc group; see Figure 8). Colored labels distinguish functionally relevant brain networks: blue indicates MRS, yellow marks components of the SBN, green represents overlapping nodes of both (SDMN), red includes stress-regulatory nuclei implicated in social modulation, purple shows autism-associated regions not directly related to social behavior, and gray indicates control areas (150).

Differences between CTR and VPA animals under the separation condition are marked by asterisks (*), while deviations from the socially housed control group (Soc, Figure 9) are marked by additional symbols: \$ for CTR animals and \$ for VPA-treated animals. All symbols follow the same three-tiered convention: one symbol indicates a trend-level difference (0.05 < p < 0.1, Cohen's d > 0.8), two symbols denote p < 0.05, and three indicate significance after FDR correction.

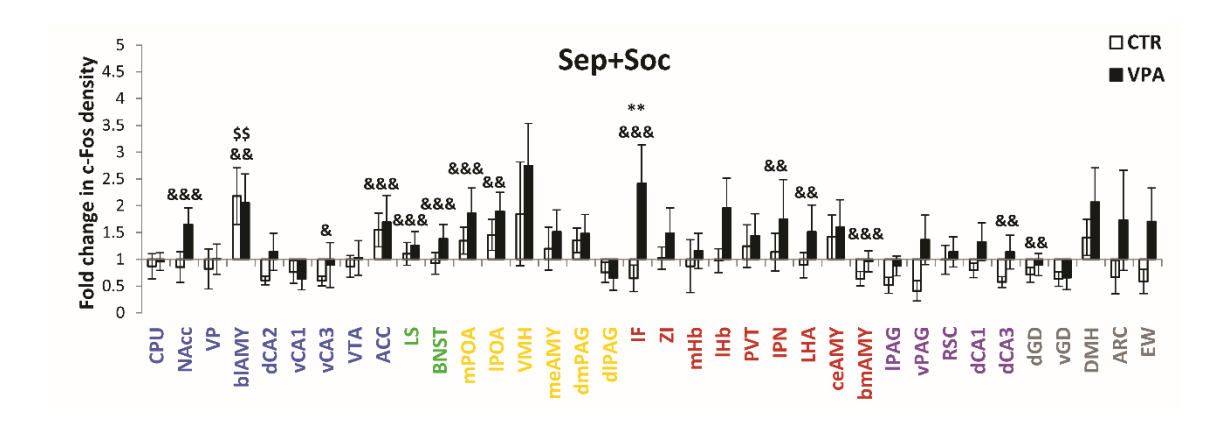


Figure 11:. Fold change in the density of c-Fos⁺ cells across brain regions in animals subjected to social reinstatement (Sep+Soc group). All values are expressed relative to the mean c-Fos density of CTR animals maintained in a consistent social environment (Soc group; see Figure 8). Colored labels distinguish functionally relevant brain networks: blue indicates MRS, yellow marks components of the SBN, green represents overlapping nodes of both (SDMN), red includes stress-regulatory nuclei implicated in social modulation, purple shows autism-associated regions not directly related to social behavior, and gray indicates control areas.

Differences between CTR and VPA animals under the separation condition are marked by asterisks (*), while deviations from the socially housed control group (Soc, Figure 9) are marked by additional symbols: \$ for CTR animals and \$ for VPA-treated animals. All symbols follow the same three-tiered convention: one symbol indicates a trend-level difference (0.05 < p < 0.1, Cohen's d > 0.8), two symbols denote p < 0.05, and three indicate significance after FDR correction.

While CTR animals presented a significant elevation ($z_{(41)} = 2.224$, p = 0.026), the VPA-treated group differed only marginally, though the effect size was high ($z_{(41)} = 1.915$, p = 0.056, Cohen's d = 1.321) (Figures 10, 11).

In the VP, a marginal difference was noted within the social environment between the CTR and VPA groups ($\chi^2_{(1, 48)} = 3.556$, p = 0.059). Notably, VPA-treated animals displayed diminished activity in the VP compared to CTR ($z_{(48)} = 1.736$, p = 0.083). The computed Cohen's d value (Cohen's d = 0.998) underscored a robust effect of VPA treatment (Figure 9).

For the blAMY, social reinstatement led to heightened activity in both CTR (χ^2 _(1, 50) = 4.270, p = 0.039; z₍₅₀₎ = -2.066, p = 0.039) and VPA-treated animals (z₍₅₀₎ = -2.214, p = 0.027). Social separation also resulted in marginally higher activation in the CTR animals due to the social environment (χ^2 _(1, 40) = 5.966, p = 0.015; z₍₄₀₎ = 2.443, p = 0.069, Cohen's d = 1.103) (Figures 10,11).

In the VP, a marginal difference was noted within the social environment between the CTR and VPA groups ($\chi^2_{(1, 48)} = 3.556$, p = 0.059). Notably, VPA-treated animals displayed diminished activity in the VP compared to CTR animals ($z_{(48)} = 1.736$, p = 0.083). The computed Cohen's d value (Cohen's d = 0.998) indicated a robust effect of VPA treatment (Figure 9).

For the blAMY, social reinstatement led to heightened activity in both CTR ($\chi^2_{(1, 50)}$ = 4.270, p = 0.039; $z_{(50)}$ = -2.066, p = 0.039) and VPA-treated animals ($z_{(50)}$ = -2.214, p = 0.027). Social separation also resulted in marginally higher activation in CTR animals due to the social environment ($\chi^2_{(1, 40)}$ = 5.966, p = 0.015; $z_{(40)}$ = 2.443, p = 0.069, Cohen's d = 1.103) (Figures 10, 11).

The ventral cornu ammonis 1 (vCA1) of HIP showed differences between VPA-treated and CTR animals only in the socially separated state ($\chi^2_{(1, 21)} = 4.753$, p = 0.029). In this social environment, CTR animals exhibited higher activity than the VPA-treated group ($z_{(21)} = 2.180$, p = 0.029) (Figure 10).

The ventral CA3 (vCA3) showed significantly weaker activity in VPA-treated animals in the undisturbed social environment compared to CTR animals ($\chi^2_{(1,27)} = 6.506$, p = 0.011; $z_{(27)} = 2.785$, p = 0.028). During reinstatement, vCA3 activity in VPA-treated animals increased compared to the consistent social environment ($z_{(27)} = -1.961$, p = 0.050, Cohen's d = 0.907) (Figures 9, 11).

The ventral VTA showed a difference in activity only when the animals were separated from their cage mates ($\chi^2_{(1, 41)} = 7.148$, p = 0.008). In this case, the nucleus exhibited higher activity in the CTR group than in the VPA-treated group ($z_{(41)} = 2.674$, p = 0.038) (Figure 10).

The ACC activity was significantly lower in VPA-treated animals under the long-term social environment ($\chi^2_{(1, 105)} = 6.872$, p = 0.009; $z_{(105)} = 3.074$, p = 0.011). During reinstatement, this activity significantly increased ($z_{(105)} = -3.468$, p = 0.003). These p-values remained significant after FDR analysis (FDR = 0.034, 0.014). The activity during social separation changed in the opposite direction ($\chi^2_{(1, 88)} = 6.443$, p = 0.011); in that environment, the ACC of the VPA-treated group was less active than in the CTR group ($z_{(88)} = 2.538$, p = 0.011) (Figures 9, 10, 11).

4.3.2.2 Lateral Septum and Bed Nucleus of the Stria Terminalis

The LS and BNST exhibited an identical activation pattern during reinstatement. In the standard social environment, both regions showed lower activity in VPA-treated animals compared to CTR animals (LS: $\chi^2_{(1,49)} = 5.896$, p = 0.015, $z_{(49)} = 2.095$, p = 0.036; BNST: $\chi^2_{(1,105)} = 11.105$, p = 0.001, $z_{(105)} = 2.561$, p = 0.010). Social reinstatement significantly increased activity in VPA-treated mice (LS: $z_{(49)} = -4.339$, p < 0.001; BNST: $z_{(105)} = -4.675$, p < 0.001), while no significant differences were observed in CTR animals. Following FDR correction, these results remained significant (FDR_{LS} = 0.005, FDR_{BNST} = 0.005).

During social separation, the activity of LS significantly elevated in CTR animals ($\chi^2_{(1,41)}$ = 4.452, p = 0.034; $z_{(41)}$ = 2.110, p = 0.035) and marginally in the VPA group ($z_{(41)}$ = 1.716, p = 0.086, Cohen's d = 0.937). Despite the elevation caused by the separation, the basic difference between CTR and VPA groups remained ($z_{(41)}$ = 2.018, p = 0.044) (Figures 9, 10, 11).

In the case of BNST, activity increased in both CTR ($\chi^2_{(1, 85)} = 4.871$, p = 0.027; $z_{(85)} = 2.207$, p = 0.027) and VPA groups ($z_{(85)} = 2.858$, p = 0.022). The pairwise comparison of CTR and VPA treatments during separation resulted in a marginal difference with a high effect size ($z_{(85)} = 1.786$, p = 0.074, Cohen's d = 1.156) (Figures 9, 10, 11).

4.3.2.3 Social Network

In the POA, none of the subregions differed in activation in the social environment due to embryonic treatment. However, the medial preoptic area (mPOA) $(\chi^2_{(1,39)} = 5.638, p =$

0.018) exhibited higher c-Fos activity as a result of social reinstatement, but only in CTR animals ($z_{mPOA(39)} = 2.374$, $p_{mPOA} = 0.082$, Cohen's $d_{mPOA} = 1.312$; $z_{IPOA(41)} = 3.094$, $p_{IPOA} = 0.011$). The activity of mPOA increased due to social stimulation ($\chi^2_{(1, 49)} = 4.081$, p = 0.043; $z_{(49)} = -3.787$, p < 0.001, FDR_{mPOA} = 0.007). Social separation also resulted in increased activity in the mPOA of CTR animals ($\chi^2_{(1, 39)} = 5.638$, p = 0.018; $z_{(39)} = 2.374$, p = 0.018), though a marginal difference was observed between the CTR and VPA groups in this environment ($z_{(39)} = 1.837$, p = 0.066, Cohen's d = 1.111) (Figures 10, 11).

The lateral preoptic area (IPOA) showed a less pronounced difference during reinstatement ($\chi^2_{(1, 49)} = 3.373$, p = 0.066), but pairwise analysis revealed a difference caused by stimulation within VPA-treated animals ($z_{(49)} = -2.847$, p = 0.004). During separation, this nucleus presented the same pattern of activity change as the mPOA ($\chi^2_{(1, 41)} = 9.572$, p = 0.002). The activity of the CTR animals significantly increased ($z_{(41)} = 3.094$, p = 0.011), resulting in a marginal difference between the activity of CTR and VPA animals in this environment ($z_{(39)} = 1.767$, p = 0.077, Cohen's d = 1.554) (Figures 10, 11).

The activation of the VMH differed only during social separation ($\chi^2_{(1, 37)} = 7.888$, p = 0.005). In this case, VPA-treated animals exhibited marginally lower activation, though with a high effect size in the constant social environment ($z_{(37)} = -2.409$, p = 0.075, Cohen's d = 1.342). Additionally, their activity was significantly lower than that of CTR animals in the same social environment ($z_{(37)} = 3.732$, p = 0.001) (Figure 10).

The activation pattern of the dorsolateral periaqueductal gray (dlPAG) differed only in the separated animals ($\chi^2_{(1, 41)} = 4.293$, p = 0.038). During separation, the dlPAG of VPA-treated animals was less active than in CTR animals ($z_{(41)} = 2.072$, p = 0.038) (Figure 10).

4.3.2.4 Stress Network

The most prominent change resulting from social reinstatement was the activation of the IF ($\chi^2_{(1,\,21)}$ = 12.044, p < 0.001). Under a constant social environment, no difference in activity was observed between VPA-treated and CTR animals ($z_{(21)}$ = 1.422, p = 0.155). However, following social reinstatement, the activity in VPA mice increased significantly ($z_{(21)}$ = -2.287, p < 0.001, FDR_{IF} = 0.005) and reached a significantly higher level than in CTR mice ($z_{(21)}$ = -2.716, p = 0.007) (Figure 11).

The zona incerta (ZI) only showed a significant activation difference ($\chi^2_{(1,37)} = 8.735$, p = 0.003) between socially separated CTR and VPA animals ($z_{(37)} = 2.955$, p = 0.017) (Figure 10).

The activity of the mHb differed significantly between CTR and VPA animals only while they were separated from their cage mates (χ^2 _(1, 41) = 3.953, p = 0.047). Following separation, the activity in CTR animals was higher than in the VPA group, despite the large variance in CTR activity (z₍₄₁₎ = 1.972, p = 0.049). A marginal decrease in activity was observed in VPA animals compared to the constant social environment (z₍₄₁₎ = -1.732, p = 0.083, Cohen's d = 1.074) (Figure 10).

The IPN ($\chi^2_{(1, 19)} = 3.819$, p = 0.051) exhibited lower activity in the VPA group in a constant social environment ($z_{(19)} = 2.230$, p = 0.026). As a result of reinstatement, the activation increased significantly ($z_{(19)} = -2.511$, p = 0.012) (Figures 9, 11).

In the lateral hypothalamic area (LHA) ($\chi^2_{(1, 24)} = 4.166$, p = 0.041), baseline activity in the undisturbed environment did not differ between the VPA-treated group and CTR animals ($z_{(24)} = 1.548$, p = 0.122). However, the activity increased significantly in VPA-treated mice due to reinstatement ($z_{(24)} = -2.771$, p = 0.006) (Figures 9, 11).

The activation of the basomedial amygdala (bmAMY) ($\chi^2_{(1,50)} = 10.824$, p = 0.001) was significantly lower in the VPA group than in CTR animals ($z_{(50)} = 3.201$, p = 0.001, FDR_{bmAMY}= 0.029). Additionally, due to reinstatement, the activity increased significantly in the VPA group ($z_{(50)} = -3.250$, p = 0.001, FDR_{bmAMY}= 0.029) (Figures 9, 11).

4.3.2.5 *Putative non-social regions*

Among the areas whose impact on social behavior is not well established but might nonetheless be involved in autism, the retrosplenial cortex (RSC) showed a difference in activity ($\chi^2_{(1,41)} = 4.805$, p = 0.028) between VPA-treated and CTR animals in the socially separated situation ($z_{(41)} = 2.192$, p = 0.028) (Figure 10).

The dorsal CA3 (dCA3) ($\chi^2_{(1, 49)} = 4.726$, p = 0.030) exhibited a significant increase in activity in VPA-treated animals due to reinstatement compared to the social group ($z_{(49)} = -2.350$, p = 0.019) (Figure 11).

Additionally, the two examined regions of the dentate gyrus (dGD and vGD) displayed differences in activity under undisturbed social environments in VPA-treated animals compared to CTR animals (dGD: $\chi^2_{(1, 49)} = 5.317$, p = 0.021; vGD: $\chi^2_{(1, 27)} = 4.151$, p = 0.042). Both regions showed higher activity in VPA-treated animals (dGD: $z_{(49)} = 2.587$, p = 0.010; vGD: $z_{(27)} = 2.416$, p = 0.016), but only dGD showed a significant increase in activity due to reinstatement ($z_{(49)} = -2.624$, p = 0.009) (Figures 9, 11).

In the case of social separation, some non-social hippocampal regions were also affected. The dorsal CA1 (dCA1) presented a different activation pattern in VPA-treated and CTR animals ($\chi^2_{(1, 41)} = 7.465$, p = 0.006), with significantly higher activity in the CTR group than in the VPA group ($z_{(41)} = 2.732$, p = 0.003). Additionally, the activation of the ventral and dorsal regions of the dentate gyrus was higher in the VPA-treated group (vGD: $\chi^2_{(1, 20)} = 9.236$, p = 0.002; dGD: $\chi^2_{(1, 41)} = 4.809$, p = 0.028) due to the social environment, while the difference was marginal in the ventral dentate gyrus with a high effect size ($z_{(20)} = 2.487$, p = 0.062, Cohen's d = 2.892). In the dorsal dentate gyrus, the difference was significant ($z_{(41)} = 2.938$, p = 0.017) (Figures 9, 10, 11).

4.4 Network Analysis

4.4.1 Visual Inspection of Network Structure

As illustrated in Figure 12/B,D, VPA-treated animals exhibit a denser network compared to CTR animals (Figure 12/A,C). However, this network demonstrates less structural organization than observed in CTR animals (Figure 12/A,B). Notably, stress-related nuclei labeled in red are prominently centralized in the network of VPA-treated animals, whereas in CTR animals, network distribution appears more heterogeneous.

In socially separated animals (Figure 12/C,D), the network of the VPA group appears more condensed with more edges (Figure 12/D), while the network of CTR animals (Figure 12/C) appears more linear and contains fewer connected nuclei. However, a

condensed centrum can still be observed in CTR animals, albeit with stress-related nuclei being more dominant in this case.

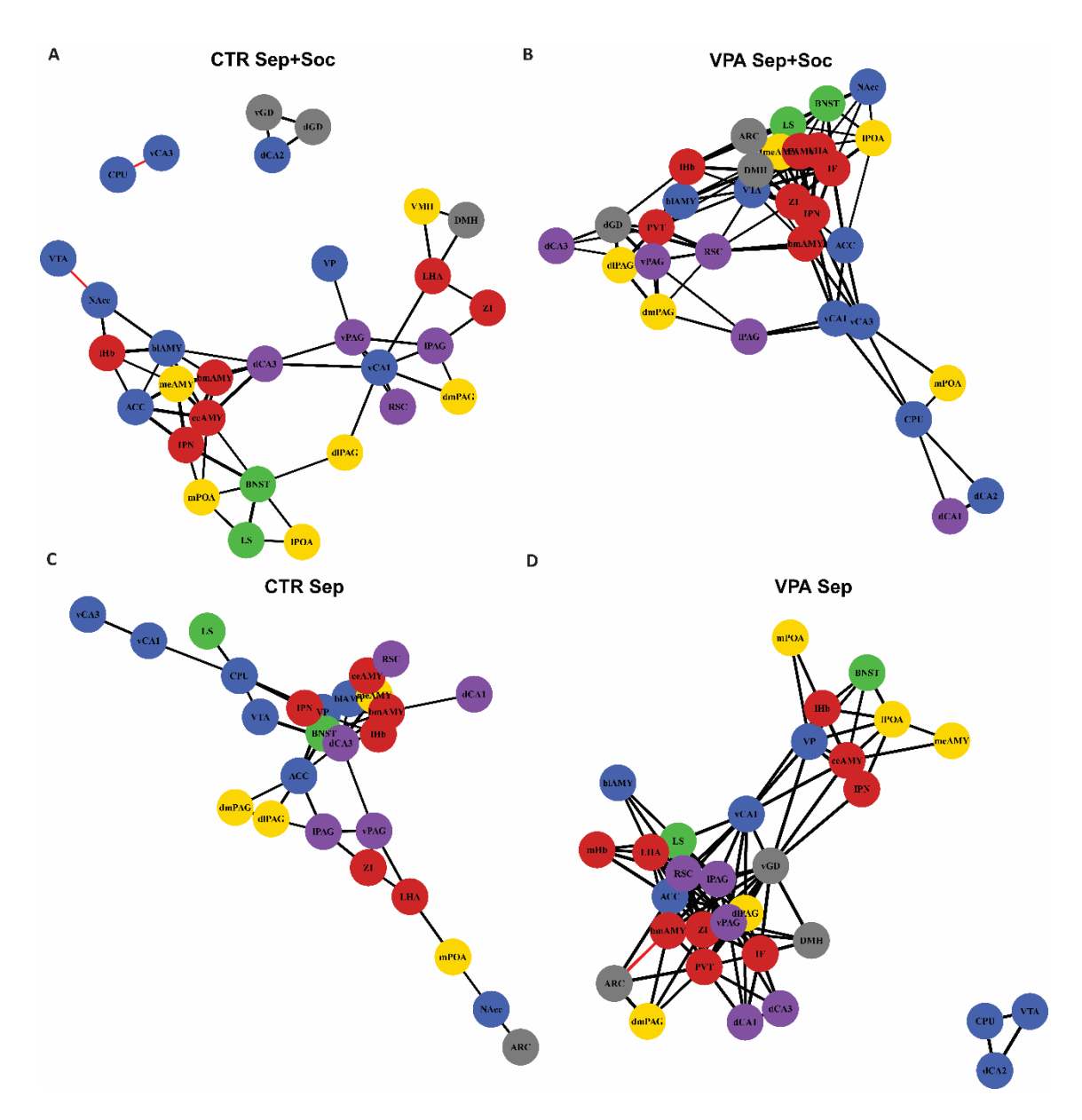


Figure 12: Functional network of the animals drawn using the thresholded matrices (see Figures 11/B,D and 12/B,D). Panels A and B represent the functional networks of the CTR and VPA-treated animals during social reinstatement (Sep+Soc). Panels C and D represent social separation (Sep). The width of the edges represents the correlation strength, with black edges indicating positive correlations and red edges indicating negative R² values. Nodes without any edges have been removed from the network figure. Different colored circles indicate the nuclei of the different subnetworks: blue indicates the MRS, green represents the intersection between MRS and SBN, yellow stands for the SBN, red labels the nuclei involved in stress modulation, purple indicates areas where changes were found in autism, and grey represents the control regions (150).

4.4.2 Validation of Connectome Threshold

4.4.2.1 Statistical Analysis

Comparing mean correlation values from areas overlapping with the connectome to those not overlapping, a significant difference was found in CTR animals (t=1.980, df = 1004.2, p=0.047). This suggests that correlations based on the observed neuronal activation are more pronounced and coherent in regions corresponding to physiological connections. This supports the notion that the observed functional connections align with known anatomical connections in control animals. However, in VPA-treated animals, no significant difference in connection strength was observed between the two networks (t=0.479, df = 1010.2, p=0.632), indicating that the co-activation of brain regions in the VPA animals are more widespread but less specific.

The average edge strength, of the network, based on the anatomical connectome, showed no difference from the strength of all edges in the socially separated animals (t = 0.027, df = 954.54, p = 0.978) Since any stimulation during the 24 social separation is necessarily less specifically activating c-Fos in the socially relevant brain regions than the sharp stimulus of social reinstatement, functional subnetwork analysis has only been conducted in the Sep+Soc groups.

4.4.3 Functional Connectivity after social stimulation

4.4.3.1 Connectome filtered and Random Matrix Analysis

In CTR animals, the average connectome-filtered correlation strength (Figure 13/A) of the entire network exhibited weaker correlations compared to VPA-treated animals (Figure 13/C) (t = 4.996, df = 1572.9, p < 0.001). Conversely, in a model simulating 1000 repetitions of correlation values between 10 randomly selected nuclei, no significant difference was found in VPA-treated animals (t = -1.280, df = 858.69, p = 0.201). However, CTR animals showed a significantly lower average correlation in the random matrix (t = -6.209, df = 830.54, p < 0.001). Such a result suggests that in VPA-treated animals, the nuclei are more interconnected, similar to a random, unspecific and possibly disfunctional network. Degree and betweenness centrality analyses also indicate that the degree values of VPA-treated animals are significantly higher than those of the CTR

group (W = 287.5, p < 0.001), showing a stronger connection between neighbouring nodes. On the other hand, the betweenness values, which represents the effectiveness of a network to convey information over larger distances do not differ significantly (W = 521.5, p = 0.142).

A similar trend was observed in the case of separated animals (Figure 14/A,C). While VPA-treated animals exhibited more edges (higher degree value) (W = 376.5, p = 0.002), the betweenness values did not differ (W = 694.5, p = 0.572).

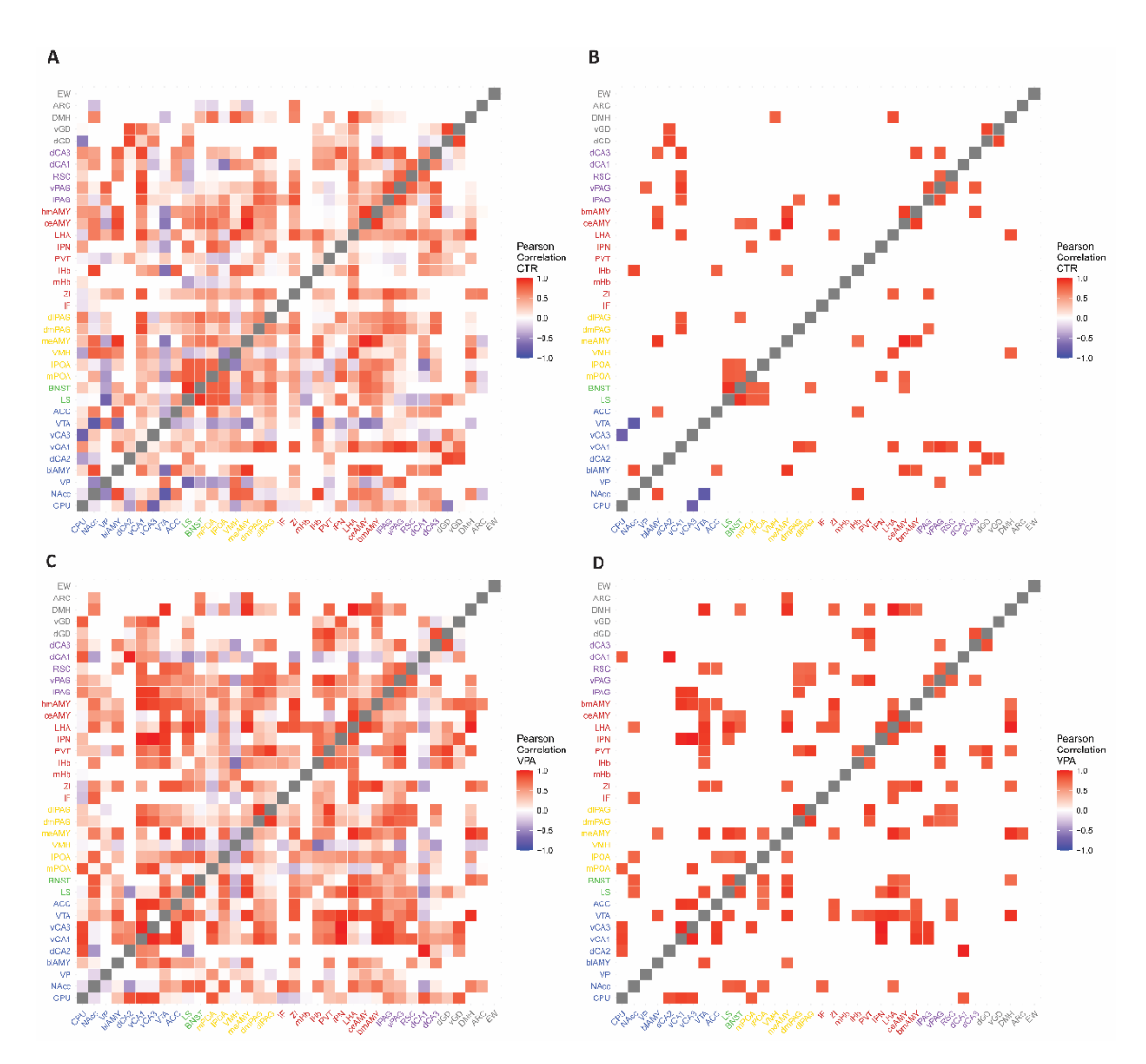


Figure 13: Heatmap illustrating the Pearson correlation strength of c-Fos activation between nuclei of the animals during social reinstatement (Sep+Soc). Panel A represents the correlation values of the CTR animals, with the connectome filter applied White areas indicate regions that are not connected anatomically according to the connectome (Figure 5). Panel C shows the correlation values of the VPA animals, also with the connectome filter applied. Panels B and D represent the connectome filtered correlations further thresholded for strong correlations (p < 0.05 and $|R^2| > 0.7$), which are considered as functional connectomes. Different colors indicate the different subnetworks: blue indicates the MRS, green represents the intersection between MRS and SBN, yellow stands for the SBN, red labels the nuclei involved in stress modulation, purple indicates areas where changes were found in autism, and grey represents the control regions.

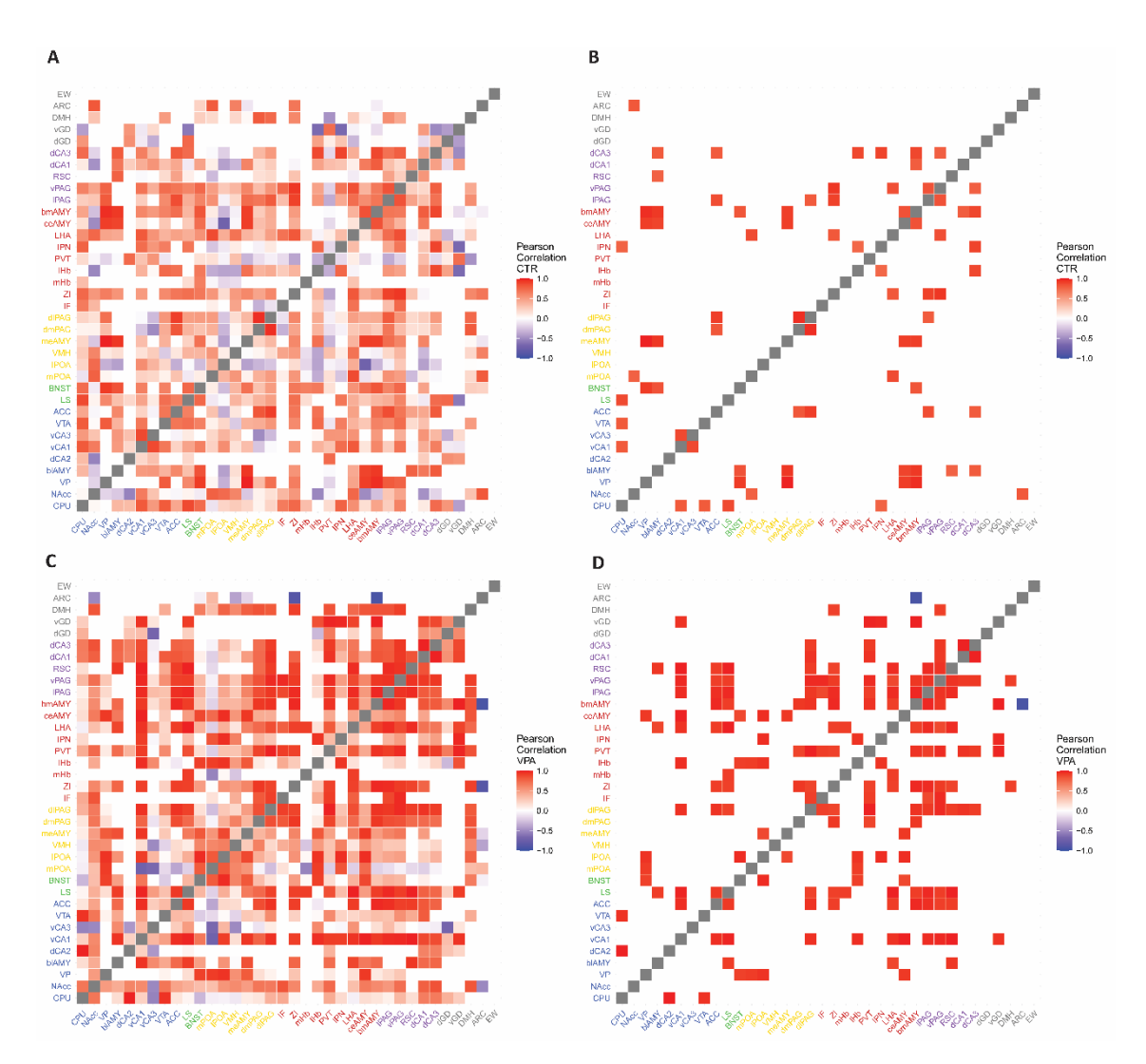


Figure 14: Heatmap illustrating the Pearson correlation strength of c-Fos activation between nuclei of the animals during social separated (Sep). Panel A represents the correlation values of the CTR animals, with the connectome filter applied White areas indicate regions that are not connected anatomically according to the connectome. (Figure 5). Panel B shows the correlation values of the VPA animals, also with the connectome filter applied. Panels B and D represent the connectome filtered correlations further thresholded for strong correlations (p < 0.05 and $|R^2| > 0.7$), which are considered as functional connectomes. Different colors indicate the different subnetworks: blue indicates the MRS, green represents the intersection between MRS and SBN, yellow stands for the SBN, red labels the nuclei involved in stress modulation, purple indicates areas where changes were found in autism, and grey represents the control regions (150).

4.4.4 Functional Sub-networks

4.4.4.1 Analysis of Sub-networks

The analysis of sub-networks revealed that the average correlation strength of the entire network is stronger than that of a network formed by randomly chosen edges from the original network (t = -6.233, df = 827.06, p < 0.001, FDR p < 0.001) (Figure 15/A). However, the correlation strength of the entire network in VPA-treated animals is stronger than in CTR animals (t = 4.996, df = 1572.9, p < 0.001, FDR p < 0.001), while the randomly generated network strength does not differ significantly from the VPA whole network (t = -1.584, df = 854.49, p = 0.114). Within the social network, a sub-network of the SDMN showed significantly weaker correlation in VPA-treated animals than in CTR animals (t = -3.010, df = 102.89, p = 0.003, FDR p = 0.009). However, the social network's correlation strength in CTR animals was stronger than the overall network strength and the randomly generated network (t = -2.694, df = 335.51, p = 0.007, FDR p = 0.001), but this was not observed in the mesolimbic network (t = 1.699, df = 156.15, p = 0.091). The SDMN did not differ between the two embryonic treatments (t = -0.707, df = 419.44, p = 0.48). However, the correlation strengths in VPA-treated animals were significantly weaker than the overall network's strengths (t = -2.694, df = 335.51, p = 0.007, FDR p = 0.0070.018).

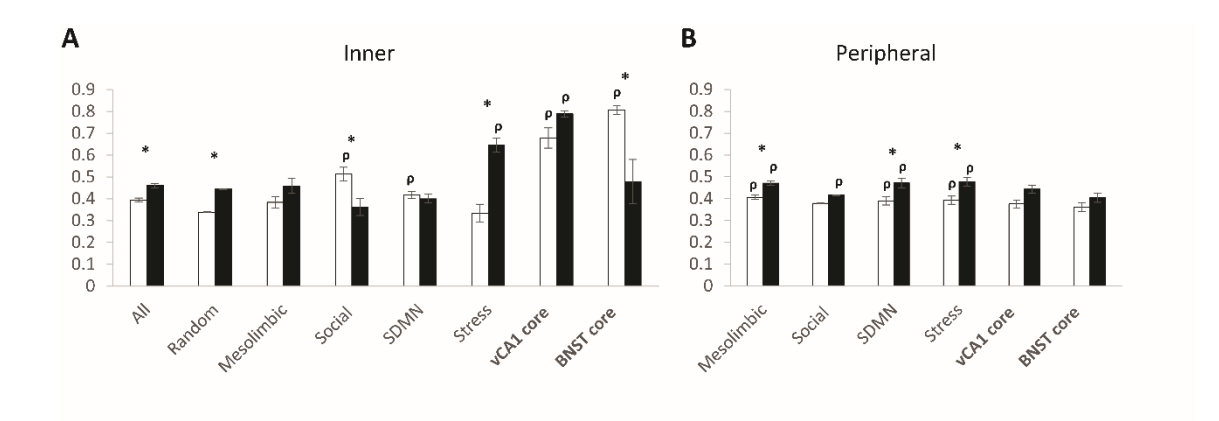


Figure 15: Average correlation strengths in the whole network (All), randomly constructed network (Random) with edges chosen randomly from the whole network's pool in subnetworks (\mathbf{A}), and the average connection strength of the network formed with nuclei that do not belong to the subnetwork (\mathbf{B}). Asterisk (*) represents the difference between CTR (white bars) and VPA (black bars) treated group, $\boldsymbol{\rho}$ denotes the difference from the randomly generated network. Symbols indicate FDR-adjusted significant differences.

The connectivity within the stress-regulating network, differed the most between VPA-treated and CTR animals (t=5.968, df=73.337, p<0.001, FDR p<0.001) The most tightly connected subnetwork in VPA-treated animals was the so-called stress network (Figure 15/A), which, in terms of its internal connections, was significantly stronger than in CTR animals (t=5.968, df=73.337, p<0.001, FDR p<0.001). The edge strength of the stress network also differed from the overall network (t=5.542, t=46.726, t=46

To test whether the connectivity differences appear only within the sub-networks we analyzed the connections outside the sub-networks (Figure 15/B) VPA-treated animals in the SDMN network presented stronger peripheral connectivity with nuclei outside SDMN (t=3.193, df=403.1, p=0.002, FDR p=0.004). In terms of peripheral connections, the two SDMN-forming subnetworks, only the mesolimbic subnetwork's connections were stronger in VPA-treated animals compared to CTR (t=2.275, df=342.21, p=0.024, FDR p=0.048), while the social network showed no difference in peripheral connections (t=1.379, df=327.51, p=0.169). The stress network also showed stronger peripheral connections in VPA-treated animals (t=2.943, t=312.27, t=0.003, FDR t=0.009).

4.4.4.2 Identification of Functional Core Networks- Social reinstatement

In addition, the mesolimbic and social networks as documented by O'Connell(149), cluster analysis revealed that in CTR animals, two subnetworks formed the functional core of the entire network. One of these two subnetworks consisted of nuclei clustered around the vCA1, while the other was centered around the BNST, as revealed by the cluster analysis (Table 1). Both regions were among the ones that exhibited the highest degree and betweenness values (Figure 16).

Following MCL analysis, the nuclei forming one cluster with vCA1 included the dmPAG, dlPAG, originally part of the social network, and vPAG, which also appeared among the nuclei with the highest betweenness values, along with the RSC, which did not belong to any of the previously mentioned networks. This network was named vCA1 core.

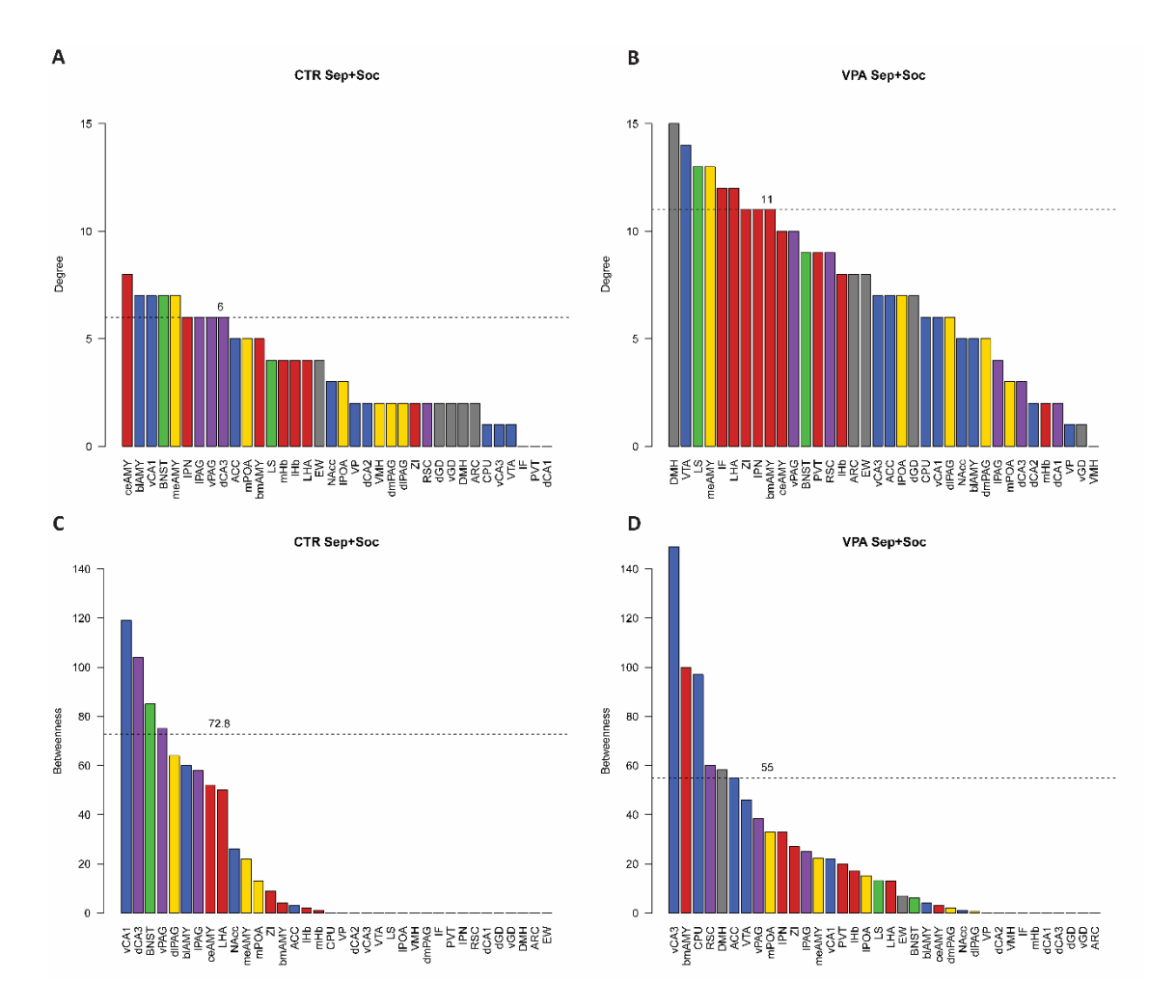


Figure 16: Degree and betweenness centrality values of the socially reinstated (Sep+Soc) of CTR (A, C) and VPA treated (B, D) animals. Degree centrality values (A, B) representing the number of connections (edges) belonging to specific nuclei. Betweenness centrality values (C, D) representing the extent to which a node (nucleus) lies on the shortest path between other nodes (nuclei). The dashed line represents the borderline of the 80% percentile of the highest centrality values. The color of the columns represents which subnetwork the nucleus belongs to: blue indicates the MRS, green represents the intersection between MRS and SBN, yellow stands for the SBN, red labels the nuclei involved in stress modulation, purple indicates areas where changes were found in autism, and grey represents the control regions.

The correlation strength in the CTR group was significantly higher in this subnetwork than in the entire network (t = 6.027, df = 20.416, p < 0.001, FDR p < 0.001; Figure 15). It was also stronger in the VPA group (t = 19.157, df = 41.881, p < 0.001, FDR p < 0.001). The connection strength differed between CTR and VPA animals, but this difference disappeared after FDR correction (t = -2.292, df = 22.479, p = 0.032, FDR p = 0.061).

The nuclei clustered around BNST included the LS, theoretically also a hub of the SDMN with BNST, the mPOA and lPOA, nuclei of the social network, and the EW, which is outside of the SDMN. This network was named BNST core. The BNST core network of the CTR group had significantly stronger connections than that of the VPA group (t = 3.156, df = 11.875, p = 0.008, FDR p = 0.019) similarly to the entire social network. The strength of the peripheral correlation values was also calculated, but none of the core networks had higher inner correlation values than the complete network.

Table 1: Clustering of brain nuclei based on MCL analysis under social separation (Sep) and social reinstatement (Sep+Soc) conditions. Nuclei within the same cluster are listed together in one cell. Clusters containing hub nuclei (underlined) are designated as cores clusters. Colors indicate functional classification: blue – MRS; green – MRS/SBN overlap; yellow – SBN; red – stress-related nuclei; purple – autism-associated areas; grey – control regions.

Socia envirom		Cluster	Nuclei	Social enviroment	Cluster	Nuclei
			dCA2, IPOA, VMH, PVT, dGD, vGD, DMH	Sep +Soc		IF, PVT, dCA1
			CPU, VTA, LS			CPU, vCA3
			NAcc, mPOA, ARC, EW		vCA1 core	vCA1, dmPAG, dlPAG, vPAG, RSC
Sep	_		vCA1, vCA3, IF			NAcc, blAMY, VTA, IHb
			ACC, dmPAG, dlPAG		BNST core	LS, <u>BNST</u> , mPOA, dlPOA, EW
			ZI, LHA, IPAG, vPAG			VMH, ZI, LHA, DMH
	IPI	IPN core	VP, blAMY, BNST, meAMY, mHb, lHb, <u>IPN</u> , ceAMY, bmAMY, RSC, dCA1, dCA3			ACC, meAMY, IPN, ceAMY, bmAMY, dCA3
						VP, mHb, IPAG, ARC
						dCA2, dGD, vGD

4.4.4.3 Identification of Functional Core Networks- Social isolation

In the brain network of socially separated animals, only the IPN was above the 80% percentile threshold in both degree and betweenness centrality values (Figure 17). However, centrality analysis revealed a more widespread network around this nucleus compared to socially reinstated animals. The VP and blAMY from the mesolimbic network, the BNST as the predicted hub region of the SDMN (and confirmed as a hub in our study for social reinstatement), the meAMY from the social network, the mHb, lHb, the ceAMY, and the bmAMY from non-social stress-regulating nuclei, and the RSC, dCA1, and dCA3, which are associated with autism but not assigned to social functions, were organized around the IPN (Table 1). The comparison of this network, which could be named core network for separation, showed that it has significantly stronger intercorrelation (t = 14.766, df = 88.439, p < 0.001) than the average correlation value of the entire examined network. Among the nuclei forming this subnetwork, the blAMY and mHb were also above the criteria for degree values, and dCA3 was above the criteria for betweenness.

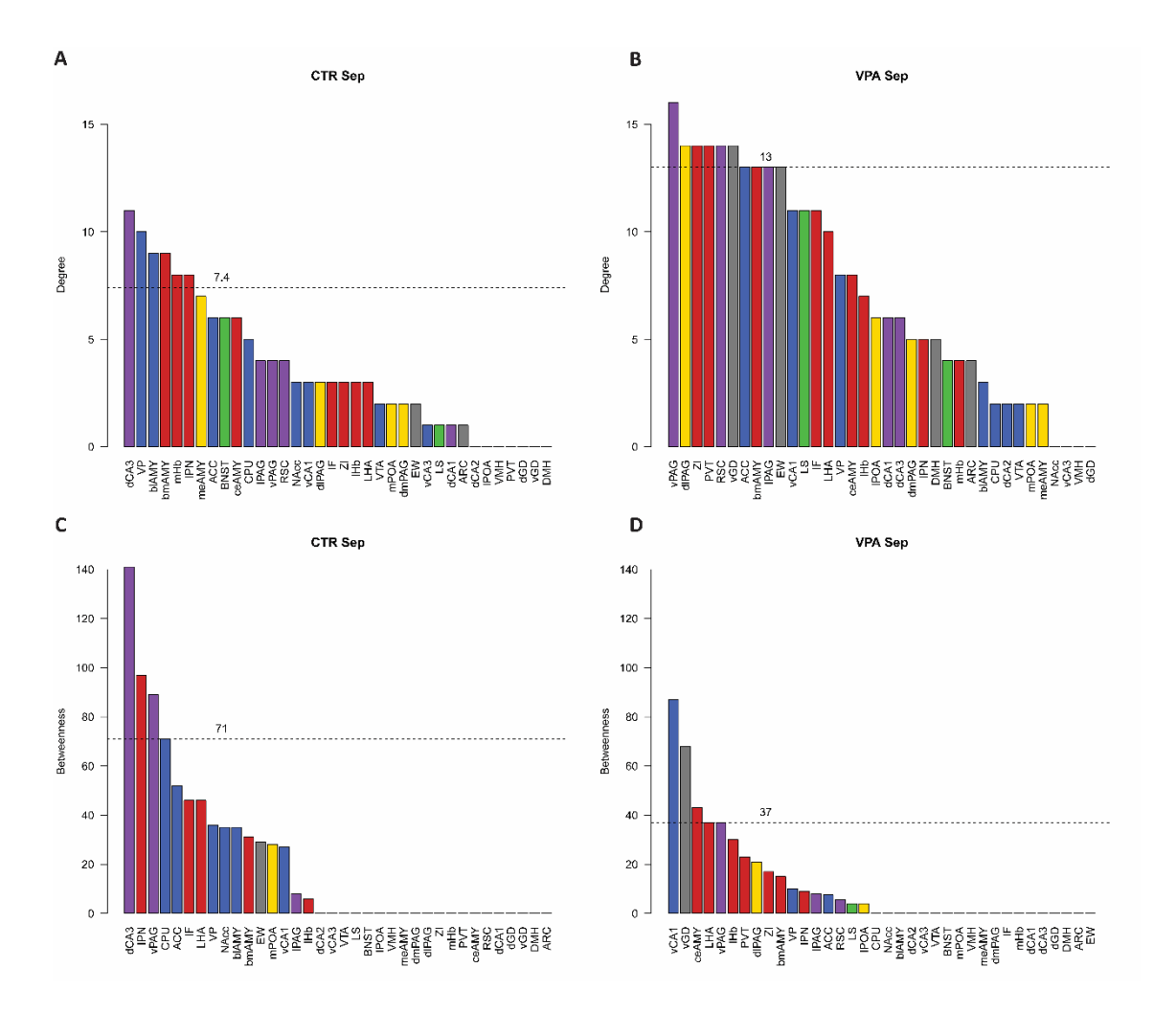


Figure 17: Degree and betweenness centrality values of the socially separated (Sep) of CTR (A, C) and VPA treated (B, D) animals. Degree centrality values (A, B) representing the number of connections (edges) belonging to specific nuclei. Betweenness centrality values (C, D) representing the extent to which a node (nucleus) lies on the shortest path between other nodes (nuclei). The dashed line represents the borderline of the 80% percentile of the highest centrality values. The color of the columns represents which subnetwork the nucleus belongs to: blue indicates the MRS, green represents the intersection between MRS and SBN, yellow stands for the SBN, red labels the nuclei involved in stress modulation, purple indicates areas where changes were found in autism, and grey represents the control regions (150).

It is notable that the BNST acts as a hub in social reinstatement and appears in the core network of socially separated animals too. Additionally, the dCA3 appears among the nuclei with the most edges in both social environments, and the blAMY holds a dominant central position in both environments.

4.4.5 Behavioral analysis

The ANOVA analysis revealed that none of the measured behavioral types differed between CTR and VPA-treated animals during the first 10-minute period of the social reinstatement ($t_{(Exploration)} = -0.210$, df = 76.6, p = 0.835; $t_{(Fight)} = -0.407$, df = 76.6, p = 0.685; $t_{(Following)} = 0.066$, df = 76.6, p = 0.948; $t_{(Grooming)} = 0.543$, df = 76.6, p = 0.589; $t_{(Run Away)} = 0.002$, df = 76.6, p = 0.999; $t_{(Self-Grooming)} = -0.134$, df = 76.6, p = 0.893; $t_{(Anogenital sniffing)} = -0.744$, df = 76.6, p = 0.459). (Figure 18).

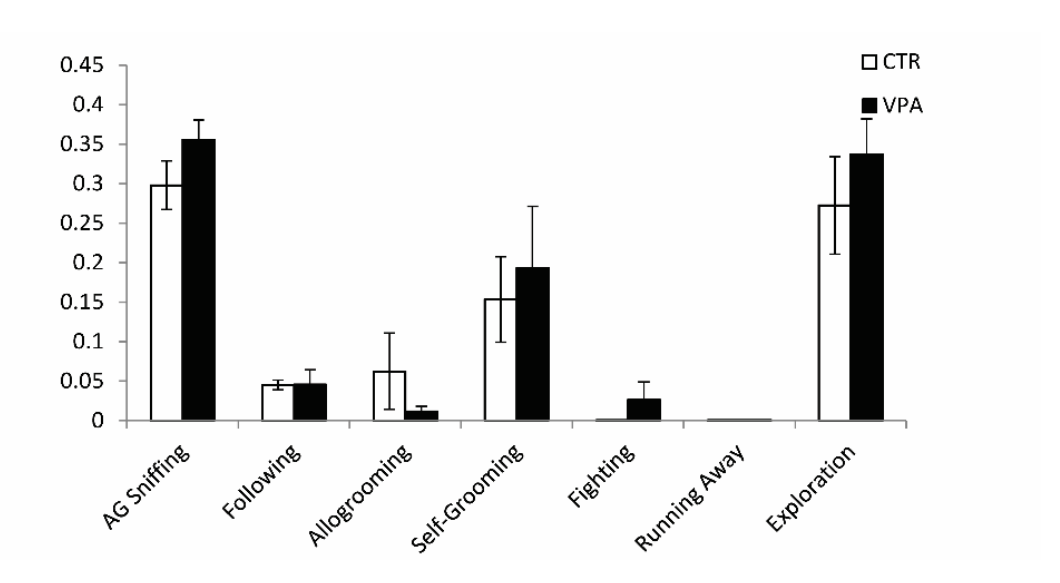


Figure 18: Results of behavioral analysis. Bar graphs illustrate the proportion of time the animal spent engaging in a specific behavior during the social reinstatement.

However, the power analysis indicated a high effect of VPA treatment on elevated time spent with anogenital sniffing (Cohen's D=0.818) and a medium effect on reduced time spent with allogrooming in VPA-treated animals (Cohen's D=0.632) and more fighting (Cohen's D=0.581) the latter only occurring in the VPA animals.

The correlation analysis showed strong associations between the time spent on different behaviors and the activation of certain brain areas (Figure 19). In CTR animals, more connections (8) were observed between brain areas and pro-social behaviors like anogenital sniffing, following, and allogrooming compared to the VPA-treated group (2). Conversely, in the case of antisocial behaviors (fight, run-away), the VPA group had slightly more correlating nuclei (5) than CTR animals (3). Additionally, for neutral behaviors (sitting, self-grooming, exploring the cage), CTR animals exhibited more correlations (13) than VPA animals (3).

This suggests that while certain regions in CTR animals are more associated to specific behaviors and are less tightly interconnected, the brain of VPA-treated individuals, with its more widespread connections, appears is somewhat more disconnected from the actual behavior of the animals.

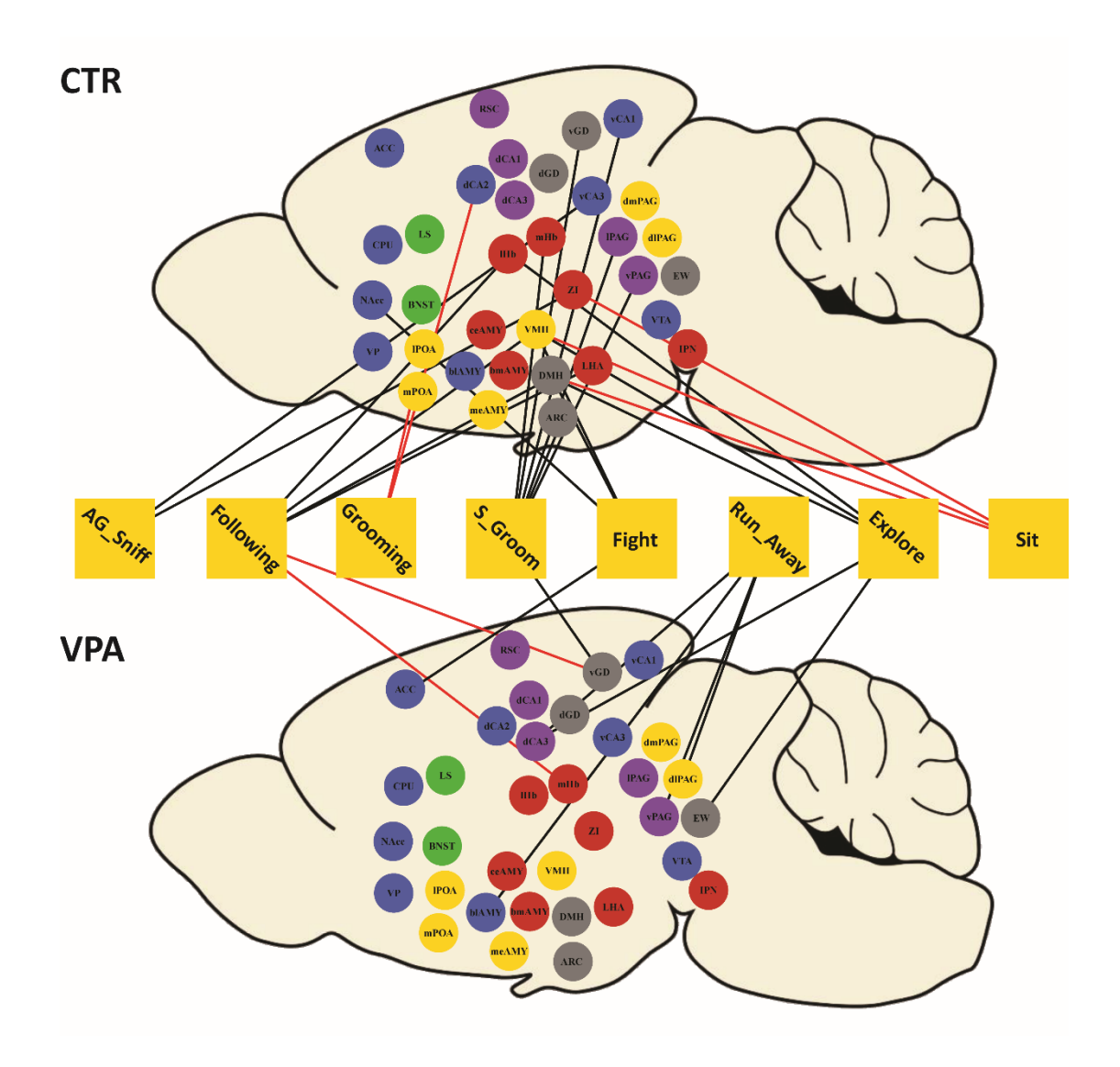


Figure 19: Correlation between behavior and c-Fos⁺ cell density in nuclei showing significant associations (p < 0.05, $R^2 > |0.8|$) during social reinstatement. Yellow squares denote behavioral variables; circles represent brain regions, Different colored circles indicate the nuclei of the different subnetworks: blue indicates the MRS, green represents the intersection between MRS and SBN, yellow stands for the SBN, red labels the nuclei involved in stress modulation, purple indicates areas where changes were found in autism, and grey represents the control regions. Edge color indicates direction of correlation: black for positive, red for negative.

4.4.6 Gene library analysis

Both the DA levels at the striatum and the functional connectome suggest an altered pathway connectivity in the brain of the VPA treated mice. To test this hypothesis, we checked in the Allen Developing Mouse Brain Atlas (214) whether there are a proportionally higher number of developmental genes related to tract development are active during the time of the embryonic development (E13.5) when the brain was exposed to VPA. At the E13.5 stage, 234 genes were identified as enriched. Of these, 28 genes were found to be crucial in regulating tract morphology development, with significant ontology enrichment (adjusted p-value = $5*10^{-5}$). At the E15.5 stage, 151 genes were identified as enriched, 16 of which were involved in tract morphology regulation, also indicating significant enrichment (adjusted p-value = $3.06*10^{-6}$).

When examining the genes that overlapped between the stages, it was found that 142 genes were unique to E13.5, while 59 genes were unique to E15.5. Further analysis of the unique genes revealed that 16 genes at the E13.5 stage were involved in tract morphology formation, showing significant enrichment (adjusted p-value = $1.15*10^{-7}$). In contrast, no significant enrichment was found for genes involved in tract morphology among the unique genes at the E15.5 stage.

These findings suggest that the regulation of tract morphology development is more prominently influenced by the genes expressed at the E13.5 stage than those at E15.5. This differential gene expression and enrichment highlight critical developmental windows and specific genetic contributions to the formation of certain tracts.

5 Discussion

5.1 Sociability deficits

The results of the three-chamber test suggest that embryonic VPA treatment effectively reduced the sociability and probably the social memory of the mice. The decreased sociability is a key diagnostic criterion for ASD (16,129,136) and it implies that VPA treated mice has an autistic like phenotype. VPA-treated animals showed less interest in an unfamiliar, age- and sex-matched animal compared to CTR animals. These observed differences were not due to motor impairments, as the number of entries into the lateral chambers during the habituation phase did not differ between groups. This aligns with previous studies demonstrating that ASD animals tend to show reduced interest in living objects compared to inanimate objects or familiar environments, in contrast with the natural tendency of rodents to explore unfamiliar mates (218).

In the social phase of the test, normally developing animals exhibited expected behavior, spending more time in the chamber containing an unfamiliar mouse. By contrast, VPA-treated animals spent equal time in the two lateral chambers, failing to exhibit this natural preference (215,219). During the social memory phase, CTR animals demonstrated a clear shift in interest towards new, unfamiliar animals. In contrast, VPA-treated animals failed to differentiate between novel and familiar mates, suggesting impairments in social memory or reduced interest in living objects. These differences may also be attributable to early olfactory learning deficits, which are known to impair social recognition in VPA-treated animals (220–222).

The lack of distinction between novel and familiar social cues, as seen in the three-chamber test, supports the hypothesis of disturbances in social memory or sensory processing, particularly olfaction. Rodents rely heavily on olfactory cues for social recognition, and VPA-treated animals are apparently less sensitive or responsive to these cues compared to normally developing animals. Previous studies have identified altered connections between the olfactory bulb, retrosplenial cortex, and NAcc in VPA-treated animals (140). These neural changes in olfactory processing could be analogous to face-processing alterations observed in human autism (56,85,223).

The fact that fighting only occurred in the VPA group further suggests that at least some of the VPA-treated animals might not recognize familiar cage mates reintroduced after separation, treating them instead as intruders. Since aggression is less frequent in adolescent mice (especially in the C57BL/6 mice) than in adults (224), it was remarkable that fights occurred in some of the VPA animals. These findings highlight the critical role of social memory deficits and sensory disturbances, particularly in olfaction, in the altered social behaviors observed in VPA-treated animals.

5.2 Activational pattern of ROI

Following the concept of the SDMN published by O'Connell and Hofmann (149), we observed that many of the nuclei they identified are activated after social stimulation. Although they did not include cortical areas, we incorporated the ACC into the MRS due to its role in physical and emotional effort-based decision-making, as mesocortical DA fibers project to it (225,226).

The activation patterns under three different social environments revealed a lateral density difference in only one brain region of VPA-treated mice. Namely, the right ceAMY of VPA-treated animals had a higher density of active cells.

These findings align with human studies, which have demonstrated that individuals with ASD exhibit enhanced inter-hemispheric and decreased intra-hemispheric variance in activity, connections, and brain area size (227,228). Such differences are observed in both cortical and subcortical regions, including the basal ganglia and thalamus (229,108) Notably, the cell density of the amygdala in ASD patients shows hemispheric differences, and the right amygdala displays hypoactivation during emotion processing tasks (73).

As a central component of the MRS, the NAcc plays a crucial role in facilitating favorable behavioral responses, either through the approach or avoidance of stimuli (149,230). In our study, the activity in VPA-treated animals significantly increased during reinstatement compared to a constant social environment. This overactivity, correlated with fighting and might represent the lack of social motivation as observed in sociability test, is most likely caused by inputs other than dopamine, since VPA treated mice had generally lower dopamine level in the NAcc (at least in a young age). The NAcc is critical for regulating motivated behaviors through subregion-specific manner (231,232). Prior

studies have shown that social defeat stress specifically induces c-Fos expression in the NAcc relative to novelty-induced exploration (233,234).

Additionally, studies using ASD model mice suggest that dopamine type 1 (D1) receptors control fundamental mechanisms for regulating excitatory synaptic transmission and glutamate-dependent forms of plasticity. Dopamine signaling through D1 receptors, but not D2 receptors, is necessary for VTA stimulation-driven social behavior (235,236). Activation of VTA-NAcc projections increases social interaction with a novel mouse, although the activity of the VTA itself did not change in this social situation (236). As the VTA plays a role in modulating salience, reward-seeking behavior, and motivation, its elevated activity in socially separated CTR animals is noteworthy (149,237).

Further supporting this perspective, our study found that the NAcc of VPA-treated animals displayed marginally elevated activity, but the VTA, which serves as the main dopamine input to the NAcc, remained significantly less active than in CTR animals. These findings suggest that the decreased dopamine levels in the NAcc of VPA-treated P7 animals, compared to control animals, may also contribute to the observed differences in activity.

Consistent with human studies, hypoactivity of the ACC in VPA-treated animals during constant social environments strongly correlates with reduced communication functions (67). Upon reinstatement to the social environment after the separation phase, VPA-treated animals exhibited significantly elevated activity. The increased activity was correlated with aggressive behavior, aligning with findings in humans that associate increased aggression with brain activity in regions of emotional and behavioral control, such as the ACC (238–240).

The most significant differential activation between CTR and VPA-treated animals during social reinstatement was observed in the IF nucleus of the VTA (241). VPA animals exhibited highly overactive IF activity during this phase. To better understand this activation, it must be examined within the context of the whole network. The IF has connections with the habenulo-peduncular pathway (formed by the mHb and IPN), which plays an important role in modulating stress aversion and withdrawal (242–244). VPA animals exhibited significantly elevated activity in the IF, IPN, and LHA during social

reinstatement, suggesting that reuniting with cagemates resulted in more stress than being kept alone. In contrast, CTR animals showed elevated activity in the mHb during social separation, which is generally associated with mild stress (245,246). Behavioral correlations indicate a similar pattern: during reinstatement, varied depending on the treatment: In control animals the activity of the mHb correlated with self-grooming, which is a non-social behavior and might be interpreted as self-separation, meanwhile in the VPA animals it negatively correlated with following, a highly social interaction. Although the causality between the brain activity and certain behaviors is undefinable by our results, it seems that the more social VPA mice has lower mHb activity, ands less social control mice has higher.

While the adjusted p-value was below the threshold for significant activation change in the blAMY from the MRS, it is noteworthy that activity elevated in both control and VPA-treated animals during social reinstatement. The blAMY, a key MRS modulator, regulates goal-directed behaviors in emotional learning, including fear conditioning (149). The overall activation of the blAMY may lead to an excitatory drive on downstream nuclei, including the NAcc, hippocampus, and hypothalamus, which modulate reward, aversion, and motivated movement through D2 receptors (247–250).

In the case of the mPOA and the IPOA, different social contexts resulted in different activation levels between CTR and VPA animals. In socially separated control animals, both parts of the POA were more active than in a constant social environment, while the activity in VPA animals did not change. The POA primarily plays a role in parental care and male-male aggression (149). The GABAergic neurons of the mPOA are crucial in regulating motivational states, which can be impaired in depression (251). The IPOA is involved in the reinstatement of reward-seeking behavior, and the activation of the general GABAergic population can generate anxiolytic effects (184,252). The fact that the POA was activated oppositely in the two groups suggest that VPA mice percieve the two social situations differently than controls.

Among the stress-regulating areas, an interestingly inactive region was observed in VPA-treated animals. The bmAMY exhibited very low activity in VPA animals under a constant social environment but became significantly more active during reinstatement. The bmAMY, critical in differentiating social contexts, may represent a target for

interventions aimed at mitigating social stress in ASD populations. This region distinguishes between safe and aversive environments, decreases fear-related freezing, and mitigates high-anxiety states (253). Chronic social stress causes a reduction in its activity.

5.3 Functional Connectivity and Network Changes

As evidenced above, social environmental changes significantly impact brain activity patterns in several brain regions. Given the correlational nature of our approach, it was impossible to infer causality between the social stimuli, the brain activity and the actual behaviors performed. Still our data were suitable to detect cross correlations between brain regions and to reconstruct functional connectivity among them. It is well established that embryonic VPA treatment induces widespread alterations in white matter volume (254,255). Our research group also identified differences in the density of tyrosine hydroxylase (TH)-positive cells in dopaminergic regions. Specifically, VPA-treated animals exhibited a higher number of TH-positive cells in the substantia nigra compared to CTR animals. Conversely, the density of TH cells in the VTA was lower in VPAtreated animals (179). The mesolimbic tracts also showed defasciculation (179), resulting alterations of the synaptic contacts within the basal forebrain (256) suggesting a disfunctional dopaminergic connectivity. To better understand the extent of such alterations and dysfunctions on the functional network of the socially relevant brain regions, we analyzed the functional connectivity of key nuclei, focusing on direct correlations supported by connectomic data.

During the social reinstatement phase, the timing of the actual social stimulus was carefully controlled, providing the most accurate onset of activation patterns. In contrast, the separation and long-term social phases lacked precise timing of c-Fos activity. Analysis revealed that functional connections in CTR animals, overlapping with anatomical projections exhibited higher correlation values compared to non-overlapping ones. This supports the hypothesis that the functional connectivity was underlined by the physiological data. Interestingly, this difference was absent in VPA-treated animals, suggesting incomplete development or improper guidance of neural tracts. Indeed, VPA-treated animals unlike controls possess widespread but poorly organized functional connections that is not different from randomly generated networks. This suggests that

embryonic VPA exposure disrupts the normal organization of neural connections, potentially contributing to ASD-like behaviors.

Overall, mean correlation values were higher in VPA-treated animals compared to CTR animals (Figure 20). These findings align with previous studies reporting structural abnormalities in ASD, such as defects in neuronal migration, delayed maturation, immature dendritic arborization, and insufficient dendritic spine pruning (80). Additional changes in axonal myelination may lead to misrouted growth, delayed target arrival, or connections failing to form altogether (84). Such disruptions manifest as intrahemispheric hyper-connectivity and interhemispheric hypo-connectivity in ASD (96,97,99,105).

One of our earlier projects also identified misplaced neurons, with a reduced number of TH+ neurons in the VTA and increased numbers in the substantia nigra. Additionally, defasciculation of the mesothelencephalic pathway further highlights these structural irregularities (179). Gene enrichment analysis during the VPA treatment window identified 16 uniquely enriched genes, of which 8 (Aff3, Arx, Dcc, Efnb1, Klf7, Sox2, Sox3, Tcf4) are implicated in autism (257–261).

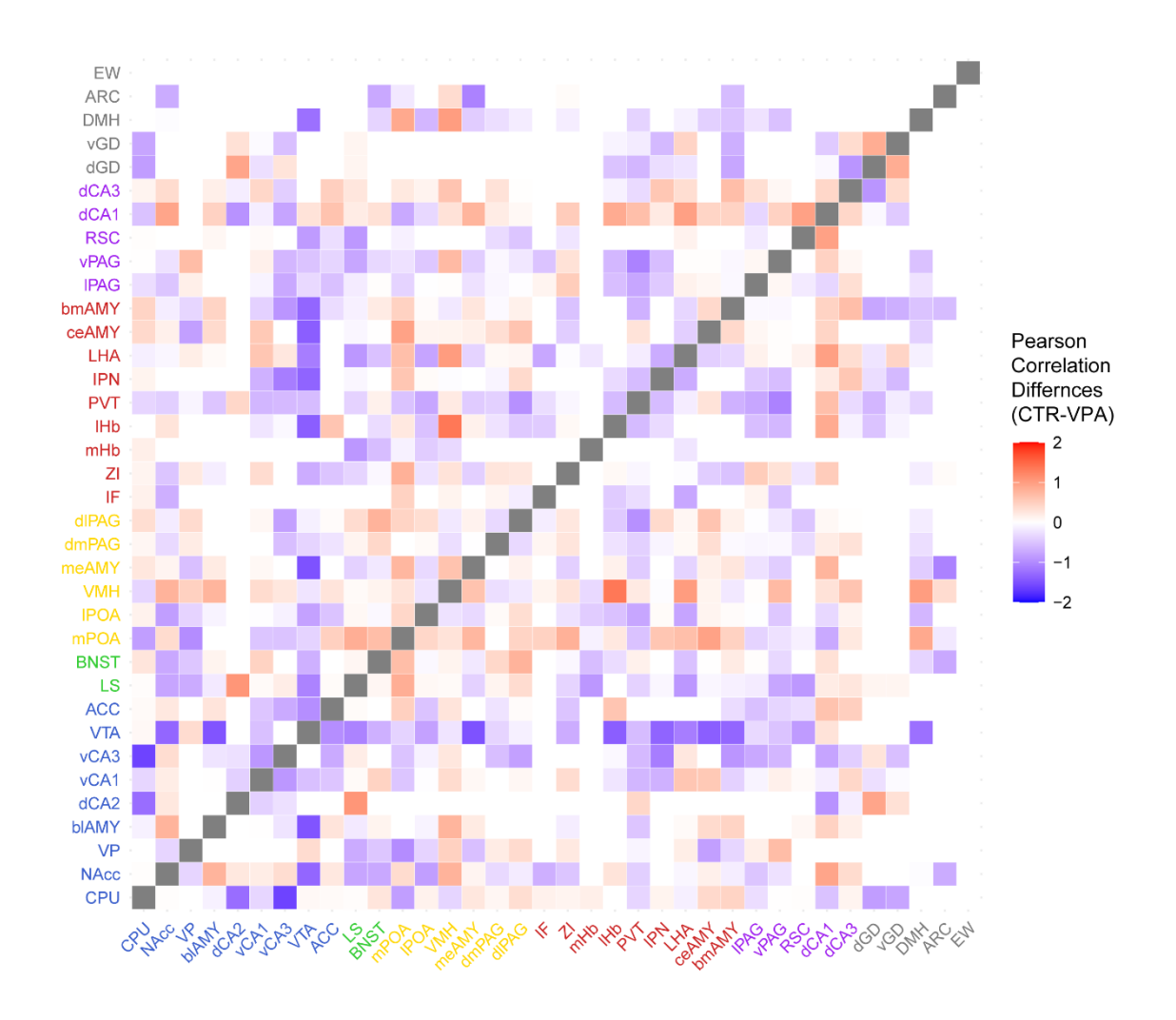


Figure 20: Heatmap illustrating the differences in Pearson correlation strengths of cFos activation between CTR and VPA-treated animals during social reinstatement
(Sep+Soc). Red squares represent functional connections that are stronger in CTR
animals, while blue squares indicate connections that are stronger in VPA-treated
animals. White areas indicate regions that are not physiologically connected according
to the connectome. Different colors in axis label indicate the different subnetworks. Blue
indicates the MRS, green represents the intersection between MRS and SBN, yellow
stands for the SBN, red labels the nuclei involved in stress modulation, purple indicates
areas where changes were found in autism, and grey represents the control regions.

As O'Connell and Hoffman (149) constructed the SDMN based on similarities in innervation and receptor characteristics across nuclei, our functional connectivity analysis revealed a divergent pattern. While the MRS did not exhibit stronger internal connectivity than random networks in the CTR group, the internal average connection strength of the SDMN was higher than expected from randomly generated networks in both the control and VPA groups The difference is clearly due to the social brain network showing a robust internal connectivity which is diminished after the embryonic VPA treatment. In contrast, the MRS, the stress network and SDMN as a whole retained stronger peripheral connectivity—that is, stronger connections with regions outside its own subnetwork—compared to random networks, particularly in VPA-treated animals. These three networks also demonstrated enhanced peripheral connectivity in the VPA group. These findings suggest that prenatal VPA exposure is associated with a shift toward a more diffusely connected and less modular network architecture in both systems (Figures 13, 18).

This finding is further supported by the observation of defasciculation of the TH+ fibers in VPA-treated animals, as the functional connections were mainly strengthened in the VTA of the VPA group (179). Notably, while the nuclei of the MRS share the characteristic of being innervated by dopaminergic input, they play roles in very different social context tasks such as motivation, aversion, reward, or social memory (149,233,249,262).

The SBN was the only a-priori defined sub network that presented increased internal connection strength only in the CTR animals compared to the overall network and these connections were also significantly stronger than in the VPA-treated animals. Such differences suggest that SBN is disproportionately affected by the embryonic VPA treatment. One of the definitions of the SBN is the occurrence of sex steroid receptors in all of its nuclei (148,263). It has been proven that sexual steroids have a major effect on the development of the grey matter, causing extreme masculinization of brain structures in individuals with autism, which is linked to regions involved in language and emotional processing (117). White matter myelination and integrity are also dependent on sexual steroids, contributing to earlier maturation and increased rigidity of connectivity patterns in male youth compared to female youth (120,121). VPA exposure decreased aromatase

expression and estradiol levels only in the prepubertal male cortex (264). This could potentially explain the sexual differences in the frequency of ASD (110,111).

Notably, the SBN primarily plays roles in sexual behavior, aggression, and parental care. In our experiment, the animals were adolescents, a sensitive period for experience-dependent social dominance plasticity (265). The disruption of the organizational effects of sex steroids by VPA treatment may inhibit the plasticity related to social dominance hierarchy, acting as a potent destabilizer of hierarchy plasticity (265,266).

The stress-regulating subnetwork, centered around the habenulo-peduncular pathway (242), was the most internally connected in VPA animals than a random network, and its outer connections were also stronger than those in CTR animals. Combining the NAcc's role in social defeat stress (233,234), the reduction in social hierarchy plasticity (265), the extensive VTA fibers (179), and the decrease in DA at terminals (266), we can conclude that the social reinstatement likely caused an environmental challenge for VPA animals likely caused an unpredictable environmental change. This challenge, coupled with their reduced ability to socially adapt, likely resulted in a significant elevation of stress. Compared to controls, both the MRS and the stress subnetwork of the VPA animals exhibited weaker internal functional connection strength but stronger outer connections. This strengthening of outer connections may be explained by the enhanced stress-regulating subnetwork in VPA-treated animals.

The differences in degree centrality values illustrate this well, as nearly all nuclei of the stress network in the VPA group have stronger connections. (Figure 21).

One of our goals was to identify the nuclei in the a-priori assigned sub networks that have central roles in the processing of social stimulation. To identify these hub nuclei in the network of CTR animals, we selected nodes/nuclei that both had the most edges/connections and the highest betweenness centrality values. Based on these two hubs we also a-posteriori identified the brain regions that form a core network around them. The clusters were formed through a cluster analysis of edges weighted by the correlation strength values of the nuclei. Nuclei within the same cluster as the hubs were designated as part of the core network.

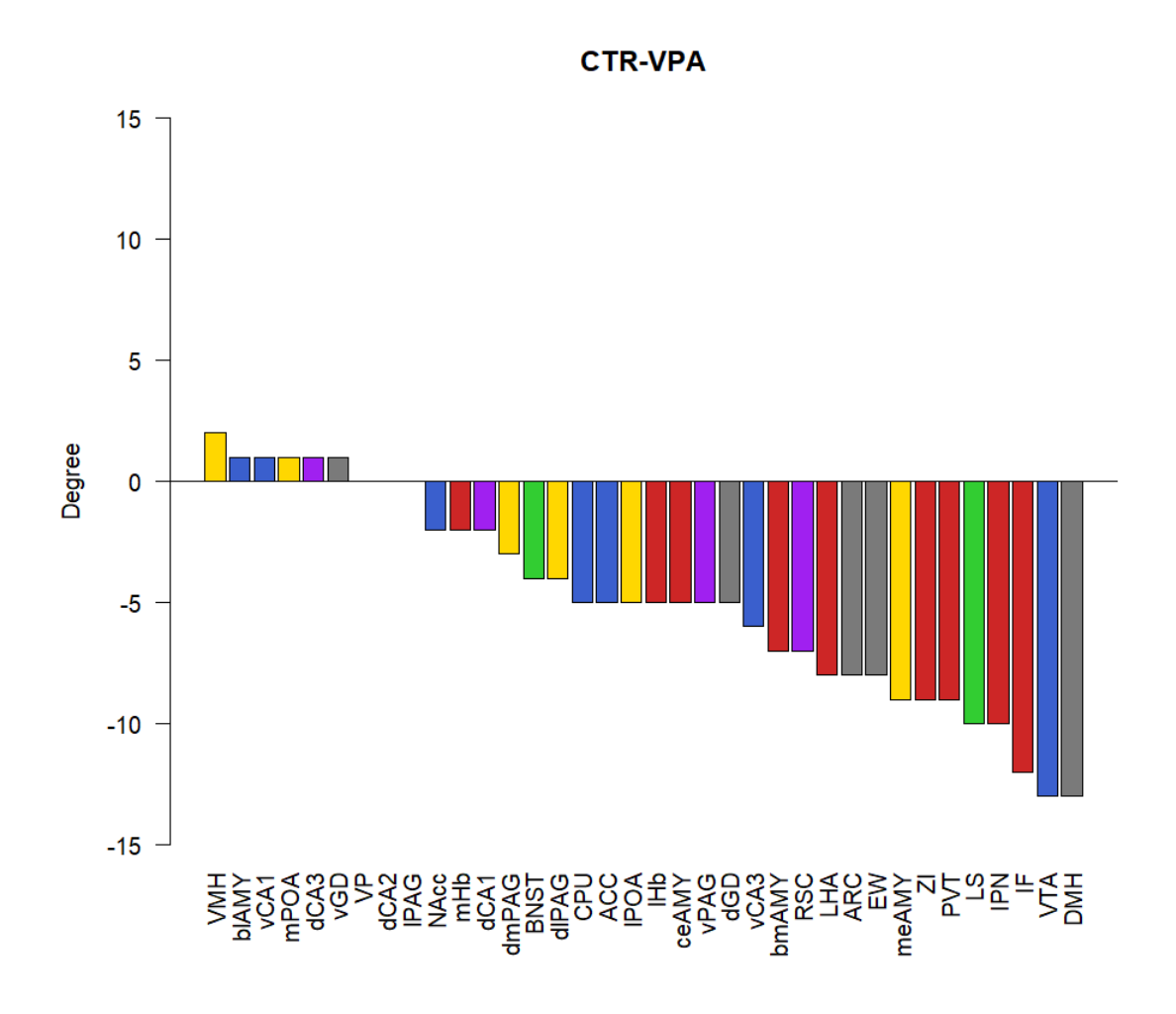


Figure 21: Difference in degree centrality values between the socially reinstated (Sep+Soc) CTR and VPA groups. The values above the x-axis represent nodes (nuclei) that have more connections (edges) in the CTR group, while the columns below the x-axis indicate nodes that have more significant connections in the VPA group. Different colors of the bars indicate the different subnetworks. Blue indicates the MRS, green represents the intersection between MRS and SBN, yellow stands for the SBN, red labels the nuclei involved in stress modulation, purple indicates areas where changes were found in autism, and grey represents the control regions.

One of the two hub nuclei identified was the vCA1 region of the hippocampus, which is part of the MRS. The vCA1 receives dopaminergic input and is involved not only in spatial memory but also in the general storage of repeated experiences (149,267). Moreover, the vCA1 specifically plays a role in regulating social recognition memory (268).

In addition to the vCA1, the dorsomedial, dorsolateral, and ventral (v) subregions of the PAG are part of this core network. The PAG is generally described as a nucleus that elicits inter-male aggressive behavior (149,269). The PAG also contains sexual steroid receptors, aligning it with the SBN (149,270). When dissected into subnuclei, it is evident that the dorsal nuclei primarily play roles in adaptive responses. These responses occur as a result of repeated exposure to threatening members of the same species and are characterized by a shift towards more socially avoidant behavioral strategies (271,272) in healthy rodents.

The dmPAG plays a key role in regulating inter-male aggression (188). It interferes with emotional judgments and mnemonic processes (187). Meanwhile, the vPAG appears to be involved in more passive patterns of behavioral responses, manifested by immobility and inhibition of the sympathetic nervous system (189,190).

Additionally, the RSC is part of this core network. The RSC is important for spatial navigation and is involved in translating information between allocentric (world-centered) and egocentric (self-centered) reference frames (273). It is also part of the complex neural circuitry that mediates social cognition and fear-inducing context memory (274,275).

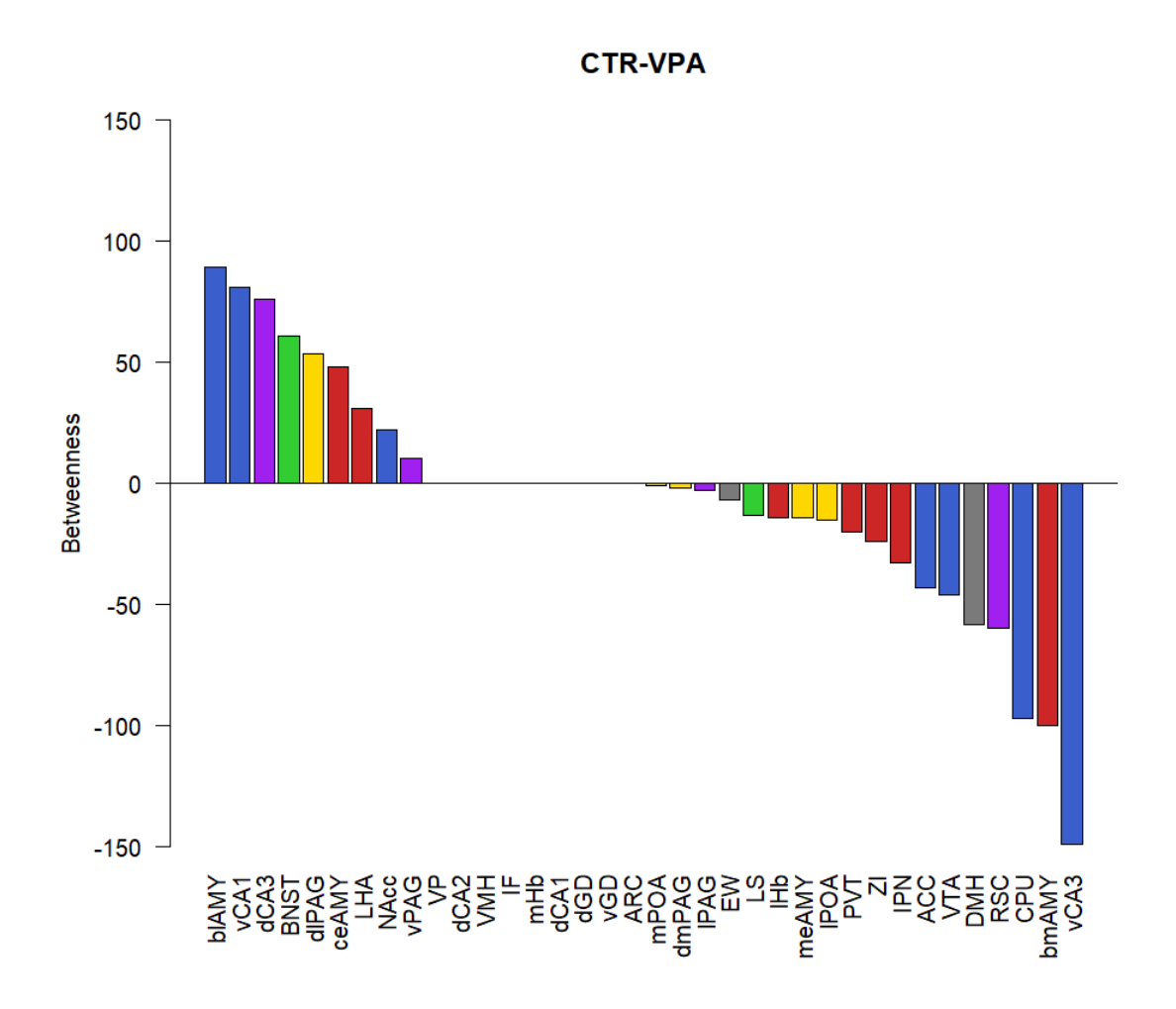


Figure 22: Difference in betweenness centrality values between the socially reinstated (Sep+Soc) CTR and VPA groups. The values above the x-axis represent nodes (nuclei) that have more central position in the network in the CTR group, while the columns below the x-axis indicate nodes that have higher betweenness values in the VPA group. Different colors of the bars indicate the different subnetworks. Blue indicates the MRS, green represents the intersection between MRS and SBN, yellow stands for the SBN, red labels the nuclei involved in stress modulation, purple indicates areas where changes were found in autism, and grey represents the control regions.

Analysis of the internal connection strength in the vCA1 core network revealed that both groups exhibited higher within-network connectivity compared to the full network of all measured nuclei (Figure 15). Notably, we cannot exclude the possibility that this internal coherence was further enhanced in VPA-treated animals (VPA vs. CTR: 0.05<p<0.1).

Such increased synchronization may reflect the coordinated recruitment of core regions involved in spatial navigation, social recognition, and defensive responses during the stimulation phase. Rather than suggesting intentional memory retrieval, this pattern is interpreted as a functional signature of network activation in response to social stimuli. In the VPA group, the enhanced connectivity might further reflect a reduction in network specificity, consistent with less segregated functional organization under altered neurodevelopmental conditions.

The hub of the second core network was the BNST, which was also previously identified as a hub area of the SDMN due to its dopaminergic input and presence of sexual steroid receptors, forming a connection between the SBN and MRS (149). The BNST plays a role in aggression and reproductive behavior (276,277). Additionally, the BNST is crucial for accurate social recognition and social context assessment through the integration of relevant sensory information such as stress history, age, and the novelty of a given conspecific (278).

The LS also belongs to this network and, like the BNST, intersects with the SDMN (149). The LS mediates social behaviors including social aggression (e.g., attack, dominance), social fear, and social play, as well as the evaluation of stimulus novelty in territorial intruder tests (279–281).

This subnetwork also includes the medial and lateral POA, which are parts of the SBN (149). The POA is primarily identified as a mediator of male-male aggression (158). Increased c-Fos activation in the mPOA is associated with aggressive behavior, but the mPOA also plays a role in regulating motivational states and social behaviors (70,251). Activation of the lPOA has been observed after social defeat, involving the LS and BNST (282). The lPOA is also involved in the reinstatement of reward-seeking behavior (184).

Surprisingly, the EW also takes part in this network. While the EW is primarily known for its classical oculomotor function, recent studies indicate its role in attention, vigilance, and fear responses (191,283–286).

The BNST core network considerably overlaps with the SBN, however it is more confined. It defines a higher level of social recognition compared to the one centered around the vCA1. In this network, the analysis of internal connection strength revealed

that in VPA-treated animals, the connectivity immensely weakened (Figure 15). This suggests that the recognition of cagemates and/or the recall of social and dominance history did not function properly in these animals (223). As this is the network that appears to be the most affected by VPA treatment, we identify it as a key pathway system in autism.

The comparison of betweenness centrality, which serves as an indicator of hub status, revealed that in the CTR group, the vCA1 and BNST occupy more central positions than in VPA-treated animals. In VPA-treated animals, the vCA3 and bmAMY take more central positions (Figure 22). The vCA3, similar to the vCA1, plays a role in social memory. However, while the vCA1 is primarily involved in social recognition memory, the vCA3 is required for the encoding, but not the recall, of social stimuli (268,287). This difference suggests that VPA animals might perceive and learn the social relations as new during reinstatement despite of the earlier experience with their former cagemates, while the controls recall the old relations in order to cope with the reinstatement (Figure 23).

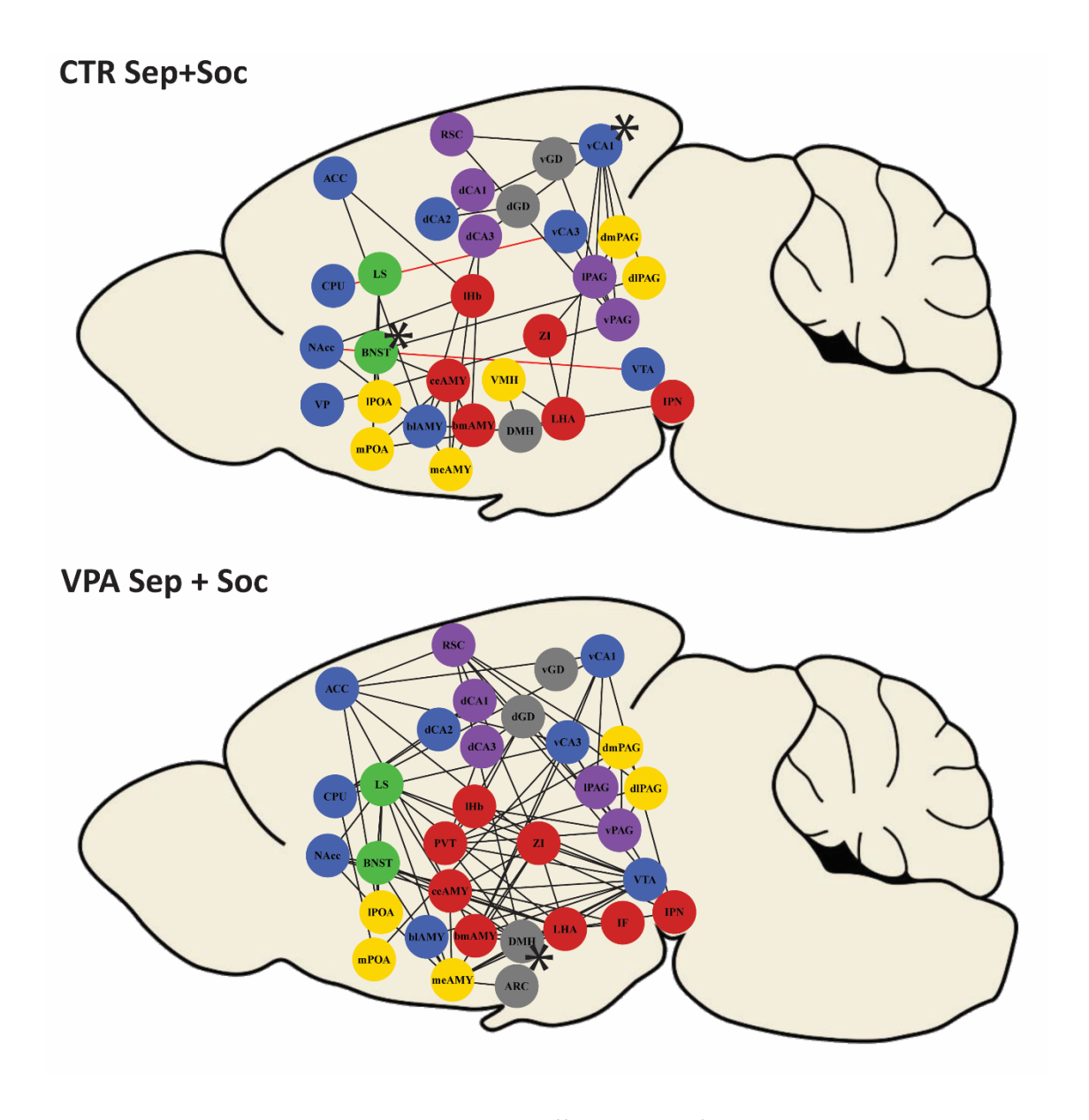


Figure 23: Functional connectivity of socially reinstated (Sep + Soc) animals, derived from the corresponding network figure (see Figure 12). Black edges depict positive correlations, while red edges indicate negative correlations. Asterisks (*) label the identified hubs. Circles represent brain nuclei, and their color denotes subnetwork: blue marks the MRS, yellow indicates the SBN, green represents overlapping nodes (SDMN), red highlights stress-regulatory regions, purple marks autism-associated areas not directly involved in social behavior, and gray denotes control regions.

In the case of socially separated CTR animals, the only hub region identified was the IPN, previously recognized as a major nucleus regulating stress (288) (Figure 24). Unsurprisingly, the cluster around the IPN contains the mHb, which plays a role in chronic unpredictable mild stress regulation and, through the habenulo-peduncular junction, modulates depression and anhedonia-like behavior (246). The IHb is also part of this network, primarily involved in avoidance and the processing of aversive information. Its activity increases in socially isolated animals (245,289,290). The IHb receives numerous afferents and functions as a core regulator of both innate and learned value-guided behavior (291). Among these afferents are the VP, BNST, and blAMY, which are involved in the core network found in the separated CTR animals and are nuclei of the MRS (149,178,292).

Although not part of our core network, the Hb is tightly connected to the VTA, significantly modulating MRS dopamine levels, and to the NAcc, regulating motivated behavior (171,233,293). The core network processing separation also includes multiple nuclei of the AMY, not just the blAMY. From the SBN, the meAMY, which is involved in anxiety-like and rewarding behaviors, may be sensitive to perturbations modulated by adolescent experience (149,294). Additionally, amygdala areas that are not part of the SDMN, such as the bmAMY and ceAMY, participate in the core network, playing important roles in regulating aversive situations and stress-induced anxiety-like behavior (192,295).

The RSC also appears in this network. Besides modulating social interaction, it plays a role in processing spatially-related social information (195). The last part of this network is the dCA3, which, through its connections with the LS, plays a major role in modulating fear and anxiety-like behaviors (296,297).

The internal connectivity strength of this network in VPA-treated animals was weaker compared to CTR animals. This may indicate that separation caused less stress for VPA-treated animals. Given that VPA-treated animals exhibit reduced sociability, decreased vocalization, and less social play(129,142,298), it is not surprising that isolation did not result in as high activation and functional connection as seen in CTR animals. However, it is important to note that this measurement was not as controlled as the reinstatement phase, as there was no specific stimulation that we could control.

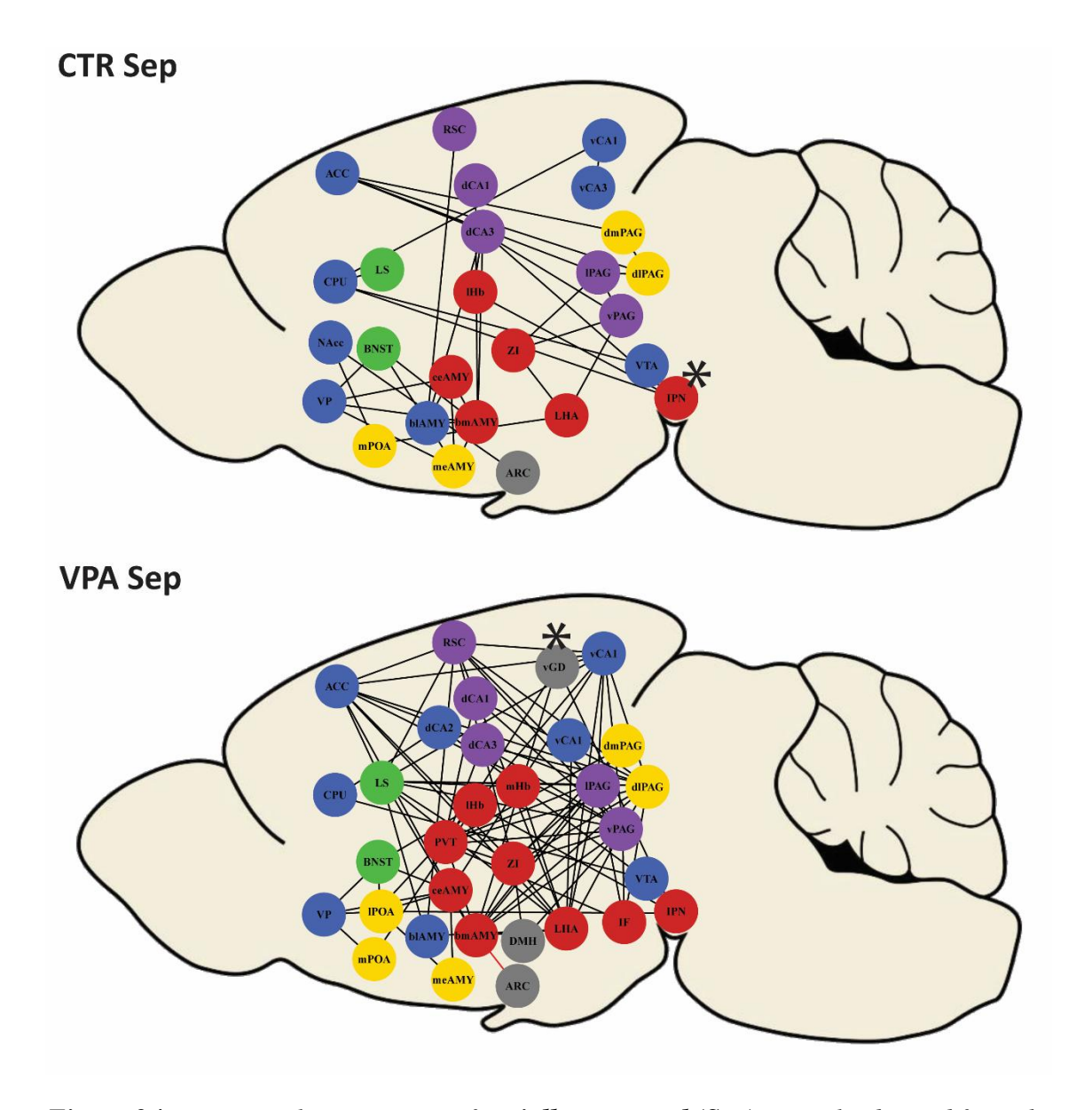


Figure 24: Functional connectivity of socially separated (Sep) animals, derived from the corresponding network figure (see Figure 12). Black edges depict positive correlations, while red edges indicate negative correlations. Asterisks (*) label the identified hubs. Circles represent brain nuclei, and their color denotes subnetwork: blue marks the MRS, yellow indicates the SBN, green represents overlapping nodes (SDMN), red highlights stress-regulatory regions, purple marks autism-associated areas not directly involved in social behavior, and gray denotes control regions (150).

6 Conclusion

Unsurprisingly, the social stimulation differentially affected the brain activation of the VPA and CTR mice in several brain regions. On the other hand, differential c-Fos activation was also observed after 24 hours of social isolation. Since c-Fos activation peaks 90 minutes after any stimulation (299), the latter result suggests that social isolation poses a continuous demand for neural adaptation for at least one day. Therefore, it is not as suitable as a control situation as one might expect. Partly for this reason, and partly because VPA affects brain development rather unspecifically (300,301), it was impossible to localize its effect to one or a few brain regions in any of the social situations used in the present study. However, when we used a network analysis based on the functional connectome, we found a priori defined brain networks to be affected.

In general, most of the brain regions were more interconnected in the VPA-treated animals, which might reflect more developed white matter a trait found in autistic patients (38,89). This parallelism is yet another factor suggesting that VPA-treated miceserve as a valid model for idiopathic autism. The enhanced connectivity within stress-regulating networks, particularly around the habenulo-peduncular pathway, and the weakened connectivity within the social network point to an increased reliance on stress-related responses in VPA-treated animals, potentially at the expense of more adaptive social behaviors.

As we expected, pathways and networks that have already been described as affecting social behavior, decision-making, and stress were disrupted by the VPA treatment. However, to identify the regions and networks most affected, we constructed new networks a posteriori using a less biased method (cluster analysis based on correlational distances). The weakened internal connection strength within these a posteriori identified networks, such as those centered around the vCA1 and BNST, suggests impaired social recognition and memory recall in VPA-treated animals. Additionally, the shift in centrality from the vCA1 and BNST to regions like the vCA3 and bmAMY underscores a reorganization of neural hubs that may contribute to the atypical social behaviors seen in these animals.

Such atypical behaviors are most likely a result of increased stress during reinstatement, as VPA-treated individuals fail to recognize their former cagemates as familiars, as suggested by the altered centrality parameters of the 'social reinstatement core network.' The VPA treatment might also have resulted in decreased stress during social isolation, probably influenced by the 'isolation core network.' These findings align with the observed decrease in sociability and increased stress responses in these animals, reinforcing the idea that VPA treatment disrupts the balance between social and stress-related neural circuits (136,142,302).

Network-based approaches (instead of focusing on just one or two brain regions) have proven to be powerful methods for assessing the effects of embryonic VPA treatment on the brain and the neural mechanisms behind social behavior. However, future research would be more effective if it does not limit itself to previously described pathways but instead measures all possible brain nuclei and identifies hub regions and affected networks a posteriori using unbiased high-throughput methods (303,304).

The results of the present study contribute to the understanding of the neural mechanisms underlying autism, particularly how prenatal exposure to VPA may lead to structural and functional changes in the brain's connectivity that manifest as social and behavioral deficits commonly observed in ASD. To maximize their impact, future research should consider focusing on hub regions identified by network-based approaches to explore the specific pathways and molecular mechanisms involved in these changes, as well as to identify potential therapeutic interventions that could mitigate the impact of these neural alterations.

7 Summary

Autism Spectrum Disorder (ASD) is characterized by deficits in social communication, repetitive behaviors, and sensory sensitivities, linked to disruptions in synaptogenesis, neuronal migration, and neurotransmitter imbalances. Increasingly, ASD is recognized as a disorder of neural connectivity, with altered synchrony across networks governing social and emotional regulation. The Social Decision-Making Network (SDMN), a conserved system regulating social behaviors, provides critical insights into ASD's neural underpinnings.

This study examines the effects of embryonic valproic acid (VPA) exposure—an established rodent model of ASD—on social behavior and brain network connectivity. Male VPA treated and control (CTR) animals underwent social separation and reinstatement paradigms, revealing reduced social preference and impaired recognition of conspecifics in VPA-treated animals. Connectivity analysis indicated significant disruptions in SDMN function, with CTR animals displaying strong internal connectivity between key regions, including the lateral septum (LS), bed nucleus of the stria terminalis (BNST), and ventral pallidum (VP). In VPA-treated animals, SDMN connectivity was diminished, while connections with stress-regulating areas, such as the interpeduncular nucleus (IPN) and lateral hypothalamic area (LHA), were strengthened, reflecting maladaptive stress engagement. c-Fos immunohistochemistry revealed hyperactivation of the nucleus accumbens (NAcc) during social reinstatement in VPA-treated animals. ELISA assays demonstrated significantly reduced dopamine (DA) levels in the NAcc, suggesting a disconnect between heightened neural activity and deficient dopaminergic signaling. Gene mapping highlighted dysregulated pathways involved in neuronal migration and tract formation during the critical period of VPA exposure, reinforcing the developmental basis of these connectivity disruptions.

These findings underscore ASD as a disorder of large-scale network dysfunction, characterized by SDMN deficits, heightened stress pathway engagement, and dopaminergic alterations. This network-level perspective offers new insights into ASD pathophysiology and potential therapeutic strategies.

8 References

- 1. Hodges H, Fealko C, Soares N. Autism spectrum disorder: definition, epidemiology, causes, and clinical evaluation. Transl Pediatr. 2020 Feb;9(Suppl 1):S55–65.
- Diagnostic and statistical manual of mental disorders: DSM-5TM, 5th ed. Arlington,
 VA, US: American Psychiatric Publishing, Inc.; 2013. xliv, 947 p. (Diagnostic and statistical manual of mental disorders: DSM-5TM, 5th ed).
- 3. PARNAS J, BOVET P, ZAHAVI D. Schizophrenic autism: clinical phenomenology and pathogenetic implications. World Psychiatry. 2002 Oct;1(3):131–6.
- 4. Bleuler E, Guttmann D former owner, King's College London. Dementia praecox, oder, Gruppe der Schizophrenien [electronic resource] [Internet]. Leipzig: Franz Deuticke; 1911 [cited 2025 May 2]. 442 p. Available from: http://archive.org/details/b21296157
- 5. Kanner L. Autistic disturbances of affective contact. Nervous Child. 1943;2:217–50.
- 6. Asperger H. Die "Autistischen Psychopathen" im Kindesalter. Archiv f Psychiatrie. 1944 Jun 1;117(1):76–136.
- 7. Asperger H. "Autistic psychopathy" in childhood. New York, NY, US: Cambridge University Press; 1991. 37 p. (Frith U, editor. Autism and Asperger syndrome).
- 8. Vicedo M. Autism's heterogeneity in historical perspective: from challenge to opportunity. Front Psychol. 2023 Aug 3;14:1188053.
- 9. Volkmar FR. DSM-III. In: Volkmar FR, editor. Encyclopedia of Autism Spectrum Disorders [Internet]. New York, NY: Springer; 2013 [cited 2024 May 1]. p. 999–1001. Available from: https://doi.org/10.1007/978-1-4419-1698-3_1442
- Volkmar FR, Bregman J, Cohen DJ, Cicchetti DV. DSM-III and DSM-III-R diagnoses of autism. Am J Psychiatry. 1988;145(11):1404–8.

- 11. Rosen NE, Lord C, Volkmar FR. The Diagnosis of Autism: From Kanner to DSM-III to DSM-5 and Beyond. J Autism Dev Disord. 2021;51(12):4253–70.
- Oberman LM, Kaufmann WE. Autism Spectrum Disorder Versus Autism Spectrum Disorders: Terminology, Concepts, and Clinical Practice. Front Psychiatry. 2020 May 25;11:484.
- 13. Lord C, Risi S, Lambrecht L, Cook EH, Leventhal BL, DiLavore PC, et al. The autism diagnostic observation schedule-generic: a standard measure of social and communication deficits associated with the spectrum of autism. J Autism Dev Disord. 2000 Jun;30(3):205–23.
- 14. Macintosh KE, Dissanayake C. Annotation: The similarities and differences between autistic disorder and Asperger's disorder: a review of the empirical evidence. J Child Psychol Psychiatry. 2004 Mar;45(3):421–34.
- 15. Fernell E, Hedvall A, Norrelgen F, Eriksson M, Höglund-Carlsson L, Barnevik-Olsson M, et al. Developmental profiles in preschool children with autism spectrum disorders referred for intervention. Res Dev Disabil. 2010;31(3):790–9.
- 16. Volkmar FR, Reichow B. Autism in DSM-5: progress and challenges. Molecular Autism. 2013 May 15;4(1):13.
- 17. Tanguay PE. Autism in DSM-5. AJP. 2011 Nov;168(11):1142–4.
- CDC. Centers for Disease Control and Prevention. 2022 [cited 2024 May 1].
 Diagnostic Criteria | Autism Spectrum Disorder (ASD) | NCBDDD | CDC.
 Available from: https://www.cdc.gov/ncbddd/autism/hcp-dsm.html
- 19. Hallmayer J, Cleveland S, Torres A, Phillips J, Cohen B, Torigoe T, et al. Genetic heritability and shared environmental factors among twin pairs with autism. Arch Gen Psychiatry. 2011;68(11):1095–102.
- Ronald A, Hoekstra RA. Autism spectrum disorders and autistic traits: a decade of new twin studies. Am J Med Genet B Neuropsychiatr Genet. 2011 Apr;156B(3):255–74.

- 21. Deth R, Muratore C, Benzecry J, Power-Charnitsky VA, Waly M. How environmental and genetic factors combine to cause autism: A redox/methylation hypothesis. Neurotoxicology. 2008;29(1):190–201.
- 22. Herbert MR. Contributions of the environment and environmentally vulnerable physiology to autism spectrum disorders. Curr Opin Neurol. 2010 Apr;23(2):103–10.
- 23. Karimi P, Kamali E, Mousavi SM, Karahmadi M. Environmental factors influencing the risk of autism. J Res Med Sci. 2017 Feb 16;22:27.
- 24. Koch-Weser J, Browne TR. Drug therapy: Valproic acid. N Engl J Med. 1980 Mar 20;302(12):661–6.
- 25. Clayton-Smith J, Bromley R, Dean J, Journel H, Odent S, Wood A, et al. Diagnosis and management of individuals with Fetal Valproate Spectrum Disorder; a consensus statement from the European Reference Network for Congenital Malformations and Intellectual Disability. Orphanet J Rare Dis. 2019 Jul 19;14:180.
- 26. Safdar A, Ismail F. A comprehensive review on pharmacological applications and drug-induced toxicity of valproic acid. Saudi Pharmaceutical Journal. 2023 Feb 1;31(2):265–78.
- 27. Robert E, Guibaud P. Maternal valproic acid and congenital neural tube defects. Lancet. 1982 Oct 23;2(8304):937.
- 28. DiLiberti JH, Farndon PA, Dennis NR, Curry CJ. The fetal valproate syndrome. Am J Med Genet. 1984;19(3):473–81.
- 29. Clayton-Smith J, Donnai D. Fetal valproate syndrome. J Med Genet. 1995 Sep;32(9):724–7.
- 30. Rasalam AD, Hailey H, Williams JHG, Moore SJ, Turnpenny PD, Lloyd DJ, et al. Characteristics of fetal anticonvulsant syndrome associated autistic disorder. Dev Med Child Neurol. 2005;47(8):551–5.

- 31. Christensen J, Grønborg TK, Sørensen MJ, Schendel D, Parner ET, Pedersen LH, et al. Prenatal Valproate Exposure and Risk of Autism Spectrum Disorders and Childhood Autism. JAMA. 2013 Apr 24;309(16):1696–703.
- 32. Deshmukh U, Adams J, Macklin EA, Dhillon R, McCarthy KD, Dworetzky B, et al. Behavioral outcomes in children exposed prenatally to lamotrigine, valproate, or carbamazepine. Neurotoxicol Teratol. 2016;54:5–14.
- 33. Moore SJ, Turnpenny P, Quinn A, Glover S, Lloyd DJ, Montgomery T, et al. A clinical study of 57 children with fetal anticonvulsant syndromes. J Med Genet. 2000 Jul;37(7):489–97.
- 34. Gottfried C, Bambini-Junior V, Baronio D, Zanatta G, Silvestrin RB, Vaccaro T, et al. Valproic Acid in Autism Spectrum Disorder: From an Environmental Risk Factor to a Reliable Animal Model. In: Recent Advances in Autism Spectrum Disorders Volume I [Internet]. IntechOpen; 2013 [cited 2024 May 1]. Available from: https://www.intechopen.com/chapters/43452
- 35. Courchesne E, Pierce K, Schumann CM, Redcay E, Buckwalter JA, Kennedy DP, et al. Mapping early brain development in autism. Neuron. 2007 Oct 25;56(2):399–413.
- 36. Herbert MR, Ziegler DA, Deutsch CK, O'Brien LM, Lange N, Bakardjiev A, et al. Dissociations of cerebral cortex, subcortical and cerebral white matter volumes in autistic boys. Brain. 2003 May;126(Pt 5):1182–92.
- 37. Sparks BF, Friedman SD, Shaw DW, Aylward EH, Echelard D, Artru AA, et al. Brain structural abnormalities in young children with autism spectrum disorder. Neurology. 2002 Jul 23;59(2):184–92.
- 38. Courchesne E, Karns CM, Davis HR, Ziccardi R, Carper RA, Tigue ZD, et al. Unusual brain growth patterns in early life in patients with autistic disorder. Neurology. 2001 Jul 24;57(2):245–54.

- 39. Riddle K, Cascio CJ, Woodward ND. Brain structure in autism: a voxel-based morphometry analysis of the Autism Brain Imaging Database Exchange (ABIDE). Brain Imaging Behav. 2017 Apr;11(2):541–51.
- 40. Wolff JJ, Jacob S, Elison JT. The journey to autism: Insights from neuroimaging studies of infants and toddlers. Development and Psychopathology. 2018 May;30(2):479–95.
- 41. Freitag CM, Luders E, Hulst HE, Narr KL, Thompson PM, Toga AW, et al. Total brain volume and corpus callosum size in medication-naïve adolescents and young adults with autism spectrum disorder. Biol Psychiatry. 2009;66(4):316–9.
- 42. Mitelman SA, Bralet MC, Haznedar MM, Hollander E, Shihabuddin L, Hazlett EA, et al. Diametrical relationship between gray and white matter volumes in autism spectrum disorder and schizophrenia. Brain Imaging Behav. 2017;11(6):1823–35.
- 43. Radua J, Via E, Catani M, Mataix-Cols D. Voxel-based meta-analysis of regional white-matter volume differences in autism spectrum disorder versus healthy controls. Psychol Med. 2011 Jul;41(7):1539–50.
- 44. Wang H, Ma ZH, Xu LZ, Yang L, Ji ZZ, Tang XZ, et al. Developmental brain structural atypicalities in autism: a voxel-based morphometry analysis. Child and Adolescent Psychiatry and Mental Health. 2022 Jan 31;16(1):7.
- 45. Courchesne E, Campbell K, Solso S. Brain growth across the life span in autism: age-specific changes in anatomical pathology. Brain Res. 2011 Mar 22;1380:138–45.
- 46. Lange N, Travers BG, Bigler ED, Prigge MBD, Froehlich AL, Nielsen JA, et al. Longitudinal volumetric brain changes in autism spectrum disorder ages 6-35 years. Autism Res. 2015 Feb;8(1):82–93.
- 47. Makris N, Pandya DN. The extreme capsule in humans and rethinking of the language circuitry. Brain Struct Funct. 2009 Feb;213(3):343–58.

- 48. Bigler ED, Mortensen S, Neeley ES, Ozonoff S, Krasny L, Johnson M, et al. Superior temporal gyrus, language function, and autism. Dev Neuropsychol. 2007;31(2):217–38.
- 49. Rizzolatti G, Sinigaglia C. The functional role of the parieto-frontal mirror circuit: interpretations and misinterpretations. Nat Rev Neurosci. 2010 Apr;11(4):264–74.
- 50. Calder AJ, Beaver JD, Winston JS, Dolan RJ, Jenkins R, Eger E, et al. Separate coding of different gaze directions in the superior temporal sulcus and inferior parietal lobule. Curr Biol. 2007;17(1):20–5.
- 51. Arunachalam Chandran V, Pliatsikas C, Neufeld J, O'Connell G, Haffey A, DeLuca V, et al. Brain structural correlates of autistic traits across the diagnostic divide: A grey matter and white matter microstructure study. NeuroImage: Clinical. 2021 Jan 1;32:102897.
- 52. Jiao Y, Chen R, Ke X, Chu K, Lu Z, Herskovits EH. Predictive models of autism spectrum disorder based on brain regional cortical thickness. Neuroimage. 2010 Apr 1;50(2):589–99.
- 53. Knaus TA, Kamps J, Foundas AL, Tager-Flusberg H. Atypical PT anatomy in children with autism spectrum disorder with expressive language deficits. Brain Imaging and Behavior. 2018;12(5):1419–30.
- 54. Fishman I, Keown CL, Lincoln AJ, Pineda JA, Müller RA. Atypical cross talk between mentalizing and mirror neuron networks in autism spectrum disorder. JAMA Psychiatry. 2014;71(7):751–60.
- 55. Hyde KL, Samson F, Evans AC, Mottron L. Neuroanatomical differences in brain areas implicated in perceptual and other core features of autism revealed by cortical thickness analysis and voxel-based morphometry. Hum Brain Mapp. 2010 Apr;31(4):556–66.
- 56. Ecker C, Bookheimer SY, Murphy DGM. Neuroimaging in autism spectrum disorder: brain structure and function across the lifespan. The Lancet Neurology. 2015 Nov 1;14(11):1121–34.

- 57. Libero LE, Stevens CE, Kana RK. Attribution of emotions to body postures: an independent component analysis study of functional connectivity in autism. Hum Brain Mapp. 2014 Oct;35(10):5204–18.
- 58. Amiez C, Petrides M. Neuroimaging evidence of the anatomo-functional organization of the human cingulate motor areas. Cereb Cortex. 2014 Mar;24(3):563–78.
- 59. Botvinick MM. Conflict monitoring and decision making: reconciling two perspectives on anterior cingulate function. Cogn Affect Behav Neurosci. 2007;7(4):356–66.
- 60. Apps MAJ, Lesage E, Ramnani N. Vicarious reinforcement learning signals when instructing others. J Neurosci. 2015 Feb 18;35(7):2904–13.
- 61. Kim SY, Choi US, Park SY, Oh SH, Yoon HW, Koh YJ, et al. Abnormal activation of the social brain network in children with autism spectrum disorder: an FMRI study. Psychiatry Investig. 2015;12(1):37–45.
- 62. Wang AT, Lee SS, Sigman M, Dapretto M. Neural basis of irony comprehension in children with autism: the role of prosody and context. Brain. 2006 Apr;129(Pt 4):932–43.
- 63. Verhoeven JS, De Cock P, Lagae L, Sunaert S. Neuroimaging of autism. Neuroradiology. 2010;52(1):3–14.
- 64. Philip RCM, Dauvermann MR, Whalley HC, Baynham K, Lawrie SM, Stanfield AC. A systematic review and meta-analysis of the fMRI investigation of autism spectrum disorders. Neurosci Biobehav Rev. 2012 Feb;36(2):901–42.
- 65. Humphreys K, Hasson U, Avidan G, Minshew N, Behrmann M. Cortical patterns of category-selective activation for faces, places and objects in adults with autism. Autism Res. 2008 Feb;1(1):52–63.
- 66. Di Martino A, Ross K, Uddin LQ, Sklar AB, Castellanos FX, Milham MP. Functional brain correlates of social and nonsocial processes in autism spectrum

- disorders: an activation likelihood estimation meta-analysis. Biol Psychiatry. 2009;65(1):63–74.
- 67. Urbain CM, Pang EW, Taylor MJ. Atypical spatiotemporal signatures of working memory brain processes in autism. Transl Psychiatry. 2015;5(8):e617.
- 68. Thakkar KN, Polli FE, Joseph RM, Tuch DS, Hadjikhani N, Barton JJS, et al. Response monitoring, repetitive behaviour and anterior cingulate abnormalities in autism spectrum disorders (ASD). Brain. 2008 Sep;131(Pt 9):2464–78.
- 69. Langen M, Leemans A, Johnston P, Ecker C, Daly E, Murphy CM, et al. Frontostriatal circuitry and inhibitory control in autism: Findings from diffusion tensor imaging tractography. Cortex. 2012;48(2):183–93.
- 70. Sato W, Kubota Y, Kochiyama T, Uono S, Yoshimura S, Sawada R, et al. Increased putamen volume in adults with autism spectrum disorder. Frontiers in Human Neuroscience. 2014;8(NOV).
- 71. Schuetze M, Park MTM, Cho IY, MacMaster FP, Chakravarty MM, Bray SL. Morphological Alterations in the Thalamus, Striatum, and Pallidum in Autism Spectrum Disorder. Neuropsychopharmacol. 2016 Oct;41(11):2627–37.
- 72. Alexander-Bloch A, Giedd JN, Bullmore E. Imaging structural co-variance between human brain regions. Nature Reviews Neuroscience. 2013;14(5):322–36.
- 73. Duan X, Wang R, Xiao J, Li Y, Huang X, Guo X, et al. Subcortical structural covariance in young children with autism spectrum disorder. Progress in Neuro-Psychopharmacology and Biological Psychiatry. 2020 Apr 20;99:109874.
- 74. Buxhoeveden DP, Semendeferi K, Buckwalter J, Schenker N, Switzer R, Courchesne E. Reduced minicolumns in the frontal cortex of patients with autism. Neuropathology and Applied Neurobiology. 2006;32(5):483–91.
- 75. Casanova MF, van Kooten IAJ, Switala AE, van Engeland H, Heinsen H, Steinbusch HWM, et al. Minicolumnar abnormalities in autism. Acta Neuropathologica. 2006;112(3):287–303.

- 76. Casanova M, Trippe J. Radial cytoarchitecture and patterns of cortical connectivity in autism. Philosophical Transactions of the Royal Society B: Biological Sciences. 2009 May 27;364(1522):1433–6.
- 77. Huberman AD, Clandinin TR, Baier H. Molecular and Cellular Mechanisms of Lamina-specific Axon Targeting. Cold Spring Harb Perspect Biol. 2010 Jan 3;2(3):a001743.
- 78. Martineau FS, Sahu S, Plantier V, Buhler E, Schaller F, Fournier L, et al. Correct Laminar Positioning in the Neocortex Influences Proper Dendritic and Synaptic Development. Cerebral Cortex. 2018 Aug 1;28(8):2976–90.
- 79. Ben-Ari Y. The GABA excitatory/inhibitory developmental sequence: A personal journey. Neuroscience. 2014 Oct 24;279:187–219.
- 80. Weigel B, Tegethoff JF, Grieder SD, Lim B, Nagarajan B, Liu YC, et al. MYT1L haploinsufficiency in human neurons and mice causes autism-associated phenotypes that can be reversed by genetic and pharmacologic intervention. Mol Psychiatry. 2023 May;28(5):2122–35.
- 81. Kemper TL, Bauman M. Neuropathology of infantile autism. J Neuropathol Exp Neurol. 1998 Jul;57(7):645–52.
- 82. Oblak AL, Rosene DL, Kemper TL, Bauman ML, Blatt GJ. Altered posterior cingulate cortical cyctoarchitecture, but normal density of neurons and interneurons in the posterior cingulate cortex and fusiform gyrus in autism. Autism Res. 2011 Jun;4(3):200–11.
- 83. Oblak A, Gibbs TT, Blatt GJ. Reduced serotonin receptor subtypes in a limbic and a neocortical region in autism. Autism Res. 2013;6(6):571–83.
- 84. Wilkinson M, Wang R, van der Kouwe A, Takahashi E. White and gray matter fiber pathways in autism spectrum disorder revealed by ex vivo diffusion MR tractography. Brain and Behavior. 2016;6(7):e00483.

- 85. Ha S, Sohn IJ, Kim N, Sim HJ, Cheon KA. Characteristics of Brains in Autism Spectrum Disorder: Structure, Function and Connectivity across the Lifespan. Exp Neurobiol. 2015 Dec;24(4):273–84.
- 86. Van Essen DC. A tension-based theory of morphogenesis and compact wiring in the central nervous system. Nature. 1997;385(6614):313–8.
- 87. Hardan AY, Jou RJ, Keshavan MS, Varma R, Minshew NJ. Increased frontal cortical folding in autism: a preliminary MRI study. Psychiatry Res. 2004 Sep 15;131(3):263–8.
- 88. Levitt JG, Blanton RE, Smalley S, Thompson PM, Guthrie D, McCracken JT, et al. Cortical sulcal maps in autism. Cereb Cortex. 2003 Jul;13(7):728–35.
- 89. Hazlett HC, Poe MD, Gerig G, Styner M, Chappell C, Smith RG, et al. Early brain overgrowth in autism associated with an increase in cortical surface area before age 2 years. Arch Gen Psychiatry. 2011 May;68(5):467–76.
- 90. Keehn B, Shih P, Brenner LA, Townsend J, Müller RA. Functional connectivity for an "island of sparing" in autism spectrum disorder: an fMRI study of visual search. Hum Brain Mapp. 2013 Oct;34(10):2524–37.
- 91. Shih P, Shen M, Ottl B, Keehn B, Gaffrey MS, Müller RA. Atypical network connectivity for imitation in autism spectrum disorder. Neuropsychologia. 2010;48(10):2931–9.
- 92. Just MA, Keller TA, Malave VL, Kana RK, Varma S. Autism as a neural systems disorder: a theory of frontal-posterior underconnectivity. Neurosci Biobehav Rev. 2012 Apr;36(4):1292–313.
- 93. Schipul SE, Keller TA, Just MA. Inter-regional brain communication and its disturbance in autism. Front Syst Neurosci. 2011;5:10.
- 94. Lynch CJ, Uddin LQ, Supekar K, Khouzam A, Phillips J, Menon V. Default mode network in childhood autism: posteromedial cortex heterogeneity and relationship with social deficits. Biol Psychiatry. 2013;74(3):212–9.

- 95. Solso S, Xu R, Proudfoot J, Hagler DJ, Campbell K, Venkatraman V, et al. Diffusion Tensor Imaging Provides Evidence of Possible Axonal Overconnectivity in Frontal Lobes in Autism Spectrum Disorder Toddlers. Biol Psychiatry. 2016 Apr 15;79(8):676–84.
- 96. Courchesne E, Pierce K. Why the frontal cortex in autism might be talking only to itself: local over-connectivity but long-distance disconnection. Curr Opin Neurobiol. 2005 Apr;15(2):225–30.
- 97. Shukla DK, Keehn B, Smylie DM, Müller RA. Microstructural abnormalities of short-distance white matter tracts in autism spectrum disorder. Neuropsychologia. 2011 Apr;49(5):1378–82.
- 98. Di Martino A, Yan CG, Li Q, Denio E, Castellanos FX, Alaerts K, et al. The autism brain imaging data exchange: towards a large-scale evaluation of the intrinsic brain architecture in autism. Mol Psychiatry. 2014 Jun;19(6):659–67.
- 99. Sahyoun CP, Belliveau JW, Mody M. White matter integrity and pictorial reasoning in high-functioning children with autism. Brain and Cognition. 2010 Aug 1;73(3):180–8.
- 100. Jou RJ, Jackowski AP, Papademetris X, Rajeevan N, Staib LH, Volkmar FR. Diffusion tensor imaging in autism spectrum disorders: preliminary evidence of abnormal neural connectivity. Aust N Z J Psychiatry. 2011 Feb;45(2):153–62.
- 101. Woodward ND, Giraldo-Chica M, Rogers B, Cascio CJ. Thalamocortical Dysconnectivity in Autism Spectrum Disorder: An Analysis of the Autism Brain Imaging Data Exchange. Biological Psychiatry: Cognitive Neuroscience and Neuroimaging. 2017 Jan 1;2(1):76–84.
- 102. Supekar K, Uddin LQ, Khouzam A, Phillips J, Gaillard WD, Kenworthy LE, et al. Brain Hyperconnectivity in Children with Autism and its Links to Social Deficits. Cell Reports. 2013 Nov 14;5(3):738–47.

- 103. Nair A, Treiber JM, Shukla DK, Shih P, Müller RA. Impaired thalamocortical connectivity in autism spectrum disorder: a study of functional and anatomical connectivity. Brain. 2013 Jun;136(Pt 6):1942–55.
- 104. He C, Chen Y, Jian T, Chen H, Guo X, Wang J, et al. Dynamic functional connectivity analysis reveals decreased variability of the default-mode network in developing autistic brain. Autism Res. 2018;11(11):1479–93.
- 105. Edgar JC, Heiken K, Chen YH, Herrington JD, Chow V, Liu S, et al. Resting-State Alpha in Autism Spectrum Disorder and Alpha Associations with Thalamic Volume. J Autism Dev Disord. 2015 Mar 1;45(3):795–804.
- 106. Sperling RA, Bates JF, Cocchiarella AJ, Schacter DL, Rosen BR, Albert MS. Encoding novel face-name associations: A functional MRI study. Human Brain Mapping. 2001;14(3):129–39.
- 107. Cerliani L, Mennes M, Thomas RM, Di Martino A, Thioux M, Keysers C. Increased Functional Connectivity Between Subcortical and Cortical Resting-State Networks in Autism Spectrum Disorder. JAMA Psychiatry. 2015 Aug 1;72(8):767–77.
- 108. Di Martino A, Kelly C, Grzadzinski R, Zuo XN, Mennes M, Mairena MA, et al. Aberrant striatal functional connectivity in children with autism. Biol Psychiatry. 2011 May 1;69(9):847–56.
- 109. Muller CL, Anacker AMJ, Veenstra-VanderWeele J. The serotonin system in autism spectrum disorder: From biomarker to animal models. Neuroscience. 2016;321:24–41.
- 110. Icasiano F, Hewson P, Machet P, Cooper C, Marshall A. Childhood autism spectrum disorder in the Barwon region: A community based study. Journal of Paediatrics and Child Health. 2004;40(12):696–701.
- 111. Fombonne E. Epidemiology of pervasive developmental disorders. Pediatr Res. 2009 Jun;65(6):591–8.

- 112. Loomes R, Hull L, Mandy WPL. What Is the Male-to-Female Ratio in Autism Spectrum Disorder? A Systematic Review and Meta-Analysis. J Am Acad Child Adolesc Psychiatry. 2017 Jun;56(6):466–74.
- 113. Greenberg DM, Warrier V, Allison C, Baron-Cohen S. Testing the Empathizing-Systemizing theory of sex differences and the Extreme Male Brain theory of autism in half a million people. Proc Natl Acad Sci U S A. 2018;115(48):12152–7.
- 114. Srivastava DP, Woolfrey KM, Liu F, Brandon NJ, Penzes P. Estrogen receptor β activity modulates synaptic signaling and structure. J Neurosci. 2010 Oct 6;30(40):13454–60.
- 115. Auyeung B, Lombardo MV, Baron-Cohen S. Prenatal and postnatal hormone effects on the human brain and cognition. Pflugers Arch. 2013 May;465(5):557–71.
- 116. Bakker J. The Sexual Differentiation of the Human Brain: Role of Sex Hormones Versus Sex Chromosomes. Curr Top Behav Neurosci. 2019;43:45–67.
- 117. Lombardo MV, Ashwin E, Auyeung B, Chakrabarti B, Taylor K, Hackett G, et al. Fetal Testosterone Influences Sexually Dimorphic Gray Matter in the Human Brain. J Neurosci. 2012 Jan 11;32(2):674–80.
- 118. Total and Regional Brain Volumes in a Population-Based Normative Sample from 4 to 18 Years: The NIH MRI Study of Normal Brain Development. Cereb Cortex. 2012 Jan;22(1):1–12.
- 119. Satterthwaite TD, Shinohara RT, Wolf DH, Hopson RD, Elliott MA, Vandekar SN, et al. Impact of puberty on the evolution of cerebral perfusion during adolescence. Proc Natl Acad Sci U S A. 2014 Jun 10;111(23):8643–8.
- 120. Grydeland H, Walhovd KB, Tamnes CK, Westlye LT, Fjell AM. Intracortical myelin links with performance variability across the human lifespan: results from T1- and T2-weighted MRI myelin mapping and diffusion tensor imaging. J Neurosci. 2013;33(47):18618–30.

- 121. Kaczkurkin AN, Raznahan A, Satterthwaite TD. Sex differences in the developing brain: insights from multimodal neuroimaging. Neuropsychopharmacology. 2019;44(1):71–85.
- 122. Vijayakumar N, Op de Macks Z, Shirtcliff EA, Pfeifer JH. Puberty and the human brain: Insights into adolescent development. Neurosci Biobehav Rev. 2018 Sep;92:417–36.
- 123. Belzung C, Lemoine M. Criteria of validity for animal models of psychiatric disorders: focus on anxiety disorders and depression. Biol Mood Anxiety Disord. 2011;1(1):9.
- 124. Mabunga DFN, Gonzales ELT, Kim J woon, Kim KC, Shin CY. Exploring the Validity of Valproic Acid Animal Model of Autism. Experimental Neurobiology. 2015 Dec 30;24(4):285–300.
- 125. DiCicco-Bloom E, Lord C, Zwaigenbaum L, Courchesne E, Dager SR, Schmitz C, et al. The developmental neurobiology of autism spectrum disorder. Journal of Neuroscience. 2006;26(26):6897–906.
- 126. Frith U, Happé F. Language and communication in autistic disorders. Philosophical Transactions of the Royal Society B: Biological Sciences. 1994;346(1315):97–104.
- 127. Lord C, Leventhal BL, Cook Jr. EH. Quantifying the phenotype in autism spectrum disorders. American Journal of Medical Genetics. 2001;105(1):36–8.
- 128. Lord C, Risi S, DiLavore PS, Shulman C, Thurm A, Pickles A. Autism from 2 to 9 years of age. Archives of General Psychiatry. 2006;63(6):694–701.
- 129. Chaliha D, Albrecht M, Vaccarezza M, Takechi R, Lam V, Al-Salami H, et al. A Systematic Review of the Valproic-Acid-Induced Rodent Model of Autism. Developmental Neuroscience. 2020 Aug 18;42(1):12–48.
- 130. Gzielo K, Potasiewicz A, Hołuj M, Litwa E, Popik P, Nikiforuk A. Valproic acid exposure impairs ultrasonic communication in infant, adolescent and adult rats. European Neuropsychopharmacology. 2020 Dec 1;41:52–62.

- 131. Zhang Y, Sun Y, Wang F, Wang Z, Peng Y, Li R. Downregulating the canonical Wnt/β-catenin signaling pathway attenuates the susceptibility to autism-like phenotypes by decreasing oxidative stress. Neurochem Res. 2012 Jul;37(7):1409–19.
- 132. Gandal MJ, Edgar JC, Ehrlichman RS, Mehta M, Roberts TPL, Siegel SJ. Validating γ oscillations and delayed auditory responses as translational biomarkers of autism. Biol Psychiatry. 2010;68(12):1100–6.
- 133. Mehta MV, Gandal MJ, Siegel SJ. mGluR5-antagonist mediated reversal of elevated stereotyped, repetitive behaviors in the VPA model of autism. PLoS One. 2011;6(10):e26077.
- 134. Markram K, Rinaldi T, La Mendola D, Sandi C, Markram H. Abnormal fear conditioning and amygdala processing in an animal model of autism. Neuropsychopharmacology. 2008 Mar;33(4):901–12.
- 135. Schneider T, Przewłocki R. Behavioral alterations in rats prenatally exposed to valproic acid: animal model of autism. Neuropsychopharmacology. 2005;30(1):80–9.
- 136. Barrett CE, Hennessey TM, Gordon KM, Ryan SJ, McNair ML, Ressler KJ, et al. Developmental disruption of amygdala transcriptome and socioemotional behavior in rats exposed to valproic acid prenatally. Molecular Autism. 2017 Aug 1;8(1):42.
- 137. Bertelsen F, Folloni D, Møller A, Landau AM, Scheel-Krüger J, Winterdahl M. Suppressed play behaviour and decreased oxytocin receptor binding in the amygdala after prenatal exposure to low-dose valproic acid. Behavioural Pharmacology. 2017 Sep;28(6):450.
- 138. Schneider T, Roman A, Basta-Kaim A, Kubera M, Budziszewska B, Schneider K, et al. Gender-specific behavioral and immunological alterations in an animal model of autism induced by prenatal exposure to valproic acid. Psychoneuroendocrinology. 2008 Jul;33(6):728–40.

- 139. Fombonne E. Epidemiological trends in rates of autism. Mol Psychiatry. 2002 Aug;7(2):S4–6.
- 140. Jeon SJ, Gonzales EL, Mabunga DFN, Valencia ST, Kim DG, Kim Y, et al. Sexspecific Behavioral Features of Rodent Models of Autism Spectrum Disorder. Exp Neurobiol. 2018 Oct;27(5):321–43.
- 141. Schneider T, Turczak J, Przewłocki R. Environmental Enrichment Reverses Behavioral Alterations in Rats Prenatally Exposed to Valproic Acid: Issues for a Therapeutic Approach in Autism. Neuropsychopharmacol. 2006 Jan;31(1):36–46.
- 142. Tartaglione AM, Cipriani C, Chiarotti F, Perrone B, Balestrieri E, Matteucci C, et al. Early Behavioral Alterations and Increased Expression of Endogenous Retroviruses Are Inherited Across Generations in Mice Prenatally Exposed to Valproic Acid. Mol Neurobiol. 2019 May 1;56(5):3736–50.
- 143. Douglas LA, Varlinskaya EI, Spear LP. Rewarding properties of social interactions in adolescent and adult male and female rats: Impact of social versus isolate housing of subjects and partners. Developmental Psychobiology. 2004;45(3):153–62.
- 144. Yates JR, Beckmann JS, Meyer AC, Bardo MT. Concurrent choice for social interaction and amphetamine using conditioned place preference in rats: Effects of age and housing condition. Drug and Alcohol Dependence. 2013 May 1;129(3):240–6.
- 145. Pellis SM, Pellis VC. What is play fighting and what is it good for? Learn Behav. 2017 Dec 1;45(4):355–66.
- 146. Lee NS, Beery AK. Neural circuits underlying rodent sociality: a comparative approach. Curr Top Behav Neurosci. 2019;43:211–38.
- 147. Burke AR, McCormick CM, Pellis SM, Lukkes JL. Impact of adolescent social experiences on behavior and neural circuits implicated in mental illnesses. Neurosci Biobehav Rev. 2017 May;76(Pt B):280–300.

- 148. Newman SW. The medial extended amygdala in male reproductive behavior. A node in the mammalian social behavior network. Ann N Y Acad Sci. 1999 Jun 29;877:242–57.
- 149. O'Connell LA, Hofmann HA. The Vertebrate mesolimbic reward system and social behavior network: A comparative synthesis. J Comp Neurol. 2011 Dec 15;519(18):3599–639.
- 150. Kemecsei RG, Dániel-Papp S, Balázs DB, Csillag A, Zachar G. Disrupted Functional Connectome in a Rodent Model of Autism During Social Isolation. Front Neural Circuits [Internet]. 2025 Apr 28 [cited 2025 May 5];19. Available from: https://www.frontiersin.org/https://www.frontiersin.org/journals/neural-circuits/articles/10.3389/fncir.2025.1525130/abstract
- 151. Halász J, Liposits Z, Meelis W, Kruk MR, Haller J. Hypothalamic attack areamediated activation of the forebrain in aggression. Neuroreport. 2002 Jul 19;13(10):1267–70.
- 152. Bandler R, McCulloch T, McDougall A, Prineas S, Dampney R. Midbrain neural mechanisms mediating emotional behaviour. Int J Neurol. 1985 Jan 1;19–20:40–58.
- 153. Siegel A, Shaikh MB. The neural bases of aggression and rage in the cat. Aggress Violent Behav. 1997 FAL;2(3):241–71.
- 154. Hayden-Hixson DM, Ferris CF. Steroid-specific regulation of agonistic responding in the anterior hypothalamus of male hamsters. Physiol Behav. 1991 Oct;50(4):793–9.
- 155. Delville Y, De Vries GJ, Ferris CF. Neural connections of the anterior hypothalamus and agonistic behavior in golden hamsters. Brain Behav Evol. 2000 Feb;55(2):53–76.
- 156. Nelson RJ, Trainor BC. Neural mechanisms of aggression. Nat Rev Neurosci. 2007 Jul;8(7):536–46.

- 157. Fuxjager MJ, Forbes-Lorman RM, Coss DJ, Auger CJ, Auger AP, Marler CA. Winning territorial disputes selectively enhances androgen sensitivity in neural pathways related to motivation and social aggression. Proc Natl Acad Sci U S A. 2010 Jul 6;107(27):12393–8.
- 158. Albert DJ, Walsh ML, Gorzalka BB, Mendelson S, Zalys C. Intermale social aggression: Suppression by medial preoptic area lesions. Physiology & Behavior. 1986 Jan 1;38(2):169–73.
- 159. Heimer L, Larsson K. Impairment of mating behavior in male rats following lesions in the preoptic-anterior hypothalamic continuum. Brain Research. 1967 Jan 2;3(3):248–63.
- 160. Hull EM, Dominguez JM. Getting his act together: roles of glutamate, nitric oxide, and dopamine in the medial preoptic area. Brain Res. 2006;1126(1):66–75.
- 161. Miceli MO, Malsbury CW. Sagittal knife cuts in the near and far lateral preoptic area-hypothalamus reduce ultrasonic vocalizations in female hamsters. Physiology & Behavior. 1982 Nov 1;29(5):953–6.
- 162. Lee AW, Brown RE. Comparison of medial preoptic, amygdala, and nucleus accumbens lesions on parental behavior in California mice (Peromyscus californicus). Physiol Behav. 2007;92(4):617–28.
- 163. Deco G, Rolls ET. Attention, short-term memory, and action selection: a unifying theory. Prog Neurobiol. 2005 Jul;76(4):236–56.
- 164. Wickens JR, Budd CS, Hyland BI, Arbuthnott GW. Striatal contributions to reward and decision making: making sense of regional variations in a reiterated processing matrix. Ann N Y Acad Sci. 2007 May;1104:192–212.
- 165. Cardinal RN, Parkinson JA, Hall J, Everitt BJ. Emotion and motivation: the role of the amygdala, ventral striatum, and prefrontal cortex. Neurosci Biobehav Rev. 2002 May;26(3):321–52.

- 166. Sandi C, Haller J. Stress and the social brain: behavioural effects and neurobiological mechanisms. Nat Rev Neurosci. 2015 May;16(5):290–304.
- 167. McLaughlin I, Dani JA, De Biasi M. The medial habenula and interpeduncular nucleus circuitry is critical in addiction, anxiety, and mood regulation. J Neurochem. 2017 Aug;142(Suppl 2):130–43.
- 168. Mirrione MM, Schulz D, Lapidus KAB, Zhang S, Goodman W, Henn FA. Increased metabolic activity in the septum and habenula during stress is linked to subsequent expression of learned helplessness behavior. Front Hum Neurosci. 2014;8:29.
- 169. Sugama S, Cho BP, Baker H, Joh TH, Lucero J, Conti B. Neurons of the superior nucleus of the medial habenula and ependymal cells express IL-18 in rat CNS. Brain Res. 2002;958(1):1–9.
- 170. Thompson R. Interpeduncular nucleus and avoidance conditioning in the rat. Science. 1960;132(3439):1551–3.
- 171. Boulos LJ, Darcq E, Kieffer BL. Translating the Habenula-From Rodents to Humans. Biol Psychiatry. 2017 Feb 15;81(4):296–305.
- 172. Hikosaka O, Sesack SR, Lecourtier L, Shepard PD. Habenula: crossroad between the basal ganglia and the limbic system. J Neurosci. 2008;28(46):11825–9.
- 173. Graziane NM, Neumann PA, Dong Y. A Focus on Reward Prediction and the Lateral Habenula: Functional Alterations and the Behavioral Outcomes Induced by Drugs of Abuse. Front Synaptic Neurosci. 2018;10:12.
- 174. Herkenham M, Nauta WJ. Efferent connections of the habenular nuclei in the rat. J Comp Neurol. 1979 Sep 1;187(1):19–47.
- 175. Hayakawa T, Seki M, Zyo K. Studies on the efferent projections of the interpeduncular complex in cats. Okajimas Folia Anat Jpn. 1981 May;58(1):1–15.

- 176. Shibata H, Suzuki T. Efferent projections of the interpeduncular complex in the rat, with special reference to its subnuclei: a retrograde horseradish peroxidase study. Brain Res. 1984 Apr 2;296(2):345–9.
- 177. Morley BJ. The interpeduncular nucleus. Int Rev Neurobiol. 1986;28:157–82.
- 178. Ogawa S, Parhar IS. Role of Habenula in Social and Reproductive Behaviors in Fish: Comparison With Mammals. Front Behav Neurosci. 2022 Feb 10;15:818782.
- 179. Ádám Á, Kemecsei R, Company V, Murcia-Ramón R, Juarez I, Gerecsei LI, et al. Gestational Exposure to Sodium Valproate Disrupts Fasciculation of the Mesotelencephalic Dopaminergic Tract, With a Selective Reduction of Dopaminergic Output From the Ventral Tegmental Area. Front Neuroanat. 2020;14:29.
- 180. Olson BJSC, Markwell J. Assays for Determination of Protein Concentration. Current Protocols in Protein Science. 2007;48(1):3.4.1-3.4.29.
- 181. Kaidanovich-Beilin O, Lipina T, Vukobradovic I, Roder J, Woodgett JR. Assessment of Social Interaction Behaviors. JoVE (Journal of Visualized Experiments). 2011 Feb 25;(48):e2473.
- 182. Atlas Thumbnails :: Allen Brain Atlas: Mouse Brain [Internet]. [cited 2024 Aug 9].

 Available from: https://mouse.brain-map.org/experiment/thumbnails/100048576?image_type=atlas
- 183. Schneider KN, Sciarillo XA, Nudelman JL, Cheer JF, Roesch MR. Anterior Cingulate Cortex Signals Attention in a Social Paradigm that Manipulates Reward and Shock. Current Biology. 2020 Oct 5;30(19):3724-3735.e2.
- 184. Gordon-Fennell AG, Will RG, Ramachandra V, Gordon-Fennell L, Dominguez JM, Zahm DS, et al. The Lateral Preoptic Area: A Novel Regulator of Reward Seeking and Neuronal Activity in the Ventral Tegmental Area. Front Neurosci. 2020 Jan 17;13:1433.

- 185. Zhong J, Liang M, Akther S, Higashida C, Tsuji T, Higashida H. c-Fos expression in the paternal mouse brain induced by communicative interaction with maternal mates. Molecular Brain. 2014 Sep 11;7(1):66.
- 186. Sato K, Hamasaki Y, Fukui K, Ito K, Miyamichi K, Minami M, et al. Amygdalohippocampal Area Neurons That Project to the Preoptic Area Mediate Infant-Directed Attack in Male Mice. J Neurosci. 2020 May 13;40(20):3981–94.
- 187. Kincheski GC, Mota-Ortiz SR, Pavesi E, Canteras NS, Carobrez AP. The Dorsolateral Periaqueductal Gray and Its Role in Mediating Fear Learning to Life Threatening Events. PLOS ONE. 2012 Nov 28;7(11):e50361.
- 188. Li CY, Miao C, Ge Y, Wu J, Gao P, Yin S, et al. A molecularly distinct cell type in the midbrain regulates intermale aggression behaviors in mice [Internet]. bioRxiv; 2024 [cited 2024 Jul 3]. p. 2023.10.19.562724. Available from: https://www.biorxiv.org/content/10.1101/2023.10.19.562724v2
- 189. Fanselow M. Neural organization of the defensive behavior system responsible for fear. Psychonomic Bulletin & Review. 1994 Dec 1;1:429–38.
- 190. Brandão ML, Lovick TA. Role of the dorsal periaqueductal gray in posttraumatic stress disorder: mediation by dopamine and neurokinin. Transl Psychiatry. 2019 Sep 17;9(1):1–9.
- 191. Li Y, Zeng J, Zhang J, Yue C, Zhong W, Liu Z, et al. Hypothalamic Circuits for Predation and Evasion. Neuron. 2018 Feb 21;97(4):911-924.e5.
- 192. Ventura-Silva AP, Melo A, Ferreira AC, Carvalho MM, Campos FL, Sousa N, et al. Excitotoxic lesions in the central nucleus of the amygdala attenuate stress-induced anxiety behavior. Front Behav Neurosci [Internet]. 2013 Apr 19 [cited 2024 Jul 10];7. Available from: https://www.frontiersin.org/journals/behavioral-neuroscience/articles/10.3389/fnbeh.2013.00032/full
- 193. Tang Y, Chen Z, Tao H, Li C, Zhang X, Tang A, et al. Oxytocin activation of neurons in ventral tegmental area and interfascicular nucleus of mouse midbrain. Neuropharmacology. 2014 Feb 1;77:277–84.

- 194. Hogeveen J, Krug MK, Elliott MV, Solomon M. Insula-Retrosplenial Cortex Overconnectivity Increases Internalizing via Reduced Insight in Autism. Biological Psychiatry. 2018 Aug 15;84(4):287–94.
- 195. Shang HF, Cai R, Sun H, Sheng T, Lian YN, Liu L, et al. Deconstruction of the retrosplenial granular cortex for social behavior in the mouse model of fragile X syndrome [Internet]. bioRxiv; 2021 [cited 2024 Jul 10]. p. 2021.01.24.428008. Available from: https://www.biorxiv.org/content/10.1101/2021.01.24.428008v1
- 196. Shi Y, Yan J, Xu X, Qiu Z. Inhibitory inputs from hippocampal CA1 to retrosplenial agranular cortex gate social behavior [Internet]. bioRxiv; 2023 [cited 2024 Oct 28]. p. 2022.08.09.503424. Available from: https://www.biorxiv.org/content/10.1101/2022.08.09.503424v2
- 197. Solomon Coder [Internet]. [cited 2024 Aug 26]. Available from: https://solomon.andraspeter.com/
- 198. Noguchi K, Gel YR, Brunner E, Konietschke F. nparLD: An R Software Package for the Nonparametric Analysis of Longitudinal Data in Factorial Experiments. Journal of Statistical Software. 2012 Sep 18;50:1–23.
- 199. Lakens D. Calculating and reporting effect sizes to facilitate cumulative science: a practical primer for t-tests and ANOVAs. Frontiers in Psychology [Internet]. 2013 [cited 2024 Aug 9];4. Available from: https://www.ncbi.nlm.nih.gov/pmc/articles/PMC3840331/
- 200. Vetere G, Kenney JW, Tran LM, Xia F, Steadman PE, Parkinson J, et al. Chemogenetic Interrogation of a Brain-wide Fear Memory Network in Mice. Neuron. 2017 Apr 19;94(2):363-374.e4.
- 201. Wheeler AL, Teixeira CM, Wang AH, Xiong X, Kovacevic N, Lerch JP, et al. Identification of a Functional Connectome for Long-Term Fear Memory in Mice. PLOS Computational Biology. 2013 Jan 3;9(1):e1002853.

- 202. Galili T, O'Callaghan A, Sidi J, Sievert C. heatmaply: an R package for creating interactive cluster heatmaps for online publishing. Bioinformatics. 2018 May 1;34(9):1600–2.
- 203. Oh SW, Harris JA, Ng L, Winslow B, Cain N, Mihalas S, et al. A mesoscale connectome of the mouse brain. Nature. 2014 Apr;508(7495):207–14.
- 204. Csárdi G, Nepusz T, Müller K, Horvát S, Traag V, Zanini F, et al. igraph for R: R interface of the igraph library for graph theory and network analysis [Internet]. Zenodo; 2025 [cited 2025 Mar 7]. Available from: https://zenodo.org/records/14736815
- 205. Wasserman S, Faust K. Social Network Analysis: Methods and Applications [Internet]. Cambridge: Cambridge University Press; 1994 [cited 2024 Jul 9]. (Structural Analysis in the Social Sciences). Available from: https://www.cambridge.org/core/books/social-network-analysis/90030086891EB3491D096034684EFFB8
- 206. Nguyen E. Text Mining and Network Analysis of Digital Libraries in *R*. In: Zhao Y, Cen Y, editors. Data Mining Applications with R [Internet]. Boston: Academic Press; 2014 [cited 2025 Mar 15]. p. 95–115. Available from: https://www.sciencedirect.com/science/article/pii/B9780124115118000049
- 207. Zhang J, Luo Y. Degree Centrality, Betweenness Centrality, and Closeness Centrality in Social Network. 2017.
- 208. Van Dongen S. A new cluster algorithm for graphs. Citeseer; 1998.
- 209. Projection :: Allen Brain Atlas: Mouse Connectivity [Internet]. [cited 2024 Jul 25]. Available from: https://connectivity.brain-map.org/
- 210. Yamawaki N, Corcoran KA, Guedea AL, Shepherd GMG, Radulovic J. Differential Contributions of Glutamatergic Hippocampal→Retrosplenial Cortical Projections to the Formation and Persistence of Context Memories. Cereb Cortex. 2019 Jun 1;29(6):2728–36.

- 211. Tao K, Chung M, Watarai A, Huang Z, Wang MY, Okuyama T. Disrupted social memory ensembles in the ventral hippocampus underlie social amnesia in autism-associated Shank3 mutant mice. Mol Psychiatry. 2022 Apr;27(4):2095–105.
- 212. Couto-Ovejero S, Ye J, Kind PC, Till SM, Watson TC. Cerebellar contributions to fear-based emotional processing: relevance to understanding the neural circuits involved in autism. Front Syst Neurosci. 2023 Nov 21;17:1229627.
- 213. GGally package RDocumentation [Internet]. [cited 2025 Mar 11]. Available from: https://www.rdocumentation.org/packages/GGally/versions/2.2.1
- 214. ISH Data :: Allen Brain Atlas: Developing Mouse Brain [Internet]. [cited 2024 May 30]. Available from: https://developingmouse.brain-map.org/search/show?page_num=0&page_size=3&no_paging=false&search_type =temporal&age=E11.5&age_id=5&structure=diencephalon&structure_id=16308
- 215. Kim KC, Kim P, Go HS, Choi CS, Yang SI, Cheong JH, et al. The critical period of valproate exposure to induce autistic symptoms in Sprague-Dawley rats. Toxicol Lett. 2011 Mar 5;201(2):137–42.
- 216. MouseMine: Home [Internet]. [cited 2024 May 30]. Available from: https://www.mousemine.org/mousemine/begin.do
- 217. Aickin M, Gensler H. Adjusting for multiple testing when reporting research results: the Bonferroni vs Holm methods. Am J Public Health. 1996 May;86(5):726–8.
- 218. Crawley JN. Mouse behavioral assays relevant to the symptoms of autism. Brain Pathol. 2007 Oct;17(4):448–59.
- 219. Di Y, Diao Z, Zheng Q, Li J, Cheng Q, Li Z, et al. Differential Alterations in Striatal Direct and Indirect Pathways Mediate Two Autism-like Behaviors in Valproate-Exposed Mice. J Neurosci. 2022 Oct 12;42(41):7833–47.
- 220. Shah A, Oxley G, Lovic V, Fleming AS. Effects of preweaning exposure to novel maternal odors on maternal responsiveness and selectivity in adulthood. Developmental Psychobiology. 2002;41(3):187–96.

- 221. Melo AI, Lovic V, Gonzalez A, Madden M, Sinopoli K, Fleming AS. Maternal and littermate deprivation disrupts maternal behavior and social-learning of food preference in adulthood: Tactile stimulation, nest odor, and social rearing prevent these effects. Developmental Psychobiology. 2006;48(3):209–19.
- 222. Roullet FI, Wollaston L, deCatanzaro D, Foster JA. Behavioral and molecular changes in the mouse in response to prenatal exposure to the anti-epileptic drug valproic acid. Neuroscience. 2010 Oct 13;170(2):514–22.
- 223. Fu P, Luo S, Liu Z, Furuhara K, Tsuji T, Higashida H, et al. Oral Supplementation with Maca Improves Social Recognition Deficits in the Valproic Acid Animal Model of Autism Spectrum Disorder. Brain Sciences. 2023 Feb 13;13:316.
- 224. Puglisi-Allegra S, Cabib S. The effect of age on two kinds of aggressive behavior in inbred strains of mice. Dev Psychobiol. 1985;18(6):477–82.
- 225. Berger B, Gaspar P, Verney C. Dopaminergic innervation of the cerebral cortex: unexpected differences between rodents and primates. Trends Neurosci. 1991;14(1):21–7.
- 226. Wang S, Hu SH, Shi Y, Li BM. The roles of the anterior cingulate cortex and its dopamine receptors in self-paced cost-benefit decision making in rats. Learn Behav. 2017 Mar;45(1):89–99.
- 227. Belmonte MK, Allen G, Beckel-Mitchener A, Boulanger LM, Carper RA, Webb SJ. Autism and abnormal development of brain connectivity. J Neurosci. 2004 Oct 20;24(42):9228–31.
- 228. Anderson SA, Eisenstat DD, Shi L, Rubenstein JLR. Interneuron Migration from Basal Forebrain to Neocortex: Dependence on Dlx Genes. Science. 1997 Oct 17;278(5337):474–6.
- 229. Maximo JO, Kana RK. Aberrant "deep connectivity" in autism: A cortico—subcortical functional connectivity magnetic resonance imaging study. Autism Research. 2019;12(3):384–400.

- 230. Schwartz N, Miller C, Fields HL. Cortico-Accumbens Regulation of Approach-Avoidance Behavior Is Modified by Experience and Chronic Pain. Cell Rep. 2017 May 23;19(8):1522–31.
- 231. Al-Hasani R, Gowrishankar R, Schmitz GP, Pedersen CE, Marcus DJ, Shirley SE, et al. Ventral tegmental area GABAergic inhibition of cholinergic interneurons in the ventral nucleus accumbens shell promotes reward reinforcement. Nat Neurosci. 2021 Oct;24(10):1414–28.
- 232. Meisner OC, Nair A, Chang SWC. Amygdala Connectivity and Implications for Social Cognition and Disorders. Handb Clin Neurol. 2022;187:381–403.
- 233. Yang H, de Jong JW, Tak Y, Peck J, Bateup HS, Lammel S. Nucleus Accumbens Subnuclei Regulate Motivated Behavior via Direct Inhibition and Disinhibition of VTA Dopamine Subpopulations. Neuron. 2018 Jan 17;97(2):434-449.e4.
- 234. Numa C, Nagai H, Taniguchi M, Nagai M, Shinohara R, Furuyashiki T. Social defeat stress-specific increase in c-Fos expression in the extended amygdala in mice: Involvement of dopamine D1 receptor in the medial prefrontal cortex. Sci Rep. 2019 Nov 13;9:16670.
- 235. Wolf ME, Mangiavacchi S, Sun X. Mechanisms by which Dopamine Receptors May Influence Synaptic Plasticity. Annals of the New York Academy of Sciences. 2003;1003(1):241–9.
- 236. Gunaydin LA, Grosenick L, Finkelstein JC, Kauvar IV, Fenno LE, Adhikari A, et al. Natural neural projection dynamics underlying social behavior. Cell. 2014 Jun 19;157(7):1535–51.
- 237. Tomova L, Wang KL, Thompson T, Matthews GA, Takahashi A, Tye KM, et al. Acute social isolation evokes midbrain craving responses similar to hunger. Nat Neurosci. 2020;23(12):1597–605.
- 238. Ducharme S, Hudziak JJ, Botteron KN, Ganjavi H, Lepage C, Collins DL, et al. Right anterior cingulate cortical thickness and bilateral striatal volume correlate with

- child behavior checklist aggressive behavior scores in healthy children. Biol Psychiatry. 2011;70(3):283–90.
- 239. Kawamoto T, Onoda K, Nakashima K, Nittono H, Yamaguchi S, Ura M. Is dorsal anterior cingulate cortex activation in response to social exclusion due to expectancy violation? An fMRI study. Front Evol Neurosci. 2012 Jul 27;4:11.
- 240. Lundwall RA, Stephenson KG, Neeley-Tass ES, Cox JC, South M, Bigler ED, et al. Relationship between brain stem volume and aggression in children diagnosed with autism spectrum disorder. Res Autism Spectr Disord. 2017 Feb;34:44–51.
- 241. Phillipson OT. The cytoarchitecture of the interfascicular nucleus and ventral tegmental area of tsai in the rat. Journal of Comparative Neurology. 1979;187(1):85–98.
- 242. Zhao-Shea R, Liu L, Pang X, Gardner PD, Tapper AR. Activation of GABAergic neurons in the interpeduncular nucleus triggers physical nicotine withdrawal symptoms. Curr Biol. 2013;23(23):2327–35.
- 243. Quina LA, Harris J, Zeng H, Turner EE. Specific connections of the interpeduncular subnuclei reveal distinct components of the habenulopeduncular pathway. J Comp Neurol. 2017 Aug 15;525(12):2632–56.
- 244. Morton G, Nasirova N, Sparks DW, Brodsky M, Sivakumaran S, Lambe EK, et al. Chrna5-Expressing Neurons in the Interpeduncular Nucleus Mediate Aversion Primed by Prior Stimulation or Nicotine Exposure. J Neurosci. 2018;38(31):6900–20.
- 245. van Kerkhof LWM, Damsteegt R, Trezza V, Voorn P, Vanderschuren LJMJ. Functional integrity of the habenula is necessary for social play behaviour in rats. Eur J Neurosci. 2013 Nov;38(10):10.1111/ejn.12353.
- 246. Xu C, Sun Y, Cai X, You T, Zhao H, Li Y, et al. Medial Habenula-Interpeduncular Nucleus Circuit Contributes to Anhedonia-Like Behavior in a Rat Model of Depression. Front Behav Neurosci [Internet]. 2018 Oct 9 [cited 2024 Jun 20];12. Available from: https://www.frontiersin.org/articles/10.3389/fnbeh.2018.00238

- 247. Kita H, Kitai ST. Amygdaloid projections to the frontal cortex and the striatum in the rat. J Comp Neurol. 1990;298(1):40–9.
- 248. Everitt BJ, Parkinson JA, Olmstead MC, Arroyo M, Robledo P, Robbins TW. Associative processes in addiction and reward. The role of amygdala-ventral striatal subsystems. Ann N Y Acad Sci. 1999 Jun 29;877:412–38.
- 249. Ferri SL, Kreibich AS, Torre M, Piccoli CT, Dow H, Pallathra AA, et al. Activation of Basolateral Amygdala in Juvenile C57BL/6J Mice During Social Approach Behavior. Neuroscience. 2016 Oct 29;335:184–94.
- 250. Weitekamp CA, Nguyen J, Hofmann HA. Neuromolecular Regulation of Aggression Differs by Social Role during Joint Territory Defense. Integrative and Comparative Biology. 2017 Sep 1;57(3):631–9.
- 251. Tao C, Zhang GW, Huang JJ, Li Z, Tao HW, Zhang LI. The medial preoptic area mediates depressive-like behaviors induced by ovarian hormone withdrawal through distinct GABAergic projections. Nat Neurosci. 2023 Sep;26(9):1529–40.
- 252. Zhang GW, Shen L, Tao C, Jung AH, Peng B, Li Z, et al. Medial preoptic area antagonistically mediates stress-induced anxiety and parental behavior. Nat Neurosci. 2021 Apr;24(4):516–28.
- 253. Adhikari A, Lerner TN, Finkelstein J, Pak S, Jennings JH, Davidson TJ, et al. Basomedial amygdala mediates top–down control of anxiety and fear. Nature. 2015 Nov 12;527(7577):179–85.
- 254. Rosenzweig I, Vukadinovic Z, Turner AJ, Catani M. Neuroconnectivity and valproic acid: The myelin hypothesis. Neuroscience & Biobehavioral Reviews. 2012 Sep 1;36(8):1848–56.
- 255. King C, Mali I, Strating H, Fangman E, Neyhard J, Payne M, et al. Region-Specific Brain Volume Changes Emerge in Adolescence in the Valproic Acid Model of Autism and Parallel Human Findings. Dev Neurosci. 2024 Apr 26;1–12.

- 256. Finszter CK, Kemecsei R, Zachar G, Ádám Á, Csillag A. Gestational VPA exposure reduces the density of juxtapositions between TH+ axons and calretinin or calbindin expressing cells in the ventrobasal forebrain of neonatal mice. Front Neuroanat. 2024;18:1426042.
- 257. Sherr EH. The ARX story (epilepsy, mental retardation, autism, and cerebral malformations): one gene leads to many phenotypes. Current Opinion in Pediatrics. 2003 0;15(6):567.
- 258. Joset P, Wacker A, Babey R, Ingold EA, Andermatt I, Stoeckli ET, et al. Rostral growth of commissural axons requires the cell adhesion molecule MDGA2. Neural Development. 2011;6:22.
- 259. Marsh V. The war on childhood: Commercialism in schools and the first amendment. Houston Law Review. 2017;55:511.
- 260. Gou Y, Vemaraju S, Sweet EM, Kwon HJ, Riley BB. *sox2* and *sox3* Play unique roles in development of hair cells and neurons in the zebrafish inner ear. Developmental Biology. 2018 Mar 1;435(1):73–83.
- 261. Tian H, Qiao S, Zhao Y, Jin X, Wang C, Wang R, et al. Krüppel-like Transcription Factor 7 Is a Causal Gene in Autism Development. International Journal of Molecular Sciences [Internet]. 2022 Mar [cited 2024 Jun 21];23(6). Available from: https://www.ncbi.nlm.nih.gov/pmc/articles/PMC8949233/
- 262. Meira T, Leroy F, Buss EW, Oliva A, Park J, Siegelbaum SA. A hippocampal circuit linking dorsal CA2 to ventral CA1 critical for social memory dynamics. Nat Commun. 2018 Oct 9;9(1):4163.
- 263. Goodson JL. The Vertebrate Social Behavior Network: Evolutionary Themes and Variations. Horm Behav. 2005 Jun;48(1):11–22.
- 264. Kim SA, Jang EH, Lee J, Cho SH. Neonatal Exposure to Valproate Induces Long-Term Alterations in Steroid Hormone Levels in the Brain Cortex of Prepubertal Rats. Int J Mol Sci. 2023 Apr 3;24(7):6681.

- 265. Bicks LK, Peng M, Taub A, Akbarian S, Morishita H. An Adolescent Sensitive Period for Social Dominance Hierarchy Plasticity Is Regulated by Cortical Plasticity Modulators in Mice. Frontiers in Neural Circuits [Internet]. 2021 [cited 2024 Jul 3];15. Available from: https://www.ncbi.nlm.nih.gov/pmc/articles/PMC8149998/
- 266. Bavelier D, Levi DM, Li RW, Dan Y, Hensch TK. Removing Brakes on Adult Brain Plasticity: From Molecular to Behavioral Interventions. J Neurosci. 2010 Nov 10;30(45):14964–71.
- 267. Godino A, Salery M, Minier-Toribio AM, Patel V, Fullard JF, Parise EM, et al. Dopaminoceptive D1 and D2 neurons in ventral hippocampus arbitrate approach and avoidance in anxiety. bioRxiv. 2023 Jul 28;2023.07.25.550554.
- 268. Okuyama T, Yokoi S, Abe H, Isoe Y, Suehiro Y, Imada H, et al. A Neural Mechanism Underlying Mating Preferences for Familiar Individuals in Medaka Fish. Science. 2014 Jan 3;343(6166):91–4.
- 269. Mos J, Kruk MR, Van Poel AMD, Meelis W. Aggressive behavior induced by electrical stimulation in the midbrain central gray of male rats. Aggressive Behavior. 1982;8(3):261–84.
- 270. Murphy AZ, Shupnik MA, Hoffman GE. Androgen and Estrogen (α) Receptor Distribution in the Periaqueductal Gray of the Male Rat. Hormones and Behavior. 1999 Oct 1;36(2):98–108.
- 271. Berton O, McClung CA, DiLeone RJ, Krishnan V, Renthal W, Russo SJ, et al. Essential Role of BDNF in the Mesolimbic Dopamine Pathway in Social Defeat Stress. Science. 2006 Feb 10;311(5762):864–8.
- 272. Franklin T, Silva B, Perova Z, Marrone L, Masferrer M, Zhan Y, et al. Prefrontal cortical control of a brainstem social behavior circuit. Nature neuroscience. 2017 Jan 9;20.
- 273. Vann S, Aggleton J, Maguire E. What does the retrosplenial cortex do? Nature reviews Neuroscience. 2009 Oct 1;10:792–802.

- 274. Burwell RD, Bucci DJ, Sanborn MR, Jutras MJ. Perirhinal and postrhinal contributions to remote memory for context. J Neurosci. 2004;24(49):11023–8.
- 275. Chen P, Hong W. Neural Circuit Mechanisms of Social Behavior. Neuron. 2018 Apr 4;98(1):16–30.
- 276. Valcourt RJ, Sachs BD. Penile reflexes and copulatory behavior in male rats following lesions in the bed nucleus of the stria terminalis. Brain Res Bull. 1979;4(1):131–3.
- 277. Shaikh MB, Brutus M, Siegel HE, Siegel A. Regulation of feline aggression by the bed nucleus of stria terminalis. Brain Res Bull. 1986 Feb;16(2):179–82.
- 278. Flanigan ME, Kash TL. Coordination of social behaviors by the bed nucleus of the stria terminalis. European Journal of Neuroscience. 2022;55(9–10):2404–20.
- 279. Caroline Blanchard D, Blanchard RJ, Takahashi LK, Takahashi T. Septal lesions and aggressive behavior. Behavioral Biology. 1977 Sep 1;21(1):157–61.
- 280. Kondo Y, Shinoda A, Yamanouchi K, Arai Y. Role of septum and preoptic area in regulating masculine and feminine sexual behavior in male rats. Hormones and Behavior. 1990 Sep 1;24(3):421–34.
- 281. Rizzi-Wise CA, Wang DV. Putting Together Pieces of the Lateral Septum: Multifaceted Functions and Its Neural Pathways. eNeuro [Internet]. 2021 Nov 1 [cited 2024 Jun 16];8(6). Available from: https://www.eneuro.org/content/8/6/ENEURO.0315-21.2021
- 282. Martinez M, Phillips PJ, Herbert J. Adaptation in patterns of c-fos expression in the brain associated with exposure to either single or repeated social stress in male rats. European Journal of Neuroscience. 1998;10(1):20–33.
- 283. Edinger L. Über den Verlauf der centralen Hirnnervenbahnen mit Demonstrationen von Präparaten. Arch Psychiat Nervenkr. 1885;16:858–9.

- 284. Westphal C. Ueber einen Fall von chronischer progressiver Lähmung der Augenmuskeln (Ophthalmoplegia externa) nebst Beschreibung von Ganglienzellengruppen im Bereiche des Oculomotoriuskerns. Archiv für Psychiatrie und Nervenkrankheiten. 1887;18(3):846–71.
- 285. Lovett-Barron M, Andalman AS, Allen WE, Vesuna S, Kauvar I, Burns VM, et al. Ancestral Circuits for the Coordinated Modulation of Brain State. Cell. 2017;171(6):1411-1423.e17.
- 286. Priest MF, Freda SN, Badong D, Dumrongprechachan V, Kozorovitskiy Y. Peptidergic modulation of fear responses by the Edinger-Westphal nucleus [Internet]. bioRxiv; 2021 [cited 2024 Jul 6]. p. 2021.08.05.455317. Available from: https://www.biorxiv.org/content/10.1101/2021.08.05.455317v1
- 287. Chiang MC, Huang AJY, Wintzer ME, Ohshima T, McHugh TJ. A role for CA3 in social recognition memory. Behavioural Brain Research. 2018 Nov 15;354:22–30.
- 288. Klenowski PM, Zhao-Shea R, Freels TG, Molas S, Zinter M, M'Angale P, et al. A neuronal coping mechanism linking stress-induced anxiety to motivation for reward. Science Advances. 2023;9(49):eadh9620.
- 289. Hikosaka O. The habenula: from stress evasion to value-based decision-making. Nat Rev Neurosci. 2010 Jul;11(7):503–13.
- 290. Benekareddy M, Stachniak TJ, Bruns A, Knoflach F, von Kienlin M, Künnecke B, et al. Identification of a Corticohabenular Circuit Regulating Socially Directed Behavior. Biol Psychiatry. 2018 Apr 1;83(7):607–17.
- 291. Groos D, Helmchen F. The lateral habenula: A hub for value-guided behavior. Cell Reports. 2024 Apr 23;43(4):113968.
- 292. Cobb-Lewis D, George A, Hu S, Packard K, Song M, Nguyen-Lopez O, et al. The lateral habenula integrates age and experience to promote social transitions in developing rats. bioRxiv. 2024 Jan 14;2024.01.12.575446.

- 293. Gruber C, Kahl A, Lebenheim L, Kowski A, Dittgen A, Veh RW. Dopaminergic projections from the VTA substantially contribute to the mesohabenular pathway in the rat. Neurosci Lett. 2007;427(3):165–70.
- 294. Walker DM, Zhou X, Ramakrishnan A, Cates HM, Cunningham AM, Peña CJ, et al. Adolescent Social Isolation Reprograms the Medial Amygdala: Transcriptome and Sex Differences in Reward [Internet]. bioRxiv; 2020 [cited 2024 Jul 10]. p. 2020.02.18.955187.

 Available from: https://www.biorxiv.org/content/10.1101/2020.02.18.955187v1
- 295. Ritger AC, Stickling CP, Ferrara NC. The impact of social defeat on basomedial amygdala neuronal activity in adult male rats. Behavioural Brain Research. 2023 May 28;446:114418.
- 296. Chen YH, Wu JL, Hu NY, Zhuang JP, Li WP, Zhang SR, et al. Distinct projections from the infralimbic cortex exert opposing effects in modulating anxiety and fear. J Clin Invest [Internet]. 2021 Jul 15 [cited 2024 Jul 10];131(14). Available from: https://www.jci.org/articles/view/145692
- 297. Liu Y, Deng SL, Li LX, Zhou ZX, Lv Q, Wang ZY, et al. A circuit from dorsal hippocampal CA3 to parvafox nucleus mediates chronic social defeat stress—induced deficits in preference for social novelty. Science Advances. 2022 Feb 23;8(8):eabe8828.
- 298. Servadio M, Manduca A, Melancia F, Leboffe L, Schiavi S, Campolongo P, et al. Impaired repair of DNA damage is associated with autistic-like traits in rats prenatally exposed to valproic acid. European Neuropsychopharmacology. 2018 Jan 1;28(1):85–96.
- 299. Morgan JI, Cohen DR, Hempstead JL, Curran T. Mapping Patterns of c-fos Expression in the Central Nervous System After Seizure. Science. 1987 Jul 10;237(4811):192–7.

- 300. Phiel CJ, Zhang F, Huang EY, Guenther MG, Lazar MA, Klein PS. Histone deacetylase is a direct target of valproic acid, a potent anticonvulsant, mood stabilizer, and teratogen. J Biol Chem. 2001 Sep 28;276(39):36734–41.
- 301. Kataoka S, Takuma K, Hara Y, Maeda Y, Ago Y, Matsuda T. Autism-like behaviours with transient histone hyperacetylation in mice treated prenatally with valproic acid. Int J Neuropsychopharmacol. 2013 Feb;16(1):91–103.
- 302. Campolongo M, Kazlauskas N, Falasco G, Urrutia L, Salgueiro N, Höcht C, et al. Sociability deficits after prenatal exposure to valproic acid are rescued by early social enrichment. Molecular Autism. 2018 Jun 14;9(1):36.
- 303. Chen JA, Peñagarikano O, Belgard TG, Swarup V, Geschwind DH. The Emerging Picture of Autism Spectrum Disorder: Genetics and Pathology. Annual Review of Pathology: Mechanisms of Disease. 2015 Jan 24;10(Volume 10, 2015):111–44.
- 304. Cho H, Kim CH, Knight EQ, Oh HW, Park B, Kim DG, et al. Changes in brain metabolic connectivity underlie autistic-like social deficits in a rat model of autism spectrum disorder. Sci Rep. 2017 Oct 16;7(1):13213.

9 List of Own Publications

Original publications related to the topic of the thesis:

A. Adam, R. Kemecsei, V. Company, R. Murcia-Ramon, I. Juarez, L. I. Gerecsei, G. Zachar, D. Echevarria, E. Puelles, S. Martinez, and A. Csillag, "Gestational Exposure to Sodium Valproate Disrupts Fasciculation of the Mesotelencephalic Dopaminergic Tract, With a Selective Reduction of Dopaminergic Output From the Ventral Tegmental Area," *FRONTIERS IN NEUROANATOMY*, vol. 14, 2020.

R. G. Kemecsei, S. Dániel-Papp, D. B. Balazs, E. Gebrihiwet, A. Csillag, and G. Zachar, "Disrupted functional connectome in a rodent model of autism during social isolation," *FRONTIERS IN NEURAL CIRCUITS*, vol. 19, 2025.

Other original publications not related to the topic of the thesis:

G. Zachar, C. Montagnese, E. A. Fazekas, R. G. Kemecsei, S. M. Papp, F. Dóra, É. Renner, A. Csillag, Á. Pogány, and Á. Dobolyi, "Brain Distribution and Sexually Dimorphic Expression of Amylin in Different Reproductive Stages of the Zebra Finch (*Taeniopygia guttata*) Suggest Roles of the Neuropeptide in Song Learning and Social Behaviour," *FRONTIERS IN NEUROSCIENCE*, vol. 13, 2020.

G. Zachar, R. Kemecsei, S. M. Papp, K. Wéber, T. Kisparti, T. Tyler, G. Gáspár, T. Balázsa, and A. Csillag, "D-Aspartate consumption selectively promotes intermediate-term spatial memory and the expression of hippocampal NMDA receptor subunits," *SCIENTIFIC REPORTS*, vol. 11, no. 1, 2021. (*Shared first authorship*)

C. K. Finszter, R. Kemecsei, G. Zachar, S. Holtkamp, D. Echevarría, I. Adorján, Á. Ádám, and A. Csillag, "Early cellular and synaptic changes in dopaminoceptive forebrain regions of juvenile mice following gestational exposure to valproate," *FRONTIERS IN NEUROANATOMY*, vol. 17, 2023.

C. K. Finszter, R. Kemecsei, G. Zachar, Á. Ádám, and A. Csillag, "Gestational VPA exposure reduces the density of juxtapositions between TH+ axons and calretinin or calbindin expressing cells in the ventrobasal forebrain of neonatal mice," *FRONTIERS IN NEUROANATOMY*, vol. 18, 2024.

10 Acknowledgement

I would like to express my sincere gratitude to Dr. Gergely Zachar for his intellectual input, creative ideas, and continuous support throughout the development of this thesis. His guidance was instrumental in shaping the direction of this work. I am also indebted to Dr. Csaba Dávid for his detailed and constructive critique, which contributed significantly to improving the quality and clarity of the final manuscript.

I extend my special thanks to Prof. András Csillag for his careful review of the thesis, valuable scientific advice, and his leadership and mentorship in the laboratory environment.

I acknowledge the valuable contributions of the research group members: Dr. Ágota Ádám, Dr. Catherine Montagnese, Dr. Cintia Finszter, and Dávid Balázs whose expertise and collaboration enriched the research process. I am also grateful to the TDK students, Viktória Horváth and Szizel Dániel-Papp, for their assistance in the experimental procedures.

I am thankful to Prof. Alán Alpár for the opportunity to carry out my research within the institute and for providing a supportive academic environment that fostered my professional growth.

My appreciation also goes to Dr. Andrea Székely and Dr. Károly Altdorfer for their guidance and support during my early steps as an educator, helping to shape my teaching development.

Finally, I would like to thank Szilvia Deák and Zoltán Gróti for their technical assistance in animal experimentation and express my heartfelt gratitude to my family and friends for their encouragement, patience, and unwavering support throughout this journey.